NATIONAL TECHNICAL UNIVERSITY OF ATHENS

SCHOOL OF MINING AND METALLURGICAL ENGINEERING

DEPARTMENT OF METALLURGY AND MATERIALS TECHNOLOGY

IRON OXIDE REMOVAL FROM BAUXITE RESIDUE THROUGH MICROWAVE ROASTING AND MAGNETIC SEPARATION

DOCTORAL THESIS OF

CHIARA CARDENIA

Graduate of Chemistry, University of Rome "La Sapienza", MSc

Athens 2021

ΕΘΝΙΚΟ ΜΕΤΣΟΒΙΟ ΠΟΛΥΤΕΧΝΕΙΟ

ΣΧΟΛΗ ΜΗΧΑΝΙΚΩΝ ΜΕΤΑΛΛΕΙΩΝ ΜΕΤΑΛΛΟΥΡΓΩΝ

ΤΟΜΕΑΣ ΜΕΤΑΛΛΟΥΡΓΙΑΣ ΚΑΙ ΤΕΧΝΟΛΟΓΙΑΣ ΥΛΙΚΩΝ

ΑΠΟΜΑΚΡΥΝΣΗ ΟΞΕΙΔΙΩΝ ΤΟΥ ΣΙΔΗΡΟΥ ΑΠΟ ΤΑ ΚΑΤΑΛΟΙΠΑ ΤΗΣ ΜΕΤΑΛΛΟΥΡΓΙΚΗΣ ΕΠΕΞΕΡΓΑΣΙΑΣ ΤΟΥ ΒΩΞΙΤΗ ΜΕΣΩ ΦΡΥΞΗΣ ΣΕ ΚΑΜΙΝΟ ΜΙΚΡΟΚΥΜΑΤΩΝ ΚΑΙ ΜΑΓΝΗΤΙΚΟ ΔΙΑΧΩΡΙΣΜΟ

ΔΙΔΑΚΤΟΡΙΚΗ ΔΙΑΤΡΙΒΗ

CHIARA CARDENIA

ΠΤΥΧΙΟΥΧΟΣ ΤΜΗΜΑΤΟΣ ΧΗΜΕΙΑΣ,
ΠΑΝΕΠΙΣΤΗΜΙΟΥ ΡΩΜΗΣ “La Sapienza”, MSc

Αθήνα 2021

NATIONAL TECHNICAL UNIVERSITY OF ATHENS

SCHOOL OF MINING AND METALLURGICAL ENGINEERING

DEPARTMENT OF METALLURGY AND MATERIALS TECHNOLOGY

IRON OXIDE REMOVAL FROM BAUXITE RESIDUE THROUGH MICROWAVE ROASTING AND MAGNETIC SEPARATION

DOCTORAL THESIS OF

CHIARA CARDENIA

Graduate of Chemistry, University of Rome "La Sapienza", MSc

Advisory Committee:

Ioannis Paspaliaris, Professor, NTUA (Supervisor)

Dimitrios Panias, Professor, NTUA

Maria Taxiarhou, Assist. Professor, NTUA

Examination Committee:

Ioannis Paspaliaris, Professor, NTUA

Dimitrios Panias, Professor, NTUA

Maria Taxiarhou, Assist. Professor, NTUA

Anthimos Xenidis, Professor, NTUA

Nimfodora Papasiopi, Professor, NTUA

Kostantinos Komnitsas, Professor, Technical University of Crete

Yiannis Pontikes, Assoc. Professor, KU Leuven

Bernd Friedrich, Professor, IME Aachen

Athens 2021

ΕΘΝΙΚΟ ΜΕΤΣΟΒΙΟ ΠΟΛΥΤΕΧΝΕΙΟ

ΣΧΟΛΗ ΜΗΧΑΝΙΚΩΝ ΜΕΤΑΛΛΕΙΩΝ ΜΕΤΑΛΛΟΥΡΓΩΝ

ΤΟΜΕΑΣ ΜΕΤΑΛΛΟΥΡΓΙΑΣ ΚΑΙ ΤΕΧΝΟΛΟΓΙΑΣ ΥΛΙΚΩΝ

ΑΠΟΜΑΚΡΥΝΣΗ ΟΞΕΙΔΙΩΝ ΤΟΥ ΣΙΔΗΡΟΥ ΑΠΟ ΤΑ ΚΑΤΑΛΟΙΠΑ ΤΗΣ ΜΕΤΑΛΛΟΥΡΓΙΚΗΣ ΕΠΕΞΕΡΓΑΣΙΑΣ ΤΟΥ ΒΩΞΙΤΗ ΜΕΣΩ ΦΡΥΞΗΣ ΣΕ ΚΑΜΙΝΟ ΜΙΚΡΟΚΥΜΑΤΩΝ ΚΑΙ ΜΑΓΝΗΤΙΚΟ ΔΙΑΧΩΡΙΣΜΟ

ΔΙΔΑΚΤΟΡΙΚΗ ΔΙΑΤΡΙΒΗ

CHIARA CARDENIA

Πτυχιουχος Τμηματος Χημειας, Πανεπιστημιου Ρωμης “La Sapienza”, MSc

Συμβουλευτική Επιτροπή:

Πασπαλιάρης Ιωάννης, Καθηγητής ΕΜΠ

Πάνιας Δημήτριος, Καθηγητής ΕΜΠ

Ταξιάρχου Μαρία, Αναπληρώτρια Καθηγήτρια ΕΜΠ

Εξεταστική Επιτροπή:

Πασπαλιάρης Ιωάννης, Καθηγητής ΕΜΠ

Πάνιας Δημήτριος, Καθηγητής ΕΜΠ

Ταξιάρχου Μαρία, Αναπληρώτρια Καθηγήτρια ΕΜΠ

Ξενίδης Ανθιμος, Καθηγητής ΕΜΠ

Κομνίτσας Κωνσταντίνος, Καθηγητής Πολυτεχνείου Κρήτης

Ποντίκης Ιωάννης, Αναπληρωτής Καθηγητής Καθολικού Πανεπιστημίου Λουβαίνης

Friedrich Bernd, Professor, RWTH Aachen

Αθήνα 2021

Approved by the seven-member examination committee:

Ioannis Paspaliaris
Professor, NTUA

Dimitrios Panias
Professor, NTUA

Maria Taxiarhou
Assist. Professor, NTUA

Anthimos Xenidis
Professor, NTUA

Nimfodora Papasiopi
Professor, NTUA

Kostantinos Komnitsas
Professor, Technical University of Crete

Yiannis Pontikes
Assoc. Professor, KU Leuven

Bernd Friedrich,
Professor, IME Aachen

"Approval of this doctoral thesis by the School of Mining and Metallurgical Engineering of the National Technical University of Athens (NTUA) does not constitute in any way an acceptance of the views of the author contained herein by the said academic organisation."
(L. 5343/1932, art. 202).

«Η έγκριση της διδακτορικής διατριβής από τη Σχολή Μηχανικών Μεταλλείων–Μεταλλουργών του ΕΜΠ δεν υποδηλώνει την αποδοχή των γνωμών του συγγραφέα.»

(Ν.5343/1932 άρθρο 202)

Dedicated to Giuliano, Francesco and Sara

La mia casa, my home, το σπίτι μου

Acknowledgements

Firstly, I would like to thank Professor Dimitrios Panias for his invaluable support in all stages of my PhD and excellent scientific supervision.

The PhD was held at NTUA in the laboratory of Metallurgy, and I would like to express my gratitude to those who contributed to its fulfilment. In particularly, I received technical, scientific, and academic support by Efthymios Balomenos, Ioanna Giannopoulou, Panagiotis Davris, Alexandra Alexandri, Kostantinos Kollias, Vangelis Bourbos, Dimitrios Sparis, Michalis Vafeias, Apostolos Kourtis, Paschalis Oustadakis, Katerina Vaxevanidou, Antonis Peppas and all other researchers working at NTUA whom I am grateful to meet and to have worked with. I would like to thank Irini Christodoulou, Asimina Katsiapi and Maria Gregou for their administrative support. I would like also to thank Kostantinos Sakkas for his precious help during my stay in Greece.

I would like to warmly thank all the other PhD candidates, supervisors and supporting staff of the MSCA-ETN REDMUD Project for the great experience I had the opportunity to have during the PhD period.

I wish to extend my special thanks to my friend, family, and colleague Chiara Bonomi for all the support she gave me during this our “adventure”.

I would like to thank my NTUA-REDMUD colleagues and friends Johannes Vind and Priiti Tam for the fruitful cooperation, the scientific discussions we had especially during our lunch together.

Finally, I would like to acknowledge with gratitude, the support and love of my family: Giuliano, my husband; my parents Fernanda and Bernardo; my in-laws: Rita and Bruno; Francesco, Marta e Monica. They all kept me going, believing in me and this thesis would not have been possible without them.

The research leading to these results has received funding from the European Community’s Horizon 2020 Programme (H2020/2014–2019) under Grant Agreement no. 636876 (MSCA-ETN REDMUD). This publication reflects only the authors’ views, exempting the Community from any liability. Project website: http://www.etn.redmud.org.

Abstract

Bauxite residue (BR), also known as red mud, is the reddish solid waste generated during the production of alumina from bauxite ores. In particular, the production of 1 metric ton of alumina creates between 0.9 and 1.5 metric tons of residue depending on the composition of initial bauxite ore.

Due to its high alkalinity, with a pH range between 10 and 13, the handling of this waste is a challenge for the alumina industry. In addition, the massive volume of BR produced, which exceeds 150 million metric tons per year worldwide, is causing drastic scarcity of available storage areas. However, its chemical composition encompassing iron, alumina and titania oxides turn BR into an interesting resource for base and critical metal recovery, while a large-scale and bulk utilisation is rather conceivable using BR in construction materials, such as aggregates, cements, ceramics or inorganic polymers. In the last decades, the research was concentrated to find environmentally friendly and cost-effective methods to dispose of or utilize the bauxite residue.

In this framework, the aim of this PhD was to recover iron from BR, developing two different reductive roasting processes followed by magnetic separation.

The first part of the PhD was focused on the study of optimal process for reduction of the nonmagnetic iron phases found in BR (namely hematite and goethite), to magnetic ones such as magnetite, wüstite, and metallic iron. BR was mixed with a carbon source (metallurgical coke) as a reducing agent and roasted in a resistance-heated tube furnace. The magnetic iron phases in the roasting residue were fractionated in a second stage through wet magnetic separation, forming a valuable iron concentrate and leaving a nonmagnetic residue containing rare earth elements

among other constituents. The BR-roasting process has been modeled using a thermochemical software (FactSage 6.4) to define process temperature, Carbon/Bauxite Residue mass ratio (C/BR), retention time, and process atmosphere. Roasting process experiments with different ratios of C/BR (0.112 and 0.225) and temperatures (800 and 1100 °C), 4 h retention time, and, in the presence of N_2 atmosphere, have proven almost the total conversion of hematite to iron magnetic phases (99 wt %). Subsequently, the magnetic separation process has been examined by means of a wet high-intensity magnetic separator, and the analyses have shown a marginal Fe enrichment in magnetic fraction in relation to the sinter.

In the second part of the work a microwave-assisted heating was presented as a suitable method to transform hematite and goethite contained in bauxite residue into magnetite, wüstite and metallic iron, with a short processing time. The final target was the production of a sinter with strong magnetic properties, allowing the magnetic separation of Fe from the residue. The influence of microwave energy on the sample, the effect of irradiation time together with the carbon/bauxite residue mass ratio (C/BR) were the parameters that have been analyzed to optimize the process. Their optimized combination allowed to transform the 79 % of the iron present in the sinter into metallic iron. However, hercynite ($FeAl_2O_4$) was also formed and the presence of this mineralogical phase could be considered a possible drawback for its magnetic properties, since its presence in the magnetic fraction could reduce its purity.

To avoid the formation of $FeAl_2O_4$, a combined soda sintering, and microwave reductive roasting process of bauxite residue was presented. In the first step, all the alumina phases in BR were transformed into sodium aluminates and leached out through alkali-leaching to recover alumina by adding sodium carbonate as flux to BR. Subsequently, the leaching residue have been mixed with carbon and roasted by using a microwave furnace at the optimum conditions. The iron oxide present in the sinter were converted into metallic iron (98 %). In addition, hercynite is not detected. The produced sinter is subjected to magnetic separation processes by using a wet high intensity magnetic separation to separate iron from the other elements.

Περίληψη

Τα Κατάλοιπα Βωξίτη (ΚΒ), γνωστά και ως ερυθρά ιλυς, είναι το στερεό παραπροϊόν που παράγεται κατά την εξαγωγή αλουμινας από βωξίτες. Συγκεκριμένα η παραγωγή ενός τόνου αλουμίνας παράγει από 0.9 εως 1.5 τόνους καταλοίπων βωξίτη, ανάλογα με τη χημική σύσταση του κατεργαζόμενου βωξίτη.

Εξαιτίας της μεγάλης αλκαλικότητας, με ένα pH ανάμεσα στο 10 και 13, η διαχείριση αυτού του υλικού είναι προβληματική για τη βιομηχανία αλουμίνας. Επιπλέον, η μεγάλη ποσότητα ΚΒ που παράγεται κάθε χρόνο και η οποία ξεπερνά τους 150 εκ. τόνους παγκοσμίως, δημιουργεί ελλείψεις σε χώρος απόθεσης. Όμως η χημική σύσταση των ΚΒ, που περιέχουν οξείδια σιδήρου, αλουμινίου και τιτανίου, τα καθιστά αξιόλογους πόρους για την ανάκτηση βασικών και κρίσιμων μετάλλων ενώ παράλληλα μπορούν να χρησιμοποιηθούν και σε εφαρμογές δομικών υλικών όπως αδρανή, τσιμέντο, κεραμικά και ανόργανα πολυμερή. Τις τελευταίες δεκαετίες, η έρευνα έχει επικεντρωθεί στην εύρεση οικολογικών και ανταποδοτικών μεθόδων αξιοποίησης των ΚΒ.

Σε αυτό το πλαίσιο ο σκοπός της παρούσης διδακτορικής διατριβής, είναι η ανάκτηση σιδήρου από τα ΚΒ μέσα από την ανάπτυξη δυο διαφορετικών διεργασιών αναγωγικής φρύξης των ΚΒ και μαγνητικού διαχωρισμού των παραγόμενων φρυγμάτων.

Το πρώτο μέρος του PhD επικεντρώθηκε στη μελέτη της βέλτιστης διαδικασίας για τη αναγωγή των μη μαγνητικών φάσεων σιδήρου που συναντιόνται στα ΚΒ (συγκεκριμένα αιματίτης και

γκαιτίτης), σε μαγνητικές φάσης όπως μαγνητίτης, βουστίτης και μεταλλικός σίδηρος. Τα ΚΒ αναμίχθηκαν με πηγή άνθρακα (μεταλλουργικό ΚΩΚ) ως αναγωγικό μέσο και φρυχθήκαν σε φούρνο ηλεκτρικής αντίστασης. Οι μαγνητικές φάσεις σιδήρου στο φρύγμα, διαχωρίστηκαν σε ένα δεύτερο στάδιο μέσω υγρού μαγνητικού διαχωρισμού, σχηματίζοντας ένα πολύτιμο συμπύκνωμα σιδήρου και ένα μη μαγνητικό κλάσμα που περιέχει στοιχεία σπάνιων γαιών μεταξύ άλλων συστατικών. Η διαδικασία φρύξης των ΚΒ έχει μοντελοποιηθεί χρησιμοποιώντας ένα θερμοχημικό λογισμικό πακέτο (FactSage 6.4) για τον καθορισμό της θερμοκρασίας της διαδικασίας, της αναλογίας μάζας άνθρακα / Καταλοίπων Βωξίτη (C/BR), του χρόνου παραμονής και την ατμόσφαιρα της διαδικασίας. Πειράματα φρύξης με διαφορετικές αναλογίες C/BR (0.112 και 0.225) και θερμοκρασίες (800 και 1100 °C), χρόνο παραμονής 4 ωρών και παρουσία ατμόσφαιρας N2, έχουν αποδείξει τη σχεδόν συνολική μετατροπή του σιδήρου σε μαγνητικές φάεις (99 % κ.β.). Στη συνέχεια, η διαδικασία μαγνητικού διαχωρισμού σε υγρό μαγνητικό διαχωριστή υψηλής έντασης κατέδειξε ένα οριακό εμπλουτισμό του σιδήρου στο μαγνητικό κλάσμα σε σχέση με το φρύγμα.

Στο δεύτερο μέρος της εργασίας εξετάστηκε η χρήση φούρνου μικροκυμάτων ως κατάλληλη μέθοδος για τη μετατροπή του αιματίτη και του γκαίτη που περιέχεται σε κατάλοιπα βωξίτη σε μαγνητίτη, σίδηρο και μεταλλικό σίδηρο, με σύντομο χρόνο επεξεργασίας. Ο τελικός στόχος ήταν η παραγωγή φρυαγμάτων με ισχυρές μαγνητικές ιδιότητες, επιτρέποντας τον μαγνητικό διαχωρισμό του σιδήρου από το υπόλειμμα. Η επίδραση της ενέργειας μικροκυμάτων στο δείγμα, η επίδραση του χρόνου ακτινοβολίας μαζί με την αναλογία μάζας άνθρακα / ΚΒ (C/BR) ήταν οι παράμετροι που εξετάστηκαν για τη βελτιστοποίηση της διαδικασίας. Ο βελτιστοποιημένος συνδυασμός τους επέτρεψε να μετατραπεί το 79 % του σιδήρου που υπάρχει στα ΚΒ σε μεταλλικό σίδερο. Ωστόσο, σχηματίστηκε επίσης η μαγνητική φάση του ερκινίτη ($FeAl_2O_4$), η παρουσία της οποίας θα μπορούσε να θεωρηθεί μειονέκτημα καθώς θα μειώσει τη καθαρότητα του μαγνητικού κλάσματος.

Για να αποφευχθεί ο σχηματισμός $FeAl_2O_4$, παρουσιάστηκε μια συνδυασμένη μέθοδος σύντηξης των ΚΒ με σόδας και αναγωγής σε φούρνο μικροκυμάτων. Στο πρώτο βήμα, όλες οι φάσεις αλουμίνας στα ΚΒ μετασχηματίστηκαν σε αργιλικά άλατα νατρίου και εκχυλίστηκαν μέσω αλκαλικής έκπλυσης. Στη συνέχεια, το υπόλειμμα της εκχύλισης αναμίχθηκε με άνθρακα και φρίχθηκε σε φούρνο μικροκυμάτων στις βέλτιστες συνθήκες. Τα οξείδιο του σιδήρου μετατράπηκαν σε μεταλλικό σίδηρο (98 %) στο φρύγμα. Επιπλέον, η φάση του ερκινίτη δεν εντοπίζεται πλέον. Το παραγόμενο φρυγμα υποβλήθηκε σε διεργασίες υγρου μαγνητικού διαχωρισμού.

List of abbreviations

ΔT	Temperature variation
Δt	Time variation
ε'	Dielectric constant
ε''	Dielectric loss factor
ε_r''	Relative dielectric loss
ε^*	Complex dielectric constant
ε_0	Permittivity of free space
κ	Volume magnetic susceptibility of the particle
λ_0	Wavelength of the incident wave
μ_0	Magnetic permeability of vacuum
μ_M^2	Magnetic moment
µm	Micrometer
ρ	Density
$\sum F_c^{mag}$	Sum of competing force of magnetic material
$\sum F_c^{non-mag}$	Sum of competing force of non-magnetic material
$\vec{\nabla} B$	External magnetic gradient
Å	Ångströme
°C	Celsius degrees
AAS	Atomic absorption spectrometry
A	Ampere
A % (t)	Percentage of absorbed energy from the sample at a specific time
$A_s(t)$	Absorbance value of the sample
$A_e(t)$	Absorbance value of the empty chamber
AoG	Aluminum of Greece plant
B	External magnetic force
BEC	Back electron scattering
BR	Bauxite residue
c	Constant
C	Curie constant
CBMS	Cross belt magnetic separator
C/BR	Carbon/Bauxite Residue mass ratio

C/MBR	Carbon/ Modified bauxite residue mass ratio
C_{Fix}	Carbon fix
C_p	Specific heat of the material
D_p	Microwave penetration depth
DSP	Desilication product
E (z)	Root mean square of the electric field strength
EAF	Electric arc furnace
ED-XRF	Energy Dispersive X-ray Fluorescence Spectroscopy
EU	European union
f	Frequency
$\overrightarrow{F_m}$	Magnetic force
F_m^{mag}	Magnetic force of the particle
$F_m^{non-mag}$	Weak magnetic force of the particle
g	Grams
GHz	Giga hertz
h	Hours
HGMS	High gradient magnetic separators
HGSMS	High gradient superconducting magnetic separation
ICP-MS	Inductively coupled plasma mass spectrometry
ICP-OES	Inductively coupled plasma optical emission spectrometry
IRMS	Induced roll magnetic separator
k	Boltzmann constant
K	Kelvin degrees
kW	Kilowatt
L	Liter
L/min	Liter/minute
LIMS	Wet low-intensity magnetic separators
$\log P_{O_2}$	Oxygen partial pressure
LOI	Loss of Ignition
MAG I	Magnetic I fraction
MAG II	Magnetic II fraction
MBR	Modified bauxite residue
min	Minutes
MHz	Mega hertz

mm	Millimeter
MW	Microwave
n	Number of magnetic dipoles
NM	Non-magnetic fraction
OGMS	Open gradient magnetic separator
P	Pressure
P_v (z)	Power absorbed by a sample per unit volume
ppm	Part per million
REEs	Rare earth elements
REO	Rare earth oxides
rpm	Revolutions per minute
SEI	Second electron imaging
SEM-EDS	Scanning Electron Microscopy coupled with Energy Dispersive Spectroscopy
T	Absolute temperature
T_c	Critical temperature
T_N	Néel temperature
tanδ	Dielectric loss tangent
TE	Transverse electric
TGA-DTA	Thermogravimetric Analysis and Differential Thermal Analysis
TM	Transverse magnetic
TWTs	Traveling wave tubes
V	Volume of the particle
WHIMS	Wet high-intensity high-gradient magnetic separators
XRD	X-Ray powder Diffraction

Table of contents

List of figures

List of tables

1. Introduction

Bauxite ore contains aluminum hydroxides in large percentage (30-65 wt. %)[1–3] and it is mainly employed for the production of alumina (Al_2O_3) through the two main process steps [4]. In the first, alumina is obtained by the Bayer process (based on the reaction with sodium hydroxide under heat and pressure) and in the second, the alumina is electrolyzed in a Hall-Heroult cell to yield aluminum metal [4–6]. However, the hydrothermal extraction of alumina is related with the formation of a reddish byproduct: bauxite residue [7,8] which is consisted of undissolved solids composed of iron oxides, sodium aluminosilicates, titania, silica and mineralogical phases that contain rare earth elements (REEs) [8]. The production of 1 metric ton of alumina creates between 0.9 and 1.5 metric tons of residue depending on the composition of initial bauxite ore. Due to its high alkalinity, with a pH range between 10 and 13, [5,9,10] the handling of this waste is a challenge for the alumina industry. In addition, the massive volume of BR produced, which exceeds 150 million metric tons per year worldwide [7], is causing drastic scarcity of available storage areas [7,11].

In the last decades, the valorization of the alumina by-product was the main drive for the continuous research. The aim was to find environmentally friendly and cost-effective methods to dispose of or utilize the bauxite residue [12]. In addition, an increasing demand for sustainable industrial processing and the depletion of available ores have supported technology development based on secondary raw materials with almost zero-waste production [12]. Thanks to its chemical composition, BR was classified as interesting resource for base and critical metal recovery [13].

BR is a polymetallic source, thanks to its composition, and iron (Fe) is the predominant constituent with its typical range concentration (20-45 wt. %) [2]. For this reason, in the last decades Fe

recovery from BR has attracted major attention [4,12,14,15], since the iron recovered can be used as an alternative iron sources [16,17]. Iron removal studies from bauxite residue are mainly based on pyrometallurgical processes. These works can be grouped into two methods for producing either high-grade magnetite (Fe_3O_4) or metallic Fe: the solid state reductive roasting followed by magnetic separation [18–21] and the reductive smelting process by employing different furnaces (blast furnace, electric arc furnace (EAF) and other types) [6,12,22–25]. On the other hand, the microwave treatment is an emerging technology of mineral processing, as it has several advantages in comparison to conventional heat treatment methods. [17,26–29] One of the advantages of this method is to generate instantaneously heat inside the material, rather than heating the outside surface and slowly conducting it inside as the conventional heating method [30]. This depends on the molecular interactions with the electromagnetic field generated during the process. Based on dielectric properties, materials can be classified into: absorbers (materials that absorb microwave energy and easily heat), insulators (which are transparent to microwave energy) and conductors (which reflect the energy) [31–33]. Since the absorption of microwave energy varies with the composition and structure of different phases, a selective heating is possible. Moreover, microwaves can accelerate chemical reactions [30,34,35]. Therefore microwave-assisted heating could be a suitable method to transform nonmagnetic iron phases found in BR (namely hematite and goethite), to magnetic ones such as magnetite, wüstite, and metallic iron, within a short processing time. The magnetic iron phases in the roasting residue can be fractionated in a second stage through wet magnetic separation, forming a valuable iron concentrate and leaving a nonmagnetic residue containing the other constituents.

1.1 The scope of PhD

In this framework, the aim of this research work is to develop a process for recovering valuable metals from bauxite residue such us iron. Figure 1 shows two conceptual flowsheets in approaching Fe removal.

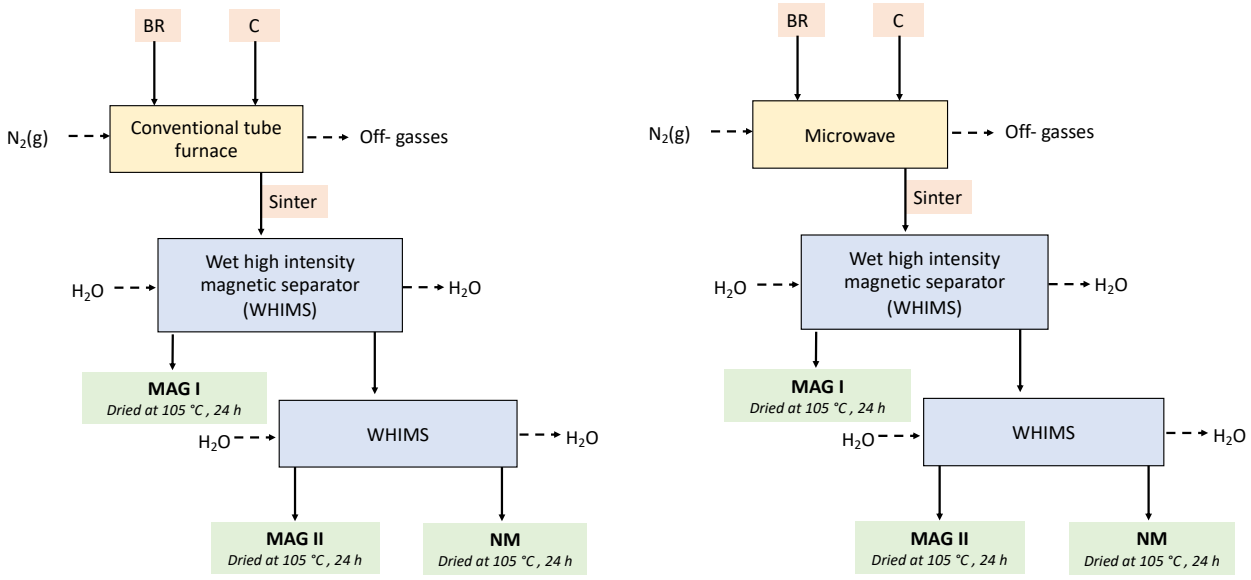

Figure 1. Conceptual flowsheets of the work presented in this PhD thesis focused on the recovery of iron from bauxite residue

The roasting process of bauxite residue using a carbon source (metallurgical coke) as a reducing agent in a resistance-heated tube furnace was investigated (Figure 1 a). The BR-roasting process has been modeled using a thermochemical software (FactSage 6.4^{TM}) to define process temperature, Carbon/Bauxite Residue mass ratio (C/BR), retention time, and process atmosphere. Roasting process experiments with different ratios of C/BR (between 0.112 and 0.225) and temperatures (between 800 and 1000 °C), 4 h retention time, and, in the presence of N_2 atmosphere were investigated. The result of the roasting process at the optimum conditions (C/BR 0.180, 800 °C, 4 h and in presence of N_2) was the production of sinter with strong magnetic properties, containing Fe_3O_4 and γ-Fe_2O_3. Subsequently, the magnetic separation process has been examined by means of a wet high-intensity magnetic separator, and the analyses have shown the existence of calcium aluminum silicon oxides on the surface of iron grains that reduced Fe enrichment in the magnetic concentrate. Other experiments were performed with high temperature (1100 °C) and C/BR ratio (0.225) to intensify reducing conditions and the result was the complete transformation of Fe^{3+}oxide into metallic iron. The following magnetic separation have shown the same problems with calcium aluminum silicon phases attached to metallic iron.

The second part of the study was focused on an optimization of a microwave reductive roasting process (Figure 1 b). Experiments have been carried out in a 2-kW microwave furnace with 3-stub tuner present in the waveguide that allowed to modify microwave energy to accomplish the highest

sample absorption for the entire experimental period. The main target was to transform hematite (Fe_2O_3) and goethite ($Fe_2O_3 \cdot H_2O$) present in BR into magnetite (Fe_3O_4), wüstite (FeO) and metallic iron (Fe^0) according with the iron reduction pathway $Fe_2O_3 \rightarrow Fe_3O_4 \rightarrow FeO \rightarrow Fe$.

Due to the fact that hematite and goethite was not good microwave receptors [36], a carbon (C) source (metallurgical coke) was mixed to BR as a reducing agent as well as microwave energy absorber. Different parameters have been studied (irradiation time, carbon/bauxite residue ratio and the influence of microwave energy on the sample) to optimize the process. The purpose was to liberate the iron-based components from the sinter produced matrix and concentrate them into the magnetic product by using a wet high intensity magnetic separator. At 0.6 kW and 0.225 C/BR with 1 l/min N_2 flow constant for 300 seconds, Fe^{3+} oxides reduction into Fe^{2+} oxides and metallic iron was facilitated by the high temperature reached during the experiment (1100 °C). In particular, the result was the production of sinter with 79 % of metallic iron, while the rest of iron mineralogical phases were attributed to magnetite (Fe_3O_4), wüstite (FeO), and hercynite ($FeAl_2O_4$). Since the formation of iron aluminum oxide was an unavoidable and it can be considered a drawback for magnetic separation process due to its paramagnetic properties, the next step was to decrease the concentration of Al in the BR.

Soda sintering process is covered extensively in many previous studies by Kaußen et al. [37,38], Zheng et al.[39], Alp et al.[40], Meher et al.[41,42] many more which is covered in Tam et al.[43] literature review section as there is potential in removing aluminum and sodium by transformation into sodium aluminate phase, removing two major components and impurities that affect other element recoveries downstream. In literatures that were focused on the carbothermic pig iron recovery from bauxite residue, it was noted that high alkali content, despite reducing melting point, contributes further to furnace lining destruction due to higher reactivity described by researchers such as Valeev et al. [44],Grafe et al. [5], Kaußen et al. [45,46], Borra et al.[23], Anisonyan et al. [47] and Ning et al. [25].

Therefore, the step of removing of aluminum and sodium have been proposed and completed in the previous studies by Tam et al.[43,48,49] using the soda sintering process of bauxite residue with sodium carbonate, which is then leached in mild alkaline solution due to the formation of leachable aluminum and sodium phases in the sinters. This produces leaching residue void of aluminum and sodium which have been optimized for the use of this thesis.

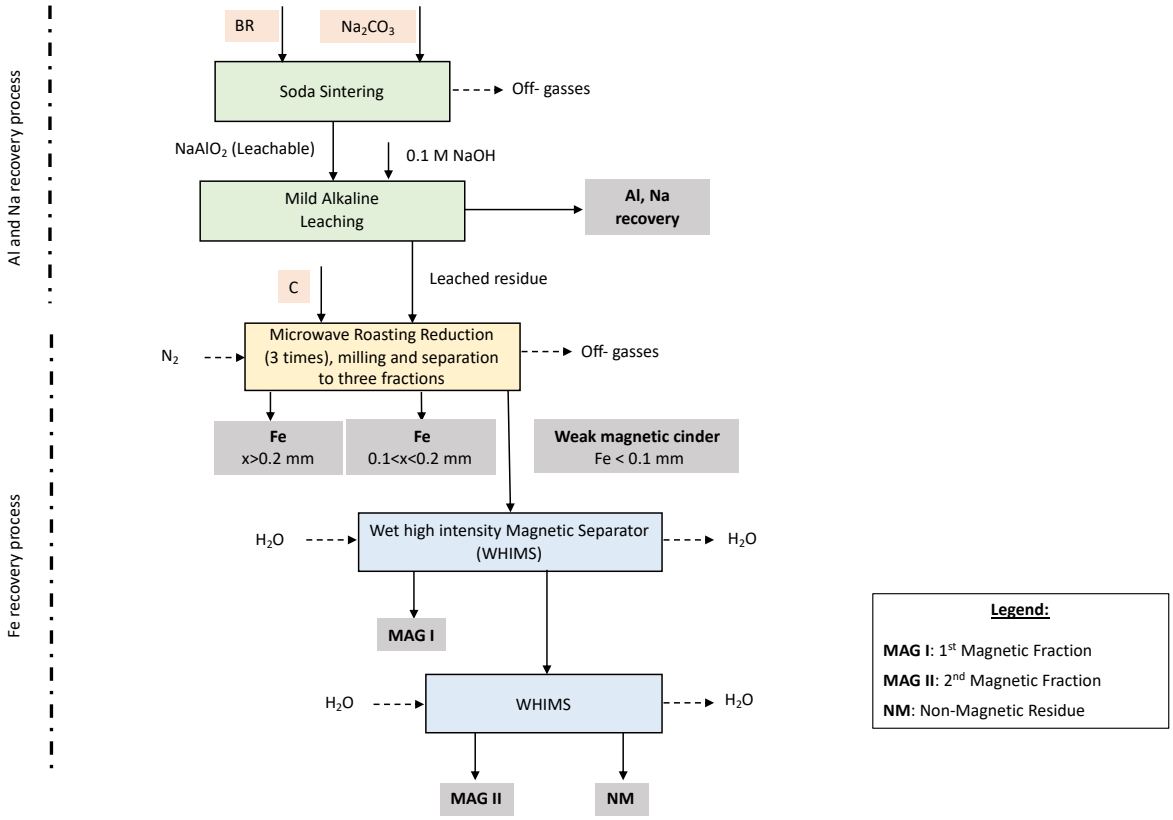

Figure 2. Conceptual flowsheet of the microwave roasting process and magnetic separation

As it presented in Figure **2**, bauxite residue was mixed with sodium carbonate as flux to transform all the alumina phases of BR to soluble sodium aluminates followed by alkali leaching to recover alumina (67 wt. % of aluminum value recovered).

Successively, the leached residue was mixed with the carbon source and treated by using the optimized parameter of microwave furnace. At these conditions, the temperature reached was 1250 °C within some seconds. The cinder resulted to be rich of spherical metallic particles entrapped in the matrix and magnetite (Fe_3O_4) and metallic iron (Fe^0) were the main iron mineralogical phases after the microwave roasting reduction. The hercynite was not detected.

To release the spheres, the sample was firstly milled and then separated by employing a manual sieve (particle size 0.2 mm). and the two fractions were fully characterized.

Since the fraction with a particle size < 0.2 mm still contained a considerable amount of iron oxide, accounting for 51 wt. %, in form of magnetite and metallic iron and due to the presence of C source, the cinder was treated again in the microwave furnace. During this experiment, temperature immediately reached 1230 °C and the result was the formation of metallic iron particles with a particle size > 0.1 mm. To release the particles from the matrix an over mentioned physical approach was used. Analyzing the results, the main component of the fraction with particle size

> 0.1 mm was metallic iron (1 wt. % of the total solid sample), while the other fraction still contains a considerable amount of iron oxide, accounting for 55 wt. % (99 wt. % of the total solid sample).

The sample was treated at the optimized condition to push the system towards the complete reduction into metallic iron to promote the magnetic separation. The analyses of the non-magnetic fraction revealed the existence of metallic iron particles (about 3 wt. %) embedded on the ceramic matrix which partially reduced Fe enrichment in the magnetic concentrate. However, microwave roasting process in combination with an Al-depleted leaching process can potentially developed into a high throughput continuous process to valorize bauxite residue a secondary raw material resource.

1.2 Outline

This PhD thesis has been divided into nine chapters. The first four chapters refer to the literature review, while from the fifth to the eighth chapter the experimental part is presented. In the ninth and final chapter conclusions and future work are given. A more detailed outline of these chapters is given below.

- **Chapter** Errore. L'origine riferimento non è stata trovata. presents the thesis background, scope of this work and the outline of this PhD thesis.
- **Chapter** Errore. L'origine riferimento non è stata trovata. describes the Bayer process in general and gives an overview on bauxite residue management, describing its potential applications. Finally, the use of bauxite residue as secondary raw material is reported and an overview of the literature on the iron recovery from bauxite residue is descript.
- **Chapter 3** specifies microwave energy characteristics and uses. It describes in detail the microwave theory and the technique application.
- **Chapter 4** describes the magnetic separation techniques analyzing the theoretical aspects and the different separators.
- **Chapter 5** describes the Bayer process in the conditions used in Aluminum of Greece plant and the fully characterization of the bauxite residue employed in this work.
- **In Chapter 6** the optimization of the conventional roasting process followed by magnetic separation process is discussed. The results of the thermodynamics software are presented compared with the analysis of the real matrix.
- **Chapter 7** is the core of this PhD thesis the optimization of microwave roasting process is extensively discussed, and the drawback of the process are also presented.

- In **Chapter 8** a combined soda sintering, and microwave reductive roasting process of bauxite residue is investigated. Some preliminary tests are presented and a multi-stage microwave roasting process following by magnetic separation process is proposed.
- **Chapter** Errore. L'origine riferimento non è stata trovata. presents the overall conclusions of the thesis.

2. Bauxite residue

2.1 From bauxite to alumina: the Bayer Process

Bauxite is a sedimentary rock composed of a heterogeneous mixture material and is characterized by aluminum hydroxide minerals found in varying proportions. The aluminum-bearing minerals present in bauxite are gibbsite ($Al(OH)_3$ or $Al_2O_3 \cdot 3H_2O$) also known as hydrargillite or alumina trihydrate or hydrate in the industry; boehmite (γ-AlOOH or $Al_2O_3 \cdot H_2O$, aluminum oxyhydroxide or monohydrate) and diaspore (α-AlOOH or $Al_2O_3 \cdot H_2O$, monohydrate) with average levels 30-65 wt. % [1,2]. Other constituents are silica (4-8 wt. %), iron oxides and hydroxides (10-35 wt. %, measured as iron oxides), titanium oxides (2-4 wt. %) [5,50] and impurities in minor or trace amounts such as scandium [51], rare earth elements [52], gallium and vanadium [53].

Due to their mineral composition, bauxites can be divided into three categories: lateritic (85 % of total), karst (14% of total), and Tikhvin-type (1 % of total) bauxites [54,55]. Lateritic bauxite is formed by weathering of aluminum silicate rocks and is typical for tropical deposits. It composed mostly of gibbsite with only small amounts of boehmite. On the other hand, karst bauxite is formed by weathering of carbonate rock and can be found primarily in Europe and Jamaica. It contains mainly boehmite accompanied with small amounts of diaspore. Since Tikhvin-type bauxites have similar mineralogical characteristic with karst, these deposits are group together [56,57]. Figure 3 shown the distribution of karst and lateritic bauxites worldwide.

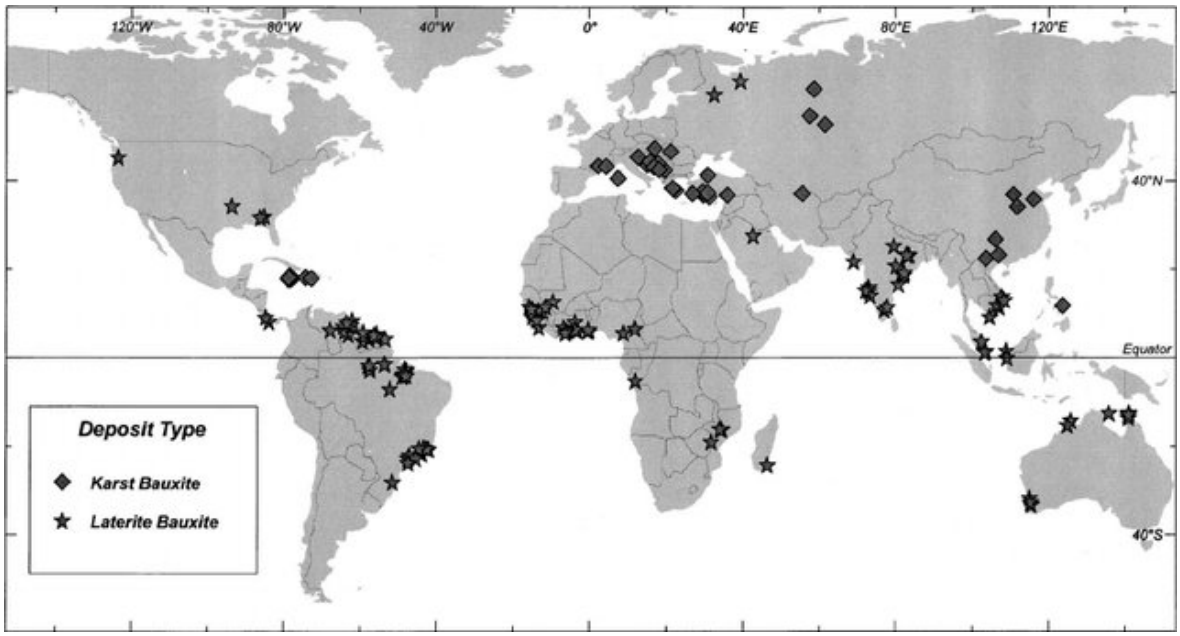

Figure 3. World distribution of karst and laterite bauxite deposits [56].

The bulk of world bauxite production, approximately 85 %, is used as feed for the hydrometallurgical extraction and refinement of pure alumina (> 98.3 % Al_2O_3) through the Bayer process [53,58–61]. Subsequently, the generated alumina is employed as the feedstock for the production of aluminum metal by electrolysis in the Hall-Héroult process [61].

The Bayer process was invented and patented by Karl Josef Bayer in 1887 and it is the primary process by which alumina is extracted from bauxite using concentrated NaOH (sodium hydroxide) solution at high pressure and temperature [2,59]. Although the alumina refineries tried to develop technological improvements to maximize the production of alumina, minimizing the energy costs and the environmental issue of this method [62,63], the Bayer process is still used to produce over 95 % of worldwide alumina supply [2].

The Bayer process is composed of a series of process steps that affect the chemical composition along with physical and mineralogical properties [59]. The essential process steps are the following: digestion, clarification, precipitation, and calcination [64] (Figure 4).

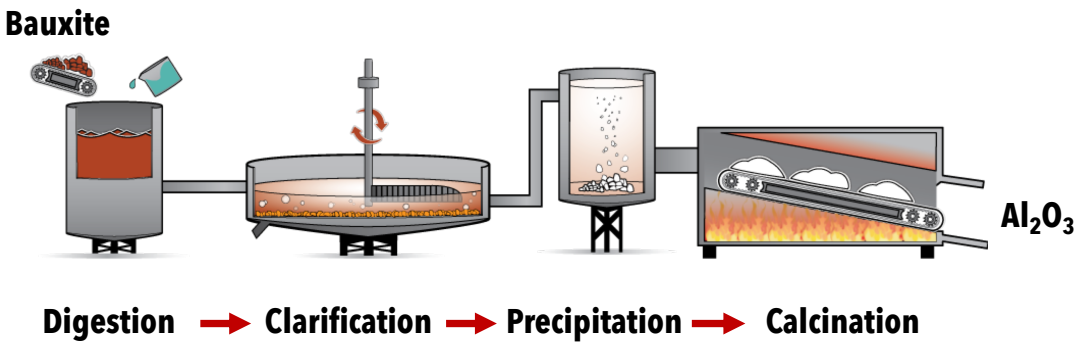

Figure 4. The Bayer Process scheme (https://aluminium.org.au/wp-content/uploads/2017/10/refining.png).

Power et al. divided the Bayer process in two parts: "red side" and "white side". The first one starts with bauxite and finishes with bauxite residue and generally includes the unit processes of bauxite milling, pre-desilication, digestion and clarification. The "white side" of Bayer process incorporates the stages after residue removal (clarification) until calcination [59].

The starting point of Bayer process involve crushing bauxite ore to reduce particle size less to 2 mm particle size [2] to facilitate the following stage.

In the 1st step of Bayer process is the digestion**.** The ground bauxite is mixed and leached with a hot caustic soda (NaOH) solution, where the aluminum-bearing minerals are dissolved selectively, and a pregnant liquor is produced ("green liquor").The high pH values and elevated temperature and pressure of this Bayer process stage, promote the solubility of Al^{3+} as aluminate ($Al(OH)_4^-$). The most of the other compounds (e.g., iron, titanium and silicates) remain insoluble in the solid residue after leaching [5]. However, the conditions (NaOH concentration, temperature and pressure) are set according to the bauxite ore mineralogy as it is possible to observe from the following reaction [5,57,65–67].

Ore with high content of gibbsite can be processed with 3.5 M NaOH [5,68] and temperature between 135-150°C. The digestion reaction is presented in the Equation (1):

$$Al(OH)_{3(s)} + NaOH \rightarrow Al(OH)^-_{4(aq)} + Na^+_{(aq)} \quad (1)$$

With a prevalent concentration of boehmite in bauxite, the temperature reached during the digestion step are between 205-245 °C and with a concentration of NaOH amounted to 3.5 M [5,68] (Equation (2)).

$$\gamma - AlOOH_{(s)} + NaOH + H_2O \rightarrow Al(OH)^-_{4(aq)} + Na^+_{(aq)} \quad (2)$$

The diasporic bauxite is dissolved by employing temperature higher than 250 °C and 5 M NaOH [5,68] (Equation (3).

$$\alpha - AlOOH_{(s)} + NaOH + H_2O \rightarrow Al(OH)^-_{4(aq)} + Na^+_{(aq)} \quad (3)$$

In general, the equilibrium in the above reaction moves to the right with an increase in caustic soda concentration [65].

During the digestion, caustic soda dissolves silica containing species like kaolinite ($Al_2O_3{\cdot}SiO_2{\cdot}2H_2O$) at low temperature (gibbsitic bauxite parameters) as it is presented in Equation (4). Under this condition quartz is less reactive then remains in the solid residue [57,65].

$$\alpha Al_2O_3 \cdot SiO_2 \cdot 2H_2O_{(s)} + 6NaOH_{(aq)} = 2\,Na_2SiO_{3(aq)} + 2\,NaAlO_{2(aq)} + 5H_2O_{(l)} \quad (4)$$

Subsequently, the silica dissolved from kaolinite is not stable and starts to precipitate according to Equation (5) [57,69,70].

$$6\,Na_2SiO_{3(aq)} + 6\,NaAlO_{2(aq)} + 6\,Na_2X_{(aq)} + 12H_2O = 3(Na_2O \cdot Al_2O_3 \cdot 2SiO_2 \cdot nH_2O) \cdot Na_2X_{(s)} + 12NaOH_{(aq)} \quad (5)$$

*Where **X** are anions like CO_3^{2-}, SO_4^{2-}, AlO_2^-, $2OH^-$, $2Cl^-$*

Pre-desilication step is often necessary to control the silica content in the bauxite to avoid a loss of caustic soda, which decrease the dissolution of aluminum-bearing minerals. Prior to the digestion process, it is possible to add at the bauxite, slaked lime ($Ca(OH)_2$) to form cancrinite instead of sodalite, which it remain insoluble in the solid residue during the alkaline leaching [5] .

The 2nd step of Bayer process is the clarification**.** It involves multiple steps, and it is achieved in a thickener (also known as a settler). Flocculants are added to facilitate the separation of residue composed with undissolved minerals (as from now on: “red mud” or “bauxite residue”) from the green liquor (saturated sodium aluminate ($NaAl(OH)_4$) solutions).

To recover NaOH and $Al(OH)_4^-$ for recycling them into the Bayer Process, the red mud slurry is washed in counter-current decantation washer. After the last washing step, the residue is usually filtered or treated in a final thickener to increase the solids content prior to being transported into a specific disposal [59].

The 3rd step is the precipitation. The $NaAl(OH)_4$) solution is pumped from the clarification settler into a series of tanks, where aluminum hydroxide seed crystals are introduced to aid the crystallization. The alumina hydrate ($Al(OH)_3$) starting to precipitate according to Equation (6):

$$Al(OH)^-_{4(aq)} + Na^+_{(aq)} \rightarrow Al(OH)_3 \downarrow + NaOH \quad (6)$$

The precipitation reaction can be considered the reverse of the digestion reaction. The difference is based on adjustment of precipitation conditions (such as type of seed material, temperature of precipitation, and cooling rate), which in this step can controlled the nature of the product [65].

The precipitated material (alumina hydrate) is separated from the caustic aluminate liquor by filtration and through evaporation. Then NaOH is washed and reused into the digestion stage. Depending from the particle size, the fine hydrate is recycled to be used as seed, while the coarse one is sent to the last step of Bayer Process, the calcination [64].

The 4th Bayer Process step is the calcination. Alumina hydrate ($Al(OH)_3$) is addressed to rotary kilns or stationary fluidized-bed flash calciners and then thermally decomposed at T > 1000 °C. The free water and the combined water evaporate at this temperature and the result is the production of pure alumina (Al_2O_3), as it is presented in Equation (7)[5,59,64]:

$$2Al(OH)_3 \rightarrow Al_2O_3 + 3H_2O \quad (7)$$

On average, to produce 1 kg of alumina are required 2.65 kg of bauxite ore [71] . The remaining amount of the solid is removed from the process as slurry (red mud).

Global bauxite production grew from 250 million tons in 2011 to over 300 million tons in 2019, due to the high demand of aluminum production. In particular, the largest producing countries are Australia with over 80 million tons (equal to 28 % of the world's output), followed by China (23 %), Guinea (15 %), Brazil (12 %) and India (9 %). Greece is the only EU country with a significant bauxite production (1.8 million tons in 2017) [72,73].

Bauxite residue (also called "red mud", "Bayer process tailings", "bauxite process tailings" [7], among other names) is the waste product left from the filtering and washing of the aluminum hydroxide crystals after the clarification step. The BR physical and chemical composition can depending on the initial ore composition, but also on the units which composed the "red side" of Bayer process (bauxite milling, pre-desilication, digestion, clarification and counter-current decantation washing) [5,14,59] (Figure 5).

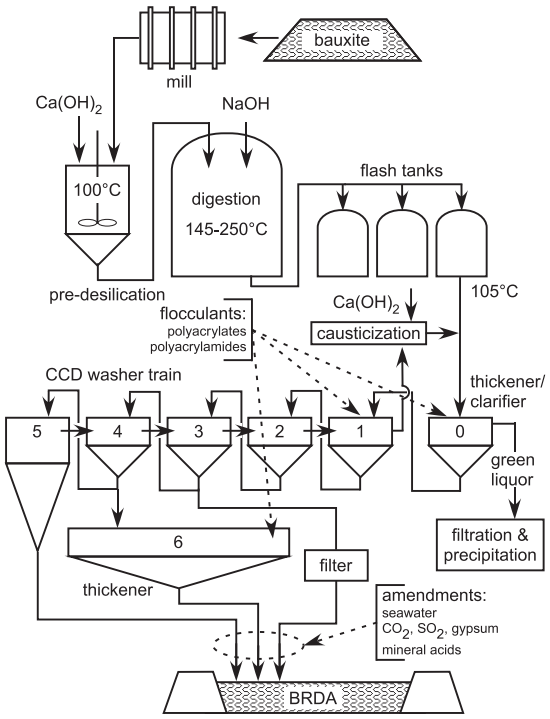

Figure 5. A schematic flowsheet of "red side" Bayer process (source Power et al.[59]).

The residue can vary in color but is typically a reddish-brown color due to the high concentration of iron oxide in the substance. The chemical composition of bauxite residue is extremely wide as it possible to observe in Table 1 [2,14,65].

Table 1. Bauxite residue chemical composition [2].

Component	Typical range (wt. %)
Fe_2O_3	20-45
Al_2O_3	10-22
TiO_2	4-20
CaO	0-14
SiO_2	5-30
Na_2O	2-8
REEs	0.1-1

After the clarification step of Bayer Process, the undissolved base elements as silicon, aluminum, iron, calcium, titanium, sodium as well as an array of minor elements namely Rare Earth Elements (REEs) are concentrated up in BR. Therefore, the material contains a significant portion of recoverable and economically valuable base metals and trace elements in terms of volume of waste produced per annum [12].

The range of minerals typically found for bauxite residues is shown Table 2. As it possible to observe the mineralogical composition of the alumina waste is complex and contain some phases which are present in the ore and others that are produced during the Bayer Process [2,7]. Some of the elements are soluble in the Bayer process and either build up in the Bayer liquor or precipitate along with the aluminium hydroxide during digestion.

Table 2. Typical range of minerals found in bauxite residue [2].

Component	Typical range (wt. %)
Sodalite ($3Na_2O{\cdot}3Al_2O_3{\cdot}6SiO_2{\cdot}Na_2SO_4$)	4-40
Al-goethite ($(Fe, Al)_2O_3{\cdot}nH_2O$)	1-55
Hematite (Fe_2O_3)	10-30
Magnetite (Fe_3O_4)	0-8
Silica (SiO_2) crystalline and amorphous	3-20
Calcium aluminate ($3CaO{\cdot}Al_2O_3{\cdot}6H_2O$)	2-20
Boehmite (AlOOH)	0-20
Titanium dioxide (TiO_2) anatase and rutile	2-15
Muscovite ($K_2O{\cdot}\ Al_2O_3{\cdot}6SiO_2{\cdot}2H_2O$)	0-15
Calcite ($CaCO_3$)	2-20
Kaolinite ($Al_2O_3{\cdot}2SiO_2{\cdot}2H_2O$)	0-5
Gibbsite ($Al(OH)_3$)	0-5
Perovskite ($CaTiO_3$)	0-12
Cancrinite ($Na_6[Al_6Si_6O_{24}]{\cdot}2CaCO_3$)	0-50
Diaspore (AlOOH)	0-5

However, due to the conditions (temperature and pressure used in the extraction process, the elements can increase or decrease in concentration in the bauxite residue compare to the bauxite ore. Sodium is the only element not found in the bauxite itself and in BR may be present as DSP as a soluble form. In fact, small quantities of soluble sodium compounds resulting from soda used during digestion will remain. The amount of this residual will depend on the de-watering and washing conditions used. These species, a mixture of sodium aluminate and sodium carbonate are

responsible for elevated pH for BR slurries, which are then neutralized by carbon dioxide from the air to form sodium carbonate and other metal carbonate species [7].

In addition to mineralogical and chemical characteristics, the physical characteristics (moisture content and particle size) are important when considering BR management. The median particle size is normally in the range of 5 – 10 μm and the grains width is extremely wide. It can extend from coarse sandy grains about 1 mm in size down to sub-micron particles and it depend from different alumina plants and the parameters employed during the Bayer process and also from the kind of bauxites used as initial material [7].

2.2 Management of bauxite residue

Bauxite residue is classified from the European Protection Agency (EPA) within the European Waste Catalogue and Hazardous Waste List as a non-hazardous mine waste (CER 01 03 09) [37]. However, the Basel Convention [38] designates the material as a non-hazardous (B2110) if the pH value is below 11.5. For this reason the high alkalinity of BR limits transportation for storage, disposal, or treatment applications and reuse options [39], since the pH of BR is spread from 9.2 to 12.8 due to the presence of multiple alkaline solids [5]. To decrease the pH value below 11.5 the alumina industries implement the filtering operation down to a desired end-point pH of 7 to 9 [34].

Although the disposal of bauxite residue is an environmental issue for the alumina refinery, due to the alkaline pH, the global demand for alumina increases rapidly. In 2019 over 130 million tons of alumina were produced worldwide, compared to 2015 where the production was attested at 115 million tons (Figure 6)[74].

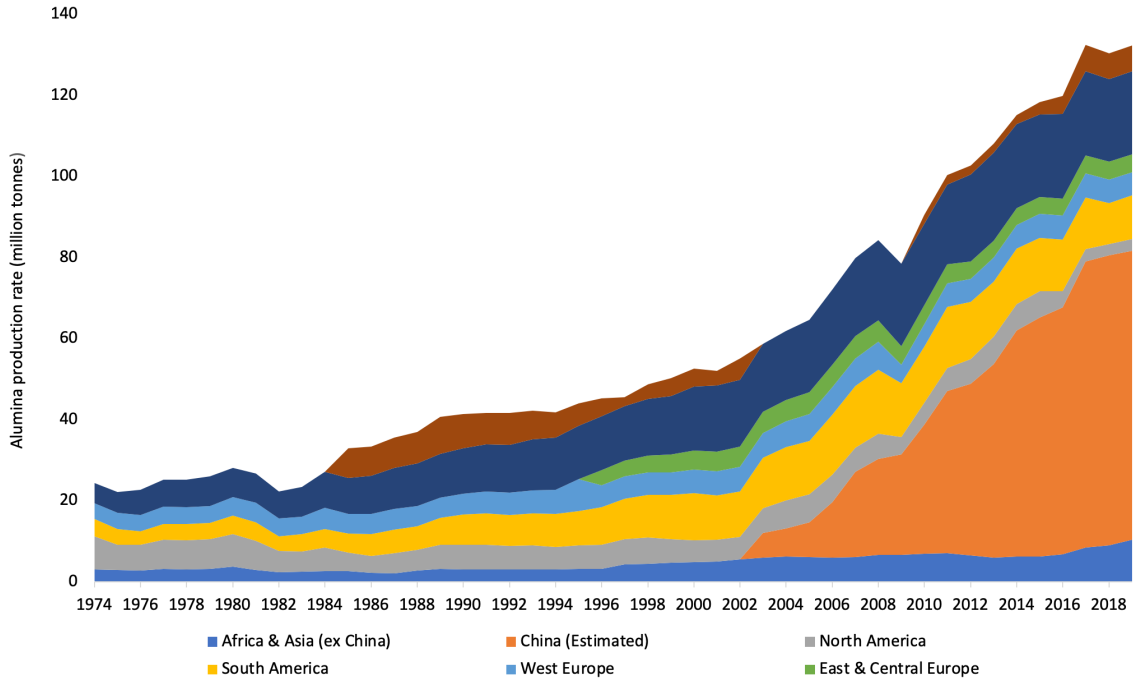

Figure 6. Global production of Al_2O_3 from 1974 to 2019 (source: http://www.world-aluminium.org/statistics/alumina-production/#histogram)

It is estimated that the production of 1 metric ton of alumina creates between 0.9 and 1.5 metric tons of residue depending on the composition of initial bauxite ore characteristics and alumina's extraction efficiency [5,7,63].

The massive volume of BR produced, which exceeds 160 million metric tons per year worldwide [7] is causing drastic scarcity of available storage areas [5,7]. There are more than 80 alumina refinery plants in the world with bauxite residue ponds and dams [75], while there are at least other 50 closed legacy sites. The combined stockpile of bauxite residue at the active and legacy sites is estimated around 3-4 billion tons [5,7,76]. The BR disposal remains a complicated issue for the aluminum/alumina industry [12] due to the waste high alkalinity [10] and the very large quantities generated [12].

The stocking method of BR can be mainly divided into two types: wet stocking and dry stocking. The method used depends on different factor as geological and environmental condition of the site, availability of the land, but also the nature of the residue and country regulations [2,59].

In the early Bayer alumina plants, the wet residue was often stockpiled close or adjacent to the alumina refinery filling depressions, valleys and mine workings. However, due to the morphology of these areas, causing high alkaline leaching of the landfill, the ponds were dammed to contain the ever-growing volume of the waste (namely lagoon-storage) [2,76].

Lagooning is the conventional wet disposal method in which the residue slurry (with a solid content of 18-30 %) is directly pumped into land-based ponds (either natural or artificial depression), and then is stocked after precipitation. The supernatant liquor above the residue was normally returned to the plant for reuse to recover most of the caustic soda and avoid the humans and wildlife contamination [7]. Prior to 1980, most of the inventory of BR was stored in lagoon-type impoundments and the practice continues at some facilities [7]. It was noticed that this approach is disadvantageous in terms of potential risk for the surrounding environment due to the high alkalinity (pH > 12 and soda level excess of 2000 mg/L) of the residue and the potential failure of the dam. Hence, the wet disposal method need high monitoring, maintenance and remediation cost to reduce the probability of a catastrophic environmental disaster, as though in the case of the accidental dam failure at Ajka, in Hungary in 2010 [7,77,78].

Another wet method largely employed between the 1940s and 1960s and definitely phased out in 2015, was marine discharge, where the slurry was directly pumped from the washing circuit to the sea or discharged into the deep ocean [2,7,59].

Since the 1980s, the trend adopted to discharge the BR was dry stacking. The residue is filtered with drum filters and plate and frame filter presses (with a solid content of 70-75 %) in order to minimize the potential for the leakage of caustic liquor to the surrounding environment and reduce the land area required. In addition, this method maximizes the recoveries of soda and alumina which can be reused in the Bayer process. Then, the alumina refinery utilized this method because environmental and safety hazards are reduced compare to lagooning. Moreover, the transport issue and cost are dramatically reduced and the dry stockpiling provides considerable economic benefits to the alumina refinery comparing with the wet [2,7,59,76,79].

The great volume of waste produced during the Bayer process and drastic scarcity of available storage areas have been the main drivers for the continuous research with the aim of reusing BR [7,80].

Its chemical composition encompassing iron, aluminum and titanium [12,13,19,65,71,81,82], but also scandium [83–85] and yttrium[86], turns BR into an interesting resource for base and critical metal recovery, while a large-scale and bulk utilization is rather conceivable using BR in construction materials, such as aggregates, cements, ceramics or inorganic polymers [87–89]. In addition, other possible BR applications can be: soil amelioration, landfill capping [80], treatment of acid mine drainage [90] and also road construction [91].

Since 1964 more than 700 patents have been presented and this also demonstrates the wide research to find a suitable method to reuse BR [80]. In Figure 7 the different areas of BR processing are shown [33, 52].

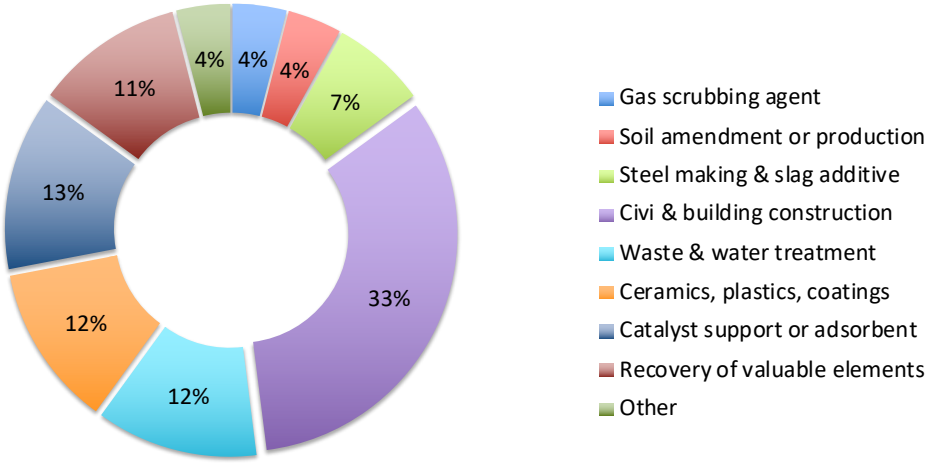

Figure 7. Patents distribution on BR processing (Klauber et al.)[11]

The high economic costing for energy requirements in drying BR, acid-consuming nature of BR due to high alkalinity, interfering elements and complex structure of minerals that inhibit the metal extraction process, and restrictions in physical and chemical parameters of extractive agents are some of the problems that the researches had to handle to utilize BR as a raw material [5,12,59,71,92]. However, Balomenos et al. reported very low exergy efficiency value 2.94 % of Bayer process indicating that the process is inefficient from the exergetic point of view mainly due to high exergy content of the unexploitable by-products [63]. As the authors suggest, the solution to improve the efficiency of the overall Bayer process, is to find possible ways for reusing BR and recovering metals from it [63,71,92].

2.3 Bauxite residue: from by-product to secondary raw material

The BR can be considered as a secondary raw material resource for the presence of valuable substances such us iron (Fe), titanium (Ti), aluminum (Al), and rare earth elements (REEs) [93–95], as it reported in Table 2, presented in paragraph **Errore. L'origine riferimento non è stata trovata.**.

In a multitude of scientific research papers, different processes have been extensively investigated to recover elements from BR (mainly hydrometallurgical or combined pyro-hydrometallurgical processes) instead of storing it [12,13,18,23,85,92,93,96–102]. None of them has reached an industrial scale due to the fact that BR utilization is either technically complicated or financially non-viable [93].

However, thanks to the demand for sustainable industrial processing and the depletion of available ores, technology development based on secondary raw materials as BR, with almost zero-waste production, was encouraged [98]. The main drivers for the continuous research founded on the BR metals extraction, were the recovery of REEs. In particular, the focus was addressed to scandium (Sc), because of high concentration (130 ppm in the Greek BR, on average) [98], which is much higher than in the Earth's crust (22 ppm) [103]. Consequently, Sc recovery from BR represents a high economic interest, since it has also been listed as a critical raw material by the European Commission due to its high economic importance and supply risk [104].

Although iron content in bauxite residue (20 – 45 wt. %) is not as high as in average iron ores (60 wt. %) used in the iron industry [94], also Fe recovery from BR has attracted major attention [4,12,14,15]. The main purpose of research community is to find an innovative, greener and economically viable routes to extract iron from BR and used it as feedstock in the iron industry [16].

2.3.1 Iron recovery studies

Three different approaches have been developed in literature to recover iron from BR: direct magnetic separation, pyrometallurgical processes and hydrometallurgical processes [12,92,105] (Figure 8)**Figure 1**. Each method will be explained in the following paragraphs.

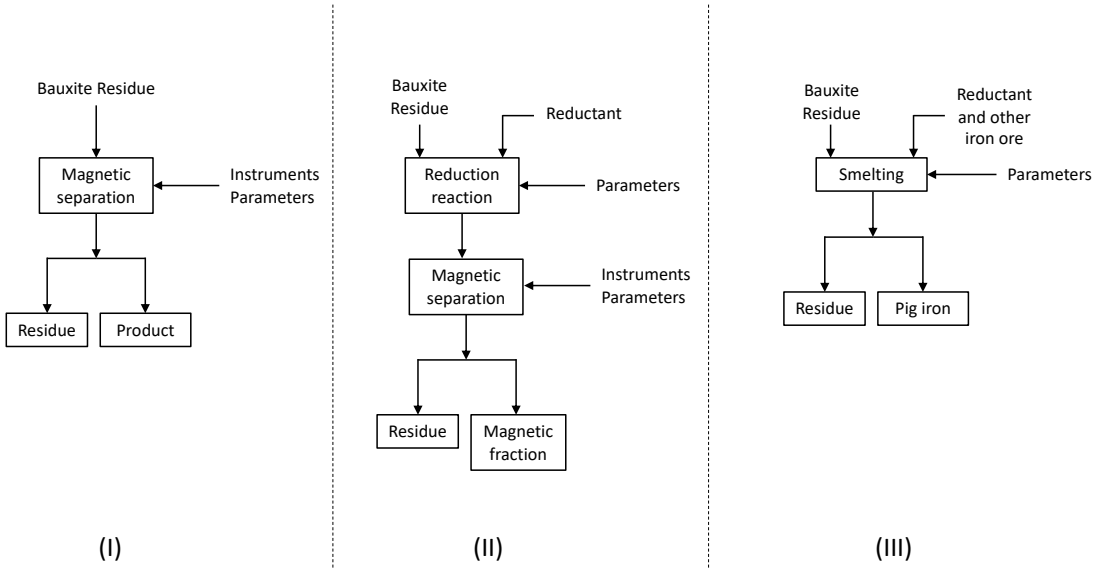

Figure 8. Simplified flowsheet illustrating iron recovery from BR by using different approaches. (I) direct magnetic separation; (II) pyrometallurgical recovery by reductive roasting and separation and (III) BR employed directly in iron ore smelting [12]

2.3.1.1 Direct magnetic separation

The technique presented in this section is the direct magnetic separation and in **Figure 8** (I) a simplified flowsheet of this method is presented. This approach is based on the interaction of material in presence of a magnetic field, due to its magnetic properties. Stickney et al. studied the direct application of high intensity magnetic separation process in Fe recovery from BR in a slurry form. Two products (magnetic and non-magnetic portions) were obtained, although the recovery of iron was low. A possible application of magnetic product can be as an ingredient for ironmaking or as a pigment for pottery making. The non-magnetic portion can be used in building materials or supplemented back into the Bayer process [106].

One of the most effective way to separate the fine magnetic particles in liquid suspensions is through the high gradient superconducting magnetic separation (HGSMS) system, as it generates stronger magnetic field and is generally inexpensive compared to the ordinary ferromagnetic-core electromagnets [107]. Li et al. developed a technique to separate the bauxite residue particles (< 100 μm) into high iron content and low iron content parts with the HGSMS system. The results of this study indicated that, after the separation process, high iron content part of BR could be the source for iron-making furnace whereas BR with low iron content could be reused in sintering process of alumina production. One of the few disadvantages of HGSMS iron recovery would be the inter-growth of Fe weak magnetic and non-metallic materials that would lead to the decrease of concentrate grade [107].

Peng and Huang investigated the Fe recovery with SLon® vertical ring and pulsating high gradient magnetic separators. Authors indicated that 53–58 % iron grade was achieved for this case study but a low overall recovery rate (28- 35 %) was reported [108].

Due to the lack of magnetic iron-bearing mineralogical phases, the direct magnetic separation approach is inefficient for Fe recovery from BR. Therefore, the Fe recovery increased when the magnetic separation was combined with a previous reductive roasting process (Figure 8 (II)). During the pyrometallurgical step, hematite and goethite are reduced into iron bearing mineralogical phases with high magnetic properties (as iron metal or magnetite). The cost of the combined route reductive roasting/magnetic separation is elevated compared to direct magnetic separation because of reductant and additives requirements as well as higher energy consumption; many attempts have been made to find an economically feasible technology for practical industrial applications [14,92,105].

2.3.1.2 Pyrometallurgical processes

Iron removal studies from bauxite residue are mainly based on pyrometallurgical processes. In particular, these works can be grouped in two methods for producing either high-grade magnetite (Fe_3O_4) or metallic Fe: the solid state reductive roasting followed by magnetic separation [18–21] (Figure 8 (II) and the reductive smelting processes by employing different furnaces (blast furnace, electric arc furnace (EAF) and other types) [12,15,22–25]((Figure 8 (III)).

Different reductants in various studies have been investigated, including carbon powder [109–111], graphite [112], soft coal [21], coal char [113], metallurgical coke [18,19] and coke [114].

Liu and Mei[115] analyzed the influence of the reactivity and ash content of coal used, on the extent and rate of metal reduction. The ideal quality of the coal used should have the following characteristics: low ash content, high reactivity, large ratio of (F_C + V_m):(A + W) (where F_C is fixed carbon content, V_m is volatile content, A is the ash content, W is the other incombustible content) and high ash composition ratio (SiO_2 + TFe):(Al_2O_3 + other) and capable of forming moderate porosity.

Moreover, the addition of additives to BR was deeply investigated. Magnesium, calcium and/or sodium salts have been proved efficient in improving the reactivity of iron oxide during the reductive roasting of BR [111]. The presence of additives decreases the apparent activation energy of iron oxides reduction and increases thus the reduction rate [116]. Rao et al. confirmed that the addition of sodium sulphate and sodium carbonate in the reduction roasting process have improved the metallization degree of iron and the extent of magnetic concentrate recovery. At optimum

conditions of experiments, iron recovery of 94.95 % and a magnetic concentrate containing 90.12 % Fe were obtained from a BR containing 48.23 % iron in the presence of 6 % Na_2SO_4 and 6 % Na_2CO_3 [117].

Several parameters to optimize the roasting-magnetic process have been studied extensively; among those were the carbon source, carbon-to-bauxite residue ratio, roasting temperature, reduction time and magnetic conditions [92]. Liu et al.[110] focused on carbon reductants influencing direct reduction roasting of bauxite residue. The optimum conditions were obtained when samples with bauxite residue, carbon and additives were mixed with the following ratio Carbon:Additives:BR = 18:6:100. The temperature was set at 1300°C and the experimental time was 110 min. After roasting, the product was separated with a magnetic separator. The total content of iron in materials was found to be 88.77 wt.%, with a metallization of 97.69 % and a recovery of 81.40 % [110]. Zhu et al. added 1 % binder and 8 % sodium carbonate to the mixture of bauxite residue and soft coal prior to direct reduction. A recovery of 95.7 % of Fe was achieved after grinding, sintering and magnetic separation [21].

Other studies are based on the simultaneous metal recovery from a polymetallic matrix as BR, by adding additives. Liu et at. used a soda-lime reductive roasting process prior to leaching and magnetic separation of the fine BR (< 75 μm). The additives promoted the formation of sodium aluminosilicate during the roasting process, which were leached and subsequently achieving 75.7 % Al and 80.7 % Na recoveries. Magnetic separation was applied on the leaching residue and 51.2 % of Fe was recovered in a magnetic concentrate [113]. Li et al. have conducted thermogravimetric analysis to further investigate the simultaneous reduction process of red mud oxides using reductants. The experiments involved reduction sintering under the optimized sintering conditions, (i.e. Reduction temperature range of 800-1075 °C in a controlled atmosphere) and a magnetic field intensity between 48 and 240 kA/m. The reduction to ferrite can be achieved with 61.78 % Fe in magnetite concentrate [109].

In addition to using of blast/electric/low shaft furnace, the microwave radiation has been used as a source of heat in pyrometallurgical applications with the presence of carbon used us a reducing agent to recovery the iron. Worth mentioning in the study of Samouhos et al.[26], where the authors used a process involving microwaves for the roasting step. This research work included the reduction of BR using lignite (30.15 wt. % C_{Fix}), followed by wet magnetic separation (feed: 10 wt. % solids, intensity: 0.3 A) to produce a raw material which was suitable for sponge or cast-iron production. Both the reductive agent content and microwave heating time controlled the reduction degree of iron. Iron reduction pathway was found to follow the sequence $Fe_2O_3 \rightarrow Fe_3O_4 \rightarrow FeO \rightarrow Fe$.

Under optimum conditions (Lignite-to-RM: 0.3, 800 W of power supply), a magnetic concentrate of iron (35.2 %) with a metallization of 69.3 % was obtained and a comparison was made between the conventional and the microwave reductive roasting techniques. They showed that the latter decreases the duration of roasting by approximately 40 %, whereas the magnetic concentrate presented higher metallization degree [26].

In addition to the reductive roasting, the reductive smelting is another pyrometallurgical approach that has been studied for iron recovery from BR.

Guo et al.[118] obtained iron nuggets containing 96.52 wt. % Fe by directly reducing the carbon-bearing pellets of BR at 1400 °C for 30 min. The nuggets composed mainly of 96.52 wt. % Fe, 3.09 wt. % C, and traces of 0.051 wt. % Si, 0.013 wt. % Mn, 0.076 wt. % P and 0.091 wt. % S. However, iron losses were observed in the slag in the forms of reduced metallic Fe and Fayalite (Fe_2SiO_4). Raspopov et al.[111] reported the results of experiments on the use of Russian BR in traditional pyrometallurgical processes. Cast iron and slag phases generated after reduction and smelting of BR (1200–1500 °C) with excess carbon, could easily be separated whereas the C content in the cast iron ranged from 2.0-2.3 % [111]. Jayasankar et al. [112] reduced BR through the use of thermal plasma technology (arc thermal plasma reactor) to produce pig iron. BR was mixed with fluxes (10 % dolomite and lime) as well as graphite as reductant and the mixture was smelted for 25 min at 1823-1923 K. These parameters allowed an optimal recovery of Fe around 71 % [112].

Within the ENEXAL project, Balomenos et al [71] extensively studied reductive smelting of BR and coke as reducing agent in an electric arc furnace (EAF) via preliminary thermodynamic modelling, laboratory experiments that translated into a full-scale pilot plant operation. This “zero-waste” process is developed for the direct transformation of BR into valuable products: pig iron with an iron content of 95.47 wt.% and mineral wool fibers. This “zero waste” process has the potential to exploit BR completely, transforming the non-iron bearing slag by-product to a high value-added thermal insulation material thus offsetting the high operating cost of the pyrometallurgical treatment.

Although reductive roasting and smelting process are the most promising to extract iron from BR, some drawbacks related for example to capital and operational expenditures as well as to several environmental issues [23] have led the research to find an alternative method to recover iron from alumina production waste.

2.3.1.3 Hydrometallurgical process

Hydrometallurgical processes have been also developed for extracting Fe from red mud. Debadatta and Pramanik have investigated the dissolution of iron from red mud using 8 N sulfuric acid achieving a low recovery of iron of 47 % [119]. Oxalic acid can also be applied as a leachate to extract Fe from red mud. The iron content of red mud was solubilized as Fe (III) oxalate and the extraction rate of iron was about 96 % after leaching process, using 1 mol/L oxalic acid at 75 °C for 2 hours. Subsequently, the solution was irradiated with UV light to reduce Fe (III) to Fe (II) and thus to accelerate its precipitation in the form of Fe (II) oxalate [120].

In the last few years, bioleaching processes have been investigated extensively as 'clean' and economically viable alternatives to traditional metal recovery techniques [92]. As written in the article of Eisele and Gabby, these processes can be efficiently applied for iron recovery from refractory ores that cannot be beneficiated by the conventional ore dressing processes [121]. Bioleaching processes have been studied and applied in various fields, such as the removal of iron from kaolin [122] and silica [123]. The high pH value of bauxite residue is not favorable field for bacterial growth therefore, no such efforts have been made for the removal of iron from bauxite residue [124–126]. Laguna et al.[127] have managed to investigate the dissolution of iron at pH >7 using mixed bacterial cultures. This study offers the possibility of using a multi-step procedure to recover iron, involving bioleaching process following by acid leaching and reduction of pH with other acidic wastes. There is potential for bioleaching technology to be a convenient and efficient way of recovery of Fe from red mud in the future [12,92,105].

3. Microwave energy

Microwave energy is a non-ionizing radiation seated between infrared radiation and radio waves in the region of the electromagnetic spectrum. More specifically, the microwave frequencies are located in the range of 0.3 to 300 GHz and a free space wavelengths of 1 m to 1 mm [31,35] (**Figure 9**).

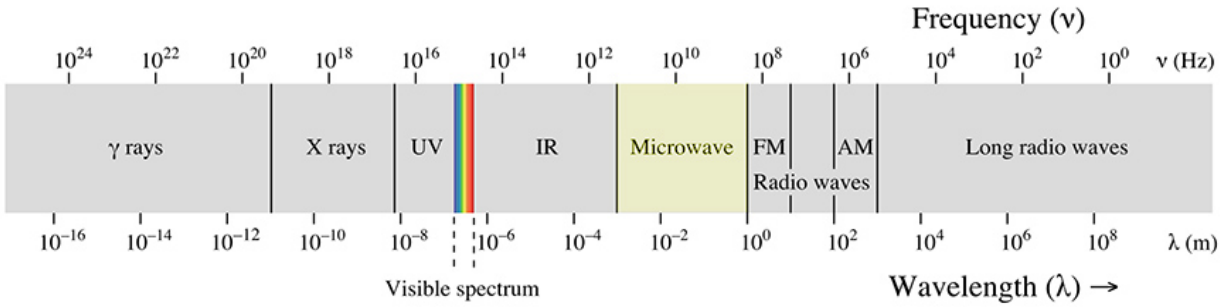

Figure 9. Microwave energy in the electromagnetic spectrum

Microwave frequencies include three bands: the ultra-high frequency UHF: 300 MHz to 3 GHz., the superhigh frequency SHF: 3 GHz to 30 GHz. and the extremely high frequency EHF: 30 GHz to 300 GHz [34] and it is commonly used in telecommunication. For this reason, Federal Communications Commission (FCC) reserved for the industrial, research, medical and domestic equipment two microwave frequencies, 0.915 and 2.45 GHz [128].

When the material is exposed to the microwave field, it could be caused molecular motion by migration of ionic species and/or rotation of dipolar species. The consequence of these interactions could be a rising of temperature inside the material [34]. In particular, in the case of polar molecules

(water and other polar fluids) the electric field component of the microwaves causes both permanent and induced dipoles to rotate as they try to align themselves with the field. This molecular movement generates friction among the rotating molecules and energy dissipates as heat. In the case of dielectric solid materials with charged particles which are free to move in a delimited region of the material, such as π-electrons, a current traveling in phase with the electromagnetic field is induced. Due to the Maxwell–Wagner effect (Interfacial or Maxwell-Wagner Polarization) energy dissipates in the form of heat since the electrons cannot couple to the changes of phase of the electric field [31,129,130].

Therefore, the heating process depends on the interaction of both the electric and the magnetic fields of the microwave radiation with both chemical and physical properties of the material [35].

3.1 Material interaction to microwave

The response of materials to the exposure to the microwave field depends on their dielectric properties. Based on these properties, materials can be classified into: absorbers (materials that absorb microwave energy and easily heat), insulators (which are transparent to microwave energy) and conductors (which reflect energy) [31–33], as it is possible to observe in Figure 10.

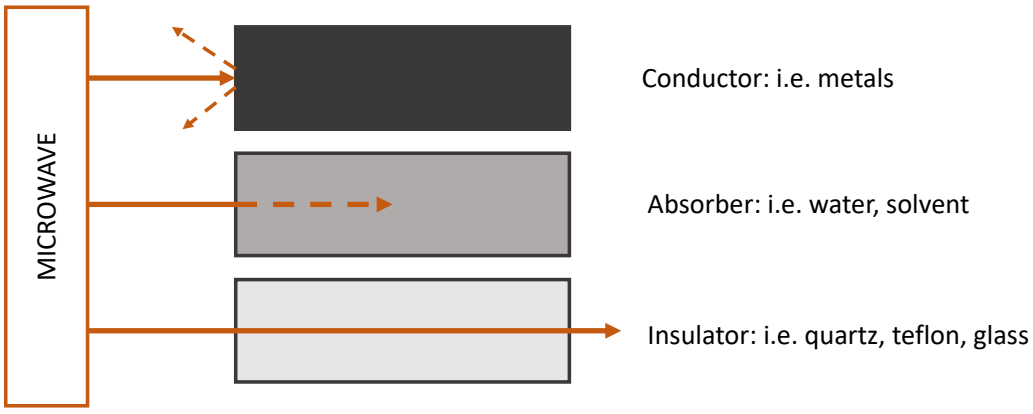

Figure 10. Classification of material based on dielectric properties

The quantitative measure of the effective heating of the material in a microwave field is the dielectric loss tangent (tanδ) (8)

$$\tan \delta = \frac{\varepsilon''}{\varepsilon'} \quad (8)$$

Where ε‘ is the dielectric constant (real permittivity) and ε ’’ is dielectric loss factor (or imaginary permittivity) [129].

These two components are also expressed in terms of complex dielectric constant (ε*) (Equation(9)) [31,128].

$$\varepsilon^* = \varepsilon' - i\varepsilon'' \quad (9)$$

The dielectric constant ε’ determines the quantity of incident energy absorbed. The dielectric loss factor ε’’ measures the quantity of electric energy dissipated in form of heat.

Therefore, the two dielectric components (ε’ and ε’’) concur to the distribution of the electric field within the material. The power absorbed by a sample per unit volume at a specific area in the material $P_v(z)$ is given in the Equation (10) [128,131,132].

$$P_v(z) = 2\pi f \varepsilon_0 \varepsilon_r'' |E(z)|^2 \quad (10)$$

where f is the frequency of microwaves, ε_0 is the permittivity of free space, ε_r" is the relative dielectric loss, which accounts for the conversion of microwave (MW) energy into heat. E (z) is the root mean square of the electric field strength. As it is possible to understand from the equation above, $P_v(z)$ directly depends on the dielectric properties of the sample and the electric field strength. Because of the absorbed energy from the given material, sample temperature increased, and this behavior is explained by the Equation(11):

$$P_v = \rho C_p \frac{\Delta T}{\Delta t} \quad (11)$$

where ρ is the density of the material, C_p is the specific heat of the material, ΔT is the temperature variation and Δt is the time variation [133,134].

Materials with a high value of dielectric loss factor (ε'') and a moderate value of ε' are able to convert microwave energy into thermal one. These are classified as absorber. On the other hand, materials which are not possess a sufficiently high loss factor to allow dielectric heating are transparent to microwaves and they are classified as insulators. Insulators are often used in microwave ovens to support the material to be heated [31,129,135].

To understand completely the behavior of materials in presence of microwave field, another parameter that needs to be analysed is the penetration depth. The microwave penetration depth (D_p) is defined as the distance at which microwave power is reduced to 1/e (e = 2.718) from the strength at the point of entry [136]. D_p is given in Equation (12) [35]:

$$D_p = \frac{\lambda_0}{2\pi(2\varepsilon_r')^{\frac{1}{2}}}\left\{\left[1+\left(\frac{\varepsilon_r''}{\varepsilon_r'}\right)^2\right]^{\frac{1}{2}}-1\right\}^{-\frac{1}{2}} \quad (12)$$

where λ_0 is the wavelength of the incident wave, ε_r' is the relative dielectric constant and ε_r'' is the relative dielectric loss. As it is possible to observe from the Equation (12) the penetration depth is inversely proportional to the frequency of the microwave radiation.

Materials with a very high conductivity, such as metals, have high loss factors, but the electric field penetration depth is very small (<< 1 mm). For this reason, most of the microwave energy is reflected and they are classified as conductors [35]. Thank to this characteristic, the conductors are used in the construction of microwave ovens, as conduits for the wavelength [31,34].

However, during the microwave process numerous factors influence the interaction between material and microwave energy. Non-homogeneous material (in terms of dielectric properties) cannot heat uniformly. This phenomenon is often referred to as thermal runaway and it could be minimized by keeping the sample in mixing or fluidized conditions [135]. Moreover, above a certain critical temperature (T_c), insulator materials become responsive to microwave heating [34]. The size of the material influences microwave heating. Metal in fine particle size can be heated by microwaves through a micro-arcing process [34,35,128,137]. In addition, the presence of a heat facilitator (such as magnetite, silicon carbide or carbon) in the sample permitted at low lossy or insulator materials to be heated by employing a microwave source. The facilitator transforms

microwave energy in thermal energy and subsequently, heats the insulator or low lossy material [34].

3.2 Microwave furnace

Microwave furnace is composed of three major parts: the microwave source, the transmission line and the applicator. Microwave energy is generated by the source, transmitted by the transmission line and in the applicator, energy is either absorbed or reflected by the material[128]. In Figure 11 the scheme of a microwave furnace is presented.

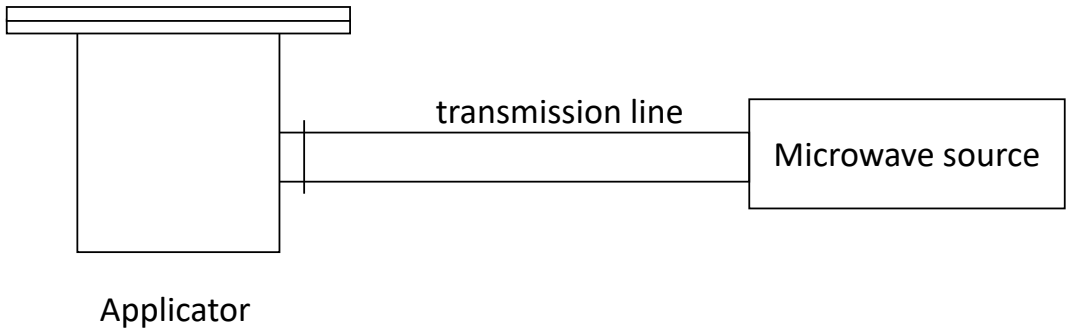

Figure 11. Schematic diagram of microwave furnace

3.2.1 Microwave source

Microwave is an electromagnetic radiation and its generation results by the acceleration charge. Usually, microwave sources are vacuum tubes to achieve the power and frequencies required for microwave heating. The tubes that are mostly used are magnetrons and traveling wave tubes (TWTs)[128,138,139].

3.2.1.1 Magnetrons

Magnetrons are efficient and reliable MW sources, and they are employed in home microwave ovens. Since magnetrons are mass produced, they are the lowest cost source available[128,140].

Magnetron are composed by vacuum tubes where a cathode and an anode are placed (Figure 12). The anode is at a high potential compared to the cathode. The potential difference produces a strong electric field, and the cathode is heated to remove the loosely bound valence electrons. Once the electrons are removed from the cathode, they are accelerated toward the anode by the electric field as presented in Figure 12 (a) [128]. A magnet is posed externally to the tube to generate a magnetic field orthogonal to the electric field. The combination of these two forces allows electrons to travel in a spiral direction, and this creates a swirling cloud of electrons.

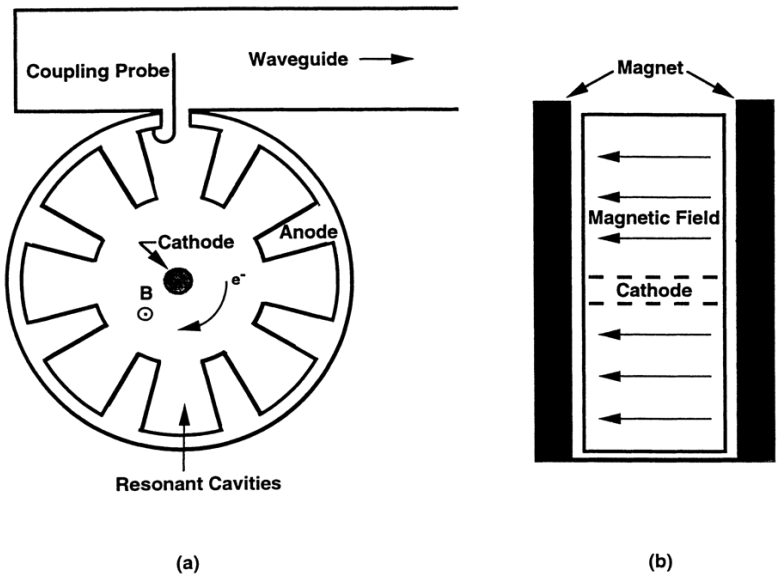

Figure 12. Magnetron schematic diagram **(a)** top view **(b)** side view[128]

As electrons pass the resonant cavities, the cavities set up oscillations in the electron cloud, and the frequency of the oscillations depends on the size of the cavities. Electromagnetic energy is coupled from one of the resonant cavities to the transmission lines through a coaxial line or waveguide launcher [128]. In addition, the average power output of magnetron tubes can be controlled through different methods. One of them is adjusting the period of operation as it happens in the home microwave ovens. The magnetron operates at full power and during a specified time, the current is turned on and off for segments of the operation period. The consequence is that the average power is reduced [141]. This on/off type of control is often referred to as duty cycle control [128].

The other method is to adjust the cathode current or magnetic field strength to control the average power output of magnetron tubes. The output power of the magnetron tube can be varied by changing the current amplitude of the cathode or the intensity of the magnetic field, when continuous microwave power is required. This allows variable control of the microwave power within the range of the source [128,135,139].

3.2.1.2 Traveling wave tubes

The traveling wave tubes (TWTs) are used as microwave source for variable microwaves frequencies. Comparing with magnetrons, where the tube is used both to create the frequency of the oscillations and to amplify the signal, the TWT amplifies a large variation of frequencies (bandwidth) within the same tube. This is because there are no resonant structures in TWT.

The TWT consists of two main components: the electron gun and the helical transmission line as it is presented in Figure 13

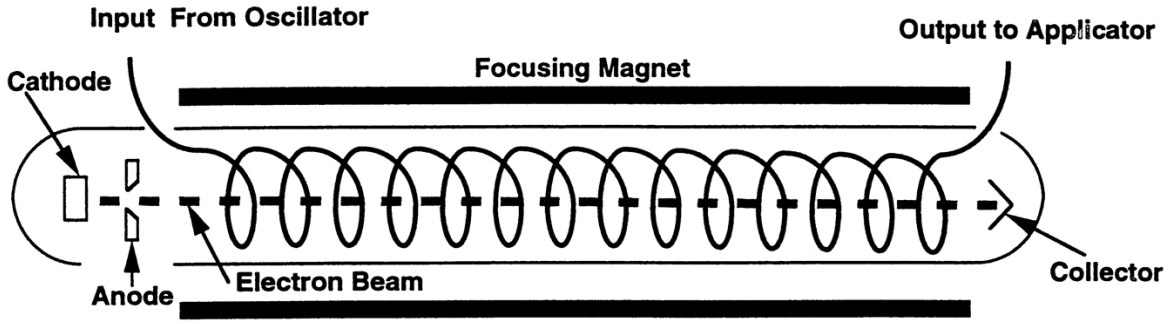

Figure 13. Schematic diagram of traveling wave tubes (TWTs)

The cathode emits a stream of electrons that is accelerated toward the anode, and the electron stream is focused by an external magnetic field. The purpose of the helical transmission line is to decrease the phase velocity of the microwave to the velocity of the electron beam. When the microwave signal propagates along the helix, the axial component of the electromagnetic field interacts with the electron beam. The amplification of the signal occurs when the electron beam is faster than the phase of the helix. In this case, the signal is amplified since energy is transferred from the electron beam to the microwave field[128,135,138].

3.2.2 Transmission lines

The transmission lines are the MW oven section where energy passes from the source to the applicator. The kind of the transmission lines utilized depends on the amount of the power system. In the low power system, the transmission line employed are coaxial cables, while at high frequencies and output power are used the waveguides. Waveguides are often employed in microwave heating systems and are hollow tubes in which the electromagnetic waves propagate. The most commonly used have rectangular shape [128]. The waves propagated through a waveguide into two broad modes: transverse electric (TE) and transverse magnetic (TM), depending on which field (electric or magnetic) is perpendicular (transverse) to the direction of wave travel. Every mathematical solution of the electromagnetic wave in a rectangular waveguide can be decomposed into a linear combination of the TE and TM modes [135,142].

Furthermore, other components are used into the transmission line to protect the equipment and couple microwaves with the material in the applicator. The circulator protects the microwave equipment by significant amount of power reflected back to the microwave source from the sample. Directional couplers are present to measure the ability of materials to absorb

electromagnetic energy by detecting the magnitude of the forward and reflected power from the sample through a power meter. Finally, tuners are employed to maximize the power absorbed by the load through impedance matching [31,128,142].

3.2.3 Applicator

The applicator, as well known as cavity, is the place in the microwave oven, where energy is transferred to the material. The design of the applicator is a critical issue, because it could interfere with the distribution of the electric fields within the applicator [34]. Common microwave applicators for processing materials include single mode cavities and multi-mode cavities. In particular, single mode, multi-mode, and variable frequency multi-mode processing systems are employed in the microwave processing research [128]. A single mode applicator has a not uniform, but predictable, electromagnetic field distribution. The design of single mode applicators is based on the Maxwell equations to support one resonant mode. The possibility to know the location of high and low field strengths offers the possibility to place the sample in the area of optimum coupling. In addition, through a single mode cavity it is possible to follow the dielectric properties of the sample. Thanks to these advantages, this cavity is used for laboratory-scale experiments to study the interaction between material and microwave. However, single mode applicators could not scale-up to industrial application due to geometric limitation and a non-uniform field [128,135].

A multi-mode applicator is a resonant cavity able to perform a large number of different spatial electromagnetic field configurations (modes) [143]. This, together with the multiple reflections from the cavity wall, implies that in the multi-mode applicator the global electromagnetic field configuration results by the addition of different electromagnetic waves propagating in different directions [128,143]. The presence of different modes results in multiple hot spots within the microwave cavity and decrease the field uniformity. Several techniques are used to reduce the presence of different hot spots, for example increasing the dimensions of cavity, operating at higher frequency or utilizing mode stirrers [128,135]. Multi-mode applicators are the most common processing systems used in industrial applications since they are more versatile than single mode applicators for batch operations [128,135,143].

3.3 Microwave process

In the last two decades, microwaves have been examined as an emerging technology of mineral processing. Compared to conventional heat treatment methods, microwave has the advantage to significantly faster reaction times and potentially lower energy [144]. This depends on the interaction between the material and the electromagnetic field generated during the process, as it

has been explained in the previous paragraph 3.1. The microwave energy instantaneously generates heat inside the absorber material, rather than heating the outside surface and slowly conducting it inside [35]. Moreover, microwave heating is a cleaner [135] and more manageable method (quick start-up and stopping) [129] and it offers promising opportunities in terms of energy reducing consumption for intensive firing processes [145]. Thank to these advantages, microwave has found applications for the processing of materials [32,35,36,144,146] and metal recovery processes such as heating [34,35,137,144,147], drying [144,148–150], grinding [151–155], hydrometallurgical process [34,144,156], pyrometallurgical process [30,32,35,36,129,146,157–160], pretreatment of refractory gold concentrate or ore [34,144,153,156,161], spent carbon regeneration [34,144,162] and waste management [26,30,34,35,144].

The main drawback of the use of microwave in the industries could be related to the capital cost comparing with a conventional treatment. Usually, microwave energy is more expensive than electrical energy, mainly due to the low conversion efficiency from electrical one (50 % for 2450 MHz and 85 % for 915 MHz). However, efficiency of microwave heating is often much higher than conventional heating and overcomes the cost of energy [34,144].

Another problem for the microwave application in the mineral processing industries is related to the amount of ore treated per day by the manufactory, as Haque concluded in his review. Usually, these industries process a large tonnage of ore or concentrate per day (several thousand to over 30,000 tons). To treat such a large tonnage of ore or concentrate, several MW generators would have to be operated in parallel, since the highest microwave power generator available is 75 kW at 915 MHz. Even though the processing costs are higher comparing to the conventional process, the high value product recovery and the low tonnage material treatment required, the use of microwave energy could offer advantages over the conventional one [34,163].

Nowadays, mineral industries are facing increasing global competition, more stringent environmental regulations, higher overhead costs and profit margins reduction. The processing industries are addressing these problems in various ways, principally focusing on peak product yield as well as performance and productivity efficiency. In this framework, microwave energy has the potential to play an important and possibly crucial role in future mineral treatment processes. However, challenges remain to be overcome through a fundamental understanding of microwave interaction with minerals and advanced engineering, especially in designing efficient applicators, processes and process control devices [34,143,144,156].

4. Magnetic separation process

Magnetic separation is a method to selectively separate and concentrate magnetic materials based on the differences in magnetic properties between particles [142–144]. Through this method it is possible to treat a wide range of materials with different particle size (from colloidal to large sizes). In addition, it can be considered an environmentally friendly technique and it can operate in wet and dry modes.

4.1 Magnetic separation theory

Magnetic separation is based on the magnetic force $\overrightarrow{F_m}$ generated when a particle is immersed in a non-uniform magnetic field (Equation(13))

$$\overrightarrow{F_m} = \frac{\kappa}{\mu_0} V B \vec{\nabla} B \tag{13}$$

where κ is the volume magnetic susceptibility of the particle and reflects how readily a material is magnetized when subjected to an applied magnetic field [167]. μ_0 is the magnetic permeability of vacuum, V is the volume of the particle, B and $\vec{\nabla} B$ are the external magnetic force and its gradient, respectively. Therefore, $\overrightarrow{F_m}$ is directly proportional to the external magnetic field and the field gradient as it is possible to observe from the Equation(13). In addition, the magnetic force has the gradient direction, indeed when $\vec{\nabla} B = 0$ (homogeneous magnetic field), the magnetic force on the particle is equal to zero [165].

The separation of one material from another depends on the particle response to the magnetic force, but also to other competing external forces, namely gravitational, inertial, hydrodynamic and centrifugal forces as it is showed in Figure 14 [168].

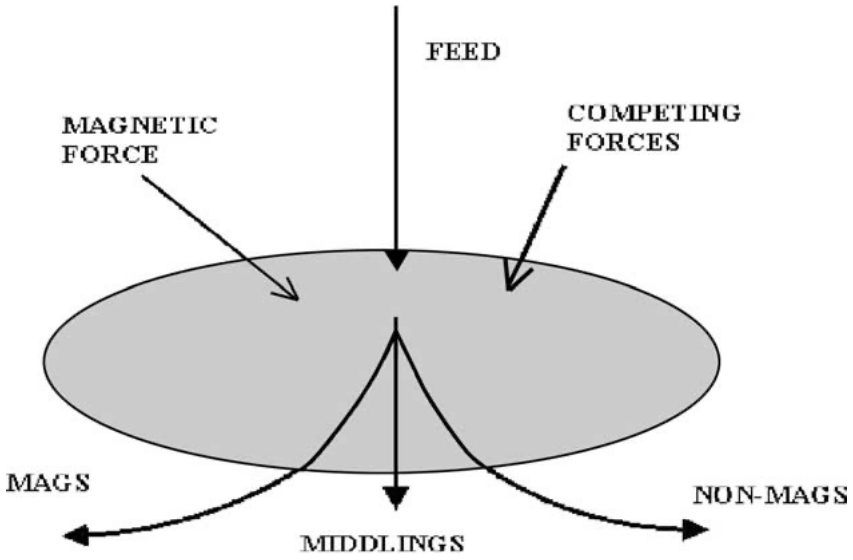

Figure 14. Schematic diagram of magnetic separation process [165]

Magnetic particles are separated from "non-magnetic" ones if the magnetic force of the particle (F_m^{mag}) is stronger compare with the sum of competing force ($\sum F_c^{mag}$) (Equation(14)).

On the other hand, if the sample has a weak magnetic force ($F_m^{non-mag}$) comparing to the sum of competing force ($\sum F_c^{non-mag}$), the material is non-magnetic (Equation (15)).

$$F_m^{mag} > \sum F_c^{mag} \tag{14}$$

$$F_m^{non-mag} < \sum F_c^{non-mag} \tag{15}$$

To achieve a high recovery of magnetic particles in a mixture, the magnetic force should be greater than the sum of the competing forces. In this way, the magnetic separator can split into two or more components depending on different magnetization of the particles. However, in any real separation, both magnetic and non-magnetic particles can be found in the magnetic fraction, non-magnetic fraction and the middle fractions. For this reason, the efficiency of the separation is expressed by the recovery of magnetic components and the grade of magnetic product [168].

4.2 Materials magnetic properties

The magnetic properties of materials lie on the orbital and spin motions of electrons. According to the magnetic response, materials can be classified into five groups: diamagnetic, paramagnetic, ferromagnetic, antiferromagnetic and ferrimagnetic. Usually, ferrimagnetic and antiferromagnetic are considered a sub-classification of ferromagnetic materials [168,169].

4.2.1 Diamagnetic

Diamagnetism occurs when the electrons orbital rotation is modified by an applied magnetic field. The resulting magnetic moment is directed opposite to the applied field, according to Lenz's law and the material is characterized by a weak magnetism [168,169]. In diamagnets, the magnetic susceptibility has a value around 10^{-5} and, with few exceptions, is independent of temperature. Many metals and most non-metals are diamagnetic. The substances which contain electrons that constitute a closed shell have no permanent magnetic moment as many inorganic and almost all organic molecules. In the case of metals which are associated with small negative susceptibility, the diamagnetism is hidden by a much stronger paramagnetic/ferromagnetic effect [168,170].

4.2.2 Paramagnetic

Paramagnetism derives from atoms, molecules, or ions which have a permanent magnetic moment associated with unpaired electron spins [170]. When an external magnetic field is applied to a paramagnetic material the magnetization is given by Equation(16)

$$M \cong \frac{c\,\mu_0 n\,\mu_M^2\,H}{kT} \tag{16}$$

where c is a constant, n is the number of magnetic dipoles, μ_M^2 is the magnetic moment, μ_0 is the magnetic permeability of vacuum, k is the Boltzmann constant and T is the absolute temperature.

The magnetic susceptibility of paramagnetic materials is defined by Equation (17)

$$\kappa = \frac{c\,\mu_0 n\,\mu_M^2}{kT} = \frac{C}{T} \tag{17}$$

where C is the Curie constant and the value are between 10^{-3} to 10^{-5}. Analyzing the Equation (17), it is possible to observe that magnetic susceptibility is inversely proportional to temperature [168].

4.2.3 Ferromagnetic

In a ferromagnetic material, the permanent magnetic moments are aligned parallel because of a strong positive interaction among neighboring atoms or ions. The strong internal field is called molecular field and depends on exchange interactions [168,169]. Ferromagnetism is normally seen in materials that have partially filled outer valence shells. The materials exhibit parallel alignment of moments, resulting in large net magnetization even in the absence of a magnetic field. However, these materials exhibit no magnetization or magnetization much smaller than saturation magnetization. This is due to the fact that the dipoles which constituted the ferromagnetic body, are line up in sections or domains. When they are not aligned in the same direction, it means that the overall magnetic moment throughout the material is zero [168,171]. Moreover, temperature affects the value of saturation magnetization. At temperature of 0 K, it is possible to observe a maximum value, while it is zero at the Curie temperature T_c. Above T_c the behavior of the ferromagnetic material become similar to a paramagnetic one, as it is shown in Figure 15.

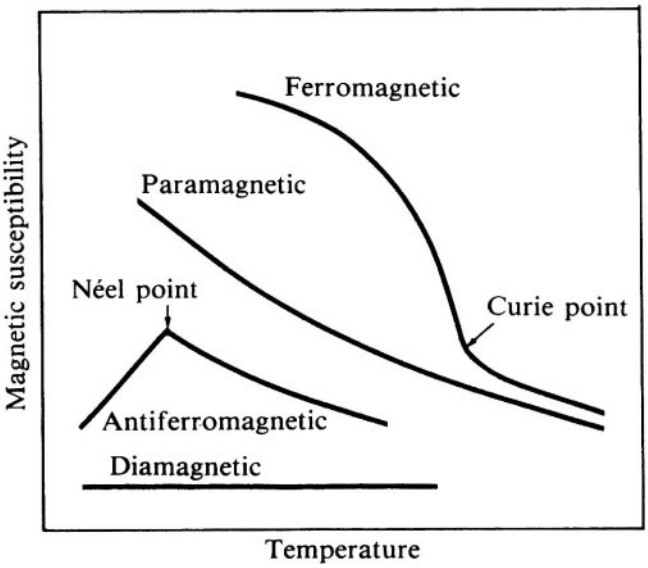

Figure 15. The temperature influence on the magnetic susceptibility [168]

For the ferromagnetic material the susceptibility is given by Equation (18)

$$\kappa = \frac{C}{T - T_c} \tag{18}$$

In order to induce permanent magnetism, a ferromagnetic compound should be placed within a strong magnetic field and the domains line up parallel to generate one strong magnetic moment. In some materials, the domains remain in this position even when the external magnetic field is removed. The ferromagnetic are thus characterized by hysteresis [168,171].

Ferromagnetism occurs in nine elements: three transition metals, iron, cobalt and nickel, and six rare earth metals, gadolinium, terbium, dysprosium, holmium, erbium and thulium. Most alloys consisting of the three transition metals are ferromagnetic, and so there are many of their alloys with non-magnetic elements. Manganese alloys are considered ferromagnetic, even though pure manganese is not ferromagnetic [168].

4.2.4 Antiferromagnetism

In the antiferromagnetic material, the permanent magnetic moments are aligned in antiparallel as a result of a strong negative interaction[169]. The interaction among neighboring atoms or ions is zero. The magnetic susceptibility is calculated by Equation (19)

$$\kappa = \frac{C}{T + T_N} \tag{19}$$

where T_N is Néel temperature. Below this temperature (T_N), the κ generally decreases with decreasing temperature, as it is shown in Figure 15 [168]. Transition metal oxides as manganese oxide (MnO), cobalt oxide (CoO) and nickel oxide (NiO) are classified antiferromagnetic. Hematite is the only mineral which has antiferromagnetic properties [168,169].

4.2.5 Ferrimagnetism

Ferrimagnet materials have magnetic properties similar to ferromagnets, the differences lie in the source of the net magnetic moments. In the ferrimagnetic material, the permanent magnetic moments are aligned in antiparallel, as in antiferromagnetism. However, in ferrimagnetic materials, the opposing moments are not equal and the net magnetic moment is different to zero [168]. Ferrites are classified as ferrimagnetic materials, but also in two of iron oxides, magnetite (Fe_3O_4) and maghemite (γ-Fe_2O_3) [168,169].

4.3 Magnetic separators

In literature various classification schemes of magnetic separation processes are presented. However, the most practical and logical way to categorize them is based on the medium carrying the sample. In this manner, the magnetic separator can be divided in two classes: dry or wet. At the same time, both of these categories can be classified depending on the magnetic field generated (a low-intensity or high-intensity magnetic field) [165,168]. Although this scheme is maneuverable, it does not consider an important parameter in magnetic separation: the gradient of the magnetic field. It can be, however, safely assumed that low-intensity separators usually generate a low magnetic field gradient while high-intensity separators can be, in general, classified as high-gradient

machines [168]. Nevertheless, there are some exceptions. The choice of the kind of separator typology is based on numerous variables, but especially on particle size distribution, distribution of magnetic properties of the particles to be separated, and by the required throughput of the machine [165,168].

4.3.1 Dry low-intensity magnetic separators

The dry low-intensity magnetic separators are employed to remove iron and strongly magnetic impurities. To accomplish the separation different devices are used, like suspended magnets, magnetic pulleys and plate and grate magnets. Moreover, through dry low-intensity magnetic separators, it is possible to concentrate a strongly magnetic valuable component. Magnetic drums are used mainly for this application [165,168].

4.3.2 Wet low-intensity magnetic separators

The main device used as wet low-intensity magnetic separators (LIMS) is drum separators and it is employed mainly for the recovery of heavy medium, such as magnetite or ferrosilicon used in dense medium separation. Another application is the concentration of strongly magnetic ores, such as magnetite. The availability of rare-earth permanent magnets extends the applicability of drum magnetic separators to medium or even weakly magnetic materials [165].

In the LIMS, the permanent magnet drum separators have two basic configurations, namely radial and axial configurations. In the first, the polarity of permanent magnets alternates across the drum width, while in an axial arrangement, the poles alternate along the circumference. Radial configuration is employed when the recovery of the strongly magnetic materials is important. The axial configuration is preferred when the quality of the magnetic product is of significance [165]. The tumbling motion of particles over the rows of the magnet facilitates the release of non-magnetic particles and thus improves the grade of the magnetic concentrate [168].

4.3.3 Dry high-intensity magnetic separator

Dry high-intensity magnetic separation has been used to remove weakly magnetic material from the material stream. There are several separators which come under high-intensity dry category and these are: cross belt magnetic separator (CBMS), permanent roll magnetic separator, induced roll magnetic separator (IRMS), lift roll magnetic separator, isodynamic separator, open gradient magnetic separator (OGMS), high gradient magnetic separators (HGMS), vibrating high gradient magnetic separator/filter, superconducting high gradient magnetic separator [165,172].

The advent of rare-earth permanent magnetic materials was crucial in this sense. Those devices allowed an implementation of the separation results due to the possibility to design rolls for

treatment of materials with different size ranges and magnetic susceptibility distributions [168]. A drawback of dry high-intensity magnetic separator is the particle size. These separators frequently yield an excellent separation on material coarser than 75 μm.

4.3.4 Wet high-intensity magnetic separator

The wet high-intensity magnetic separator generated sufficiently high gradient force to extend the process separation to fine weakly magnetic minerals. Although numerous cyclic and continuous wet high-intensity high-gradient magnetic separators (WHIMS or HGMS) were designed and built, only a few met the requirements of the mining industry. Successful application of WHIMS in mining industries are: kaolin purification, iron-ore and beach sand beneficiation [165].

5. Greek bauxite residue

5.1 From bauxite to bauxite residue

The largest deposits of bauxite, in Greece, is present in the area of Parnassus-Ghiona (Ghiona-Helicon, Oeta, Parnassus). It can be classified as karst bauxite because it is hosted within carbonate rocks and situated between limestone sequences [52,173]. The mineralogical composition of this bauxite shows that the main aluminum-bearing minerals present are boehmite and diaspore, followed by kaolinite, hematite, goethite.

Due to the high amount of bauxite, Greece is also a significant producer of aluminum [72]. Aluminum of Greece (Metallurgy Business Unit, Mytilineos S.A.; hereafter denoted as AoG) is the main Greek alumina company, which produces annually 850,000 tons of alumina, 175,000 tons of aluminum and 750,000 tons of bauxite residue [174].

To produce pure alumina from bauxite through the Bayer process, AoG mixes two types of bauxite feed: 80 % of the feed is from the karst (diasporic/boehmitic) bauxite coming from Parnassus-Ghiona, and 20 % is imported lateritic (gibbsitic) bauxite originating from Ghana or Brazil [51,53].

In Figure 16 a simplified flow diagram of AoG process is presented [53]. Before the conventional Bayer process, an additional step is introduced. The Parnassos-Ghiona karst bauxite contains trace of unwanted limestone (mainly composed of calcite), which is inevitably partly mined together with bauxite. It is necessary to remove limestone from the ore and for this reason it is separated by gravimetric heavy media separation (HMS) in Fe-Si medium, prior to the other stages [53,175,176]. The sample is ground with the presence of concentrated leach liquor to achieve granulometry <

315 μm and the resulting suspension is pre-heated at about 180 °C. The digestion conditions utilized from the AoG, require T > 250 °C and elevated pressure (5.8 – 6.0 MPa) and are also known as high-temperature digestion (HTD)[53,177]. These conditions are necessary to promote the solubility of Al^{3+} in presence of diasporic/boehmitic bauxite.

To increase the productivity of the Bayer process, the Greek alumina plant uses an optimization step (called “sweetening” process), in which lateritic bauxite is digested at a lower temperature after the digestion of karst bauxite. Lateritic bauxite suspension passes through a pre-desilication step to allow the formation of desilication products (sodalite and cancrinite) and avoid the problems of reactive silica (i.e., kaolinite) during digestion. Consequently, lateritic bauxite suspension is introduced to the main karst bauxite slurry after the HTD of karst bauxite suspension [53].

During the clarification step, the solid fraction is separated from the pregnant leach liquor as residue slurry or red mud (bauxite residue in the suspended form) by settling and washing. To obtain de-watered bauxite residue, AoG makes use of the plate and frame filter pressing of the initial residue slurry after the settling and washing unit. Then, by adding gibbsite seed crystals to supersaturated liquid, alumina trihydrate begins to precipitate. In the last step of Bayer process, the aluminium hydroxide is calcined at >1000 °C to produce anhydrous alumina (Al_2O_3) [60,178]. Aluminum of Greece adopted the frame filter press and dry stacking disposal method for the produced BR . However, in this alumina refinery, the BR disposal takes up to 1 km^2 of land for an annual 0.75 million tons of BR[93].

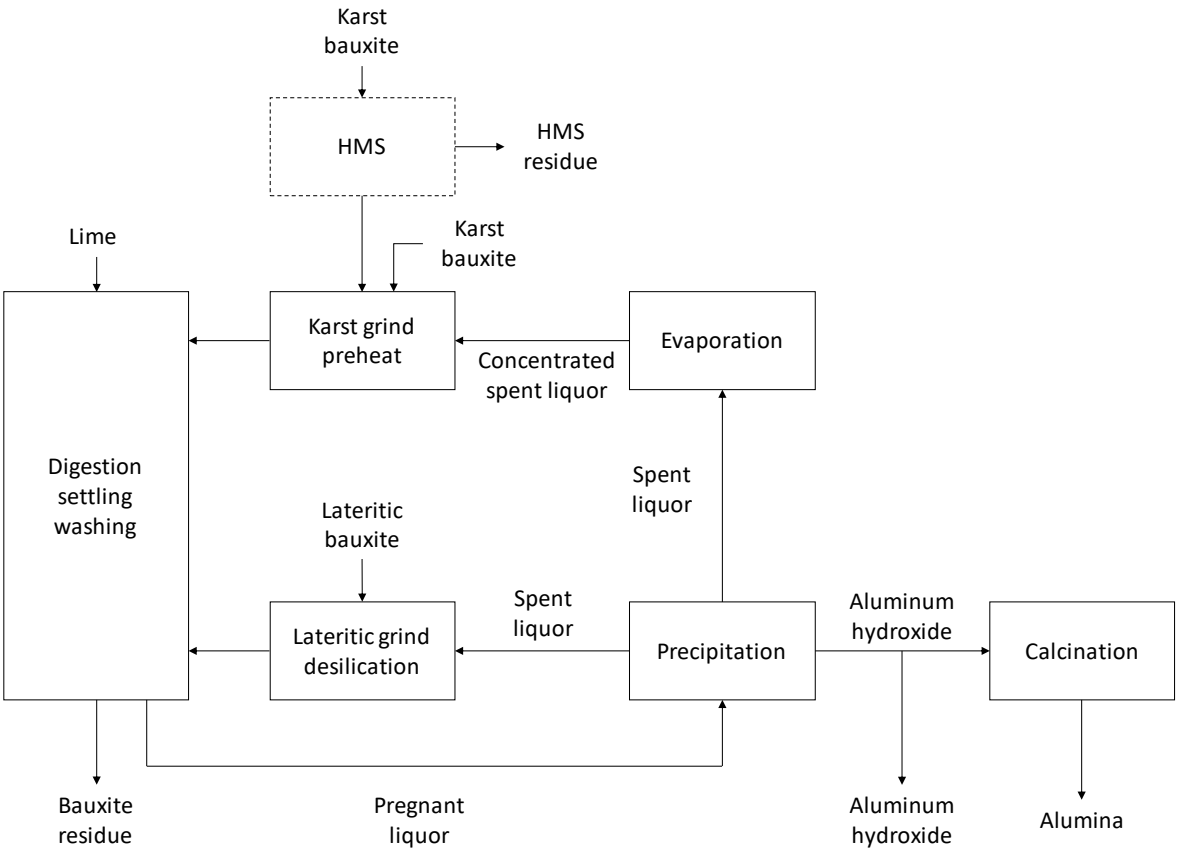

Figure 16. Simplified flow diagram of AoG's process (source Vind et al.[52])

5.2 Bauxite residue characterization

In the experiments of the present work, a filter-pressed bauxite residue cake, received from Aluminum of Greece plant, Metallurgy Business Unit, Mytilineos S.A. (AoG), was used as a raw material. A batch of about 58 kg of the as-produced BR cake was drying at 100 °C for 72 hours in a laboratory oven to eliminate the residual moisture.

Before the chemical and mineralogical composition analyses, the BR was homogenized by using laboratory sampling procedures and split to obtain a representative sample following the procedure in Figure 17.

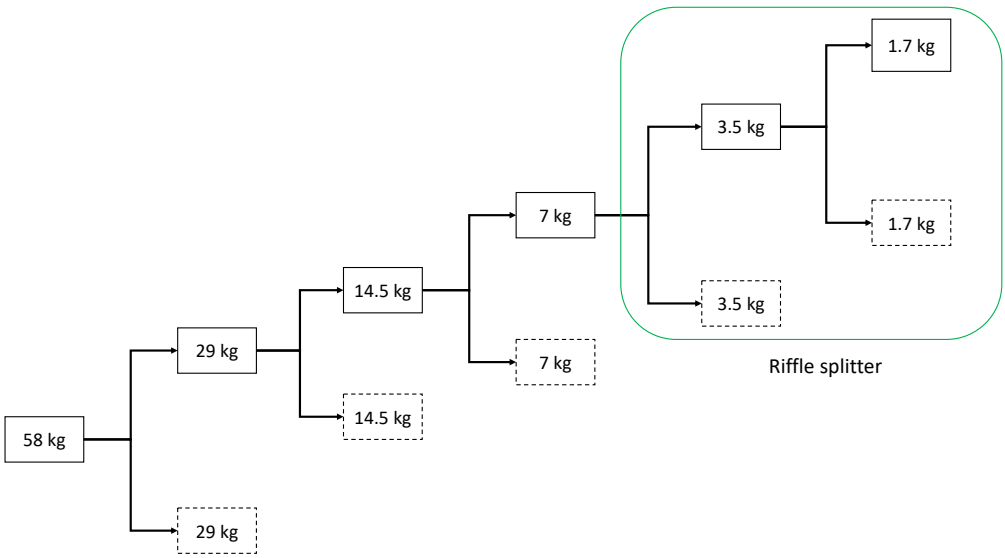

Figure 17. Homogenization procedure of BR

In particular, from 58 kg to 7 kg, the material was mixed by using “spooning” method. This method is one of the most common to obtain a homogeneous sample which involves the random insertion of a spoon into a course soil. After 7 kg the BR was separated by using a riffle splitter (also called Jones splitter), since this method ensures the representativeness of a sample and thus the reproducibility of the analysis [179].

In Figure 18 is presented a riffle splitter used to homogenize a 7 kg batch. The device is composed of a steel funnel and three collection pans. The funnel is designed to have an even number of opposing inclined chutes (the riffles) with same width and this permit the material to flow out towards two different sides. The sample then produces two equally divided subsamples.

As it is possible to observe, the sample was flowed through the alternately arranged passages (Figure 18 a) into the two collecting pans under the dividing funnel outlets, which contained about one-half of the original sample each (Figure 18 b). To obtain the required quantity of material, the operation can be repeated as many times as necessary using the following procedure. One collection pan containing one-half of the original BR was replaced with a clean pan, and the feed sample was treated again through the splitter and divided in two representative subsamples. After this step the volume was reduced to one-quarter of its original sample volume. The operation was repeated two times and a sample of about 1.7 kg was obtained and dried in a static furnace at 105 °C for 24 hours. Subsequently, the material was milled using a vibratory disc mill and the sample was fully characterized.

a b

Figure 18. Riffle splitter used to homogenize BR sample

The particle size distribution of the dried sample was measured through laser particle size analysis Malvern Mastersizer™ and it was found that 50 % of the particles were below 1.87 µm, while 90 % were smaller than 42.87 µm, as it is illustrated in Figure 19.

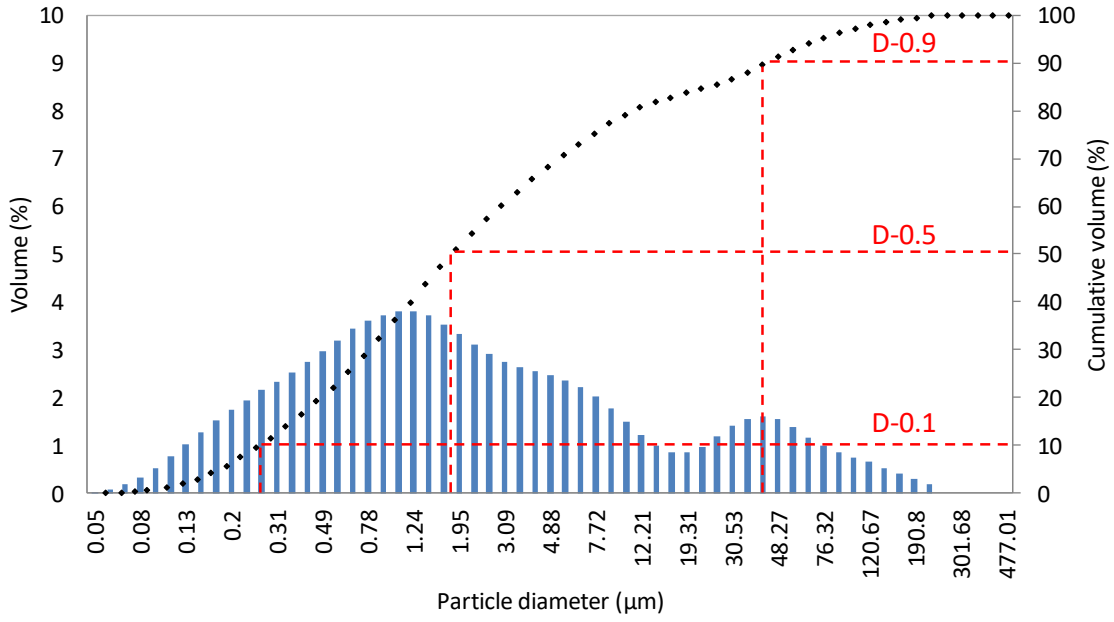

Figure 19. Particle size of BR used for the experiments

The chemical distribution and composition of microstructure of the samples were examined through a scanning electron microscope JEOL 6380LV (SEM) combined with an Oxford INCA energy dispersive spectrometer (EDS).

Chemical analyses of major and minor elements were executed via fusion method (1000 °C for 1 hour with a mixture of $Li_2B_4O_7/KNO_3$ followed by direct dissolution in 10 % v/v HNO_3 solution) through a Perkin Elmer 2100 Atomic Absorption Spectrometer (AAS), a Thermo Fisher Scientific X-series 2 Inductively Coupled Plasma Mass Spectrometer (ICP-MS) and a Perkin Elmer Optima 8000 Inductively Coupled Plasma Optical Emission Spectrometer (ICP-OES). Calcium oxide content was detected in solid samples with a Spectro Xepos Energy Dispersive X-ray fluorescence spectroscopy (ED-XRF).

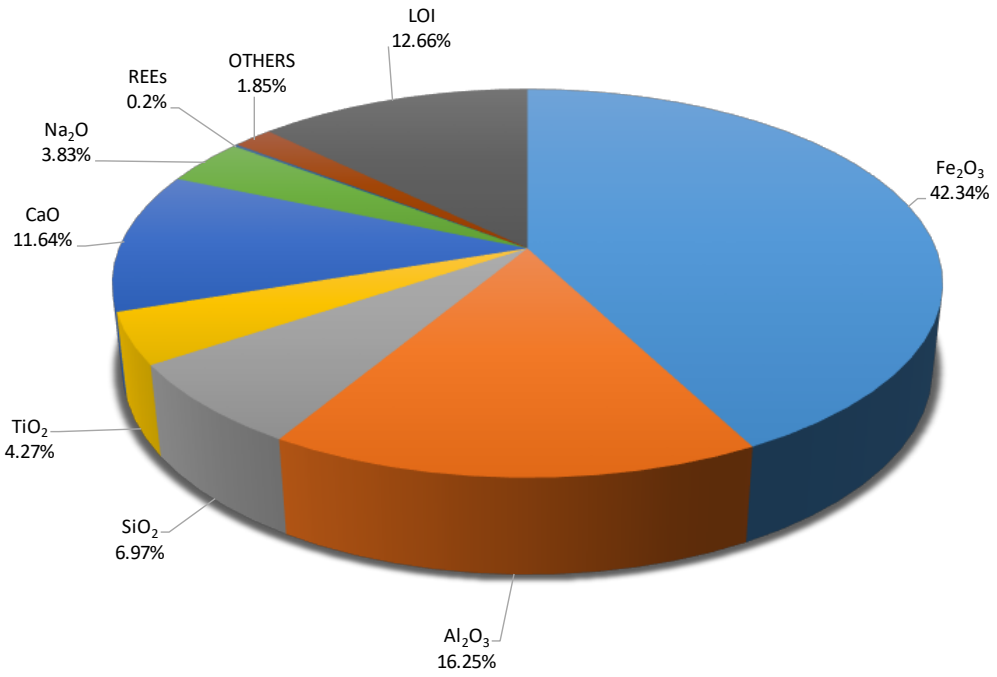

Figure 20: Bauxite residue chemical analysis

The chemical analysis results of the BR are shown in Figure 20. Iron oxide content (Fe_2O_3) is 42.34 wt. % and it can be considered the major component followed by aluminum oxide (16.25 wt. %), calcium oxide (11.64 wt. %), silicon oxide (6.97 wt. %), titanium oxide (4.27 wt. %) and sodium oxide (3.83 wt. %) while the rare earths elements (REEs) content, as oxides, is 0.19 wt. %. In particular, regarding the REEs, cerium (Ce) was determined to be the main rare earth element in concentration (402.2 ± 0.2 mg/kg), followed by lanthanum (La) (145 ± 12 mg/kg), scandium (Sc) (134 ± 4 mg/kg), neodymium (Nd) (127.1 ± 0.1 mg/kg) and yttrium (Y) (112 ± 2 mg/kg); error was calculated as the standard deviation based on the duplicate measurements.

The loss of ignition (LOI) of the sample was provided by differential thermal analysis (DTA), using a SETARAM TG Labys-DS-C system in the temperature range of 25 – 1000 °C with a 10 °C/min-heating rate, in air atmosphere (Figure 21). As it is possible to observe from the Figure 21, the value of the LOI is attested at 12.66 wt.% and it is constituted by dehydration and the decarbonation of mineral phases existing in the residue.

The composition of the Greek bauxite residue is representative of sampling of years 2010 to 2015 with an error margin of 1–10% for both chemical and mineral assays. Further variations of Greek bauxite residue is explained by Vind et al. [43,52]

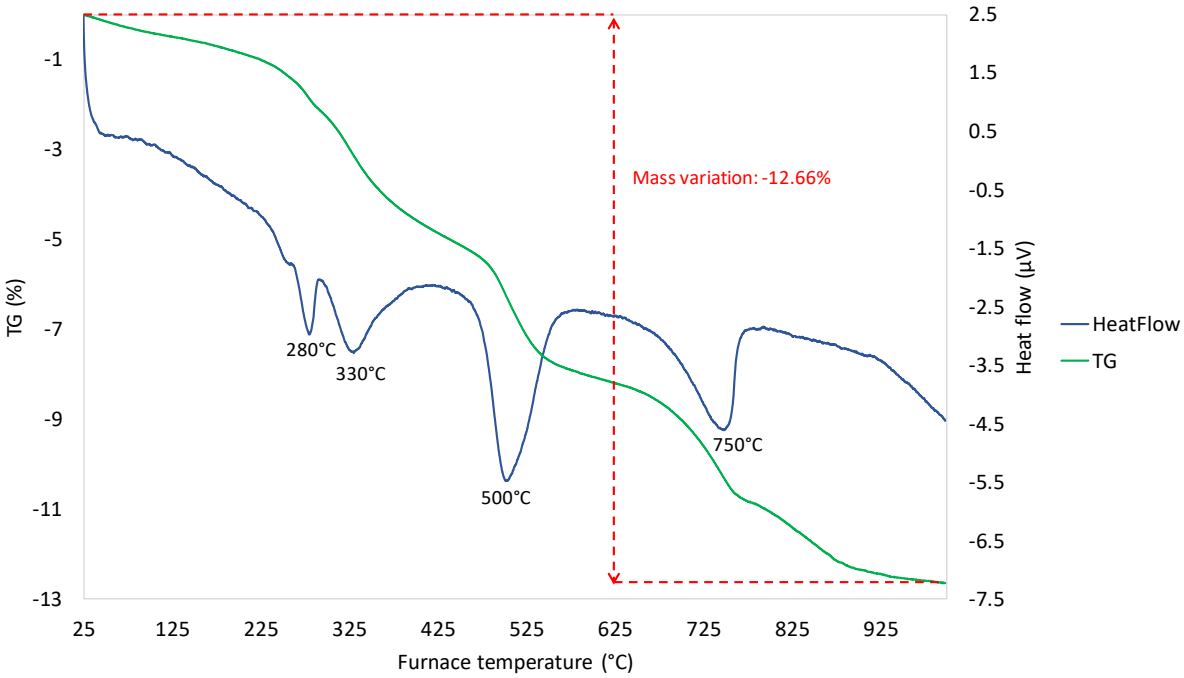

Figure 21. Thermogravimetric and differential thermal analysis (TGA-DTA) of BR

The results of TGA-DTA analysis presented four strong endothermic peaks, which correspond to four mass variation (Figure 21) [180,181]. The first peak at 280 °C is correlated to the dehydroxylation of goethite ($Fe_2O_3 \cdot H_2O$) to form hematite (Fe_2O_3). The other endothermic peaks disclosed are related to the dehydration of gibbsite ($Al_2O_3 \cdot 3H_2O$) which partially overlapped the goethite peak around 280 °C. Moreover, the dehydration of calcium aluminum iron silicate hydroxide ($Ca_3AlFe(SiO_4)(OH)_8$) is detected between 200 and 300 °C, while the dehydration of cancrinite ($Na_6Ca_2(AlSiO_4)_6(CO_3)_2(H_2O)_2$) between 400 and 625 °C. The endothermic peak at 500 °C is correlated to the dehydration of diaspore (α-AlOOH), overlapping the peak associated to the dehydration of cancrinite. The decarbonation of cancrinite ($Na_6Ca_2(AlSiO_4)_6(CO_3)_2(H_2O)_2$) appears at 750 °C [19,182].

Mineralogical phases were detected by X-ray diffraction analysis (XRD) using a Bruker D8 Focus powder diffractometer with nickel-filtered CuKα radiation (α= 1.5405 Å) coupled with XDB Powder Diffraction Phase Analytical System version 3.107 which evaluated the quantification of mineral phases via profile fitting specifically for bauxite ore and bauxite residue. The mineralogical phases of BR are presented in Figure 22 and according with the quantification analysis carried out with the XDB software (Table 3), hematite is the main mineral in BR with 30 wt. %. The other iron mineralogical phases were calcium aluminum iron silicate hydroxide, goethite, and chamosite with 17 wt. %, 9 wt. % and 4 wt. % respectively. Regarding the alumina-containing phases, diaspore was the main mineralogical phase (9 wt. %), followed by chamosite (4 wt. %), boehmite (3 wt. %), gibbsite (2 wt. %) and cancrinite (15 wt. %), while Ti was detected into perovskite, anatase and rutile with 4.5, 0.5 and 0.5 wt. % respectively.

Table 3. Bauxite residue mineralogical phases and quantification.

Mineralogical phases	**Formula**	**wt.%**
Hematite	α-Fe_2O_3	30
Goethite	$Fe_2O_3 \cdot H_2O$	9
Boehmite	γ-AlOOH	3
Diaspore	α-AlOOH	9
Gibbsite	$Al_2O_3 \cdot 3H_2O$	2
Calcite	$CaCO_3$	4
Anatase	TiO_2	0.5
Rutile	TiO_2	0.5
Perovskite	$CaTiO_3$	4.5
Cancrinite	$Na_6Ca_2(AlSiO_4)_6(CO_3)_2$	15
Calcium aluminum iron silicate hydroxide	$Ca_3AlFe(SiO_4)(OH)_8$	17
Chamosite	$(Fe^{2+},Mg)_5Al(AlSi_3O_{10})(OH)_8$	4
Sum		98.5

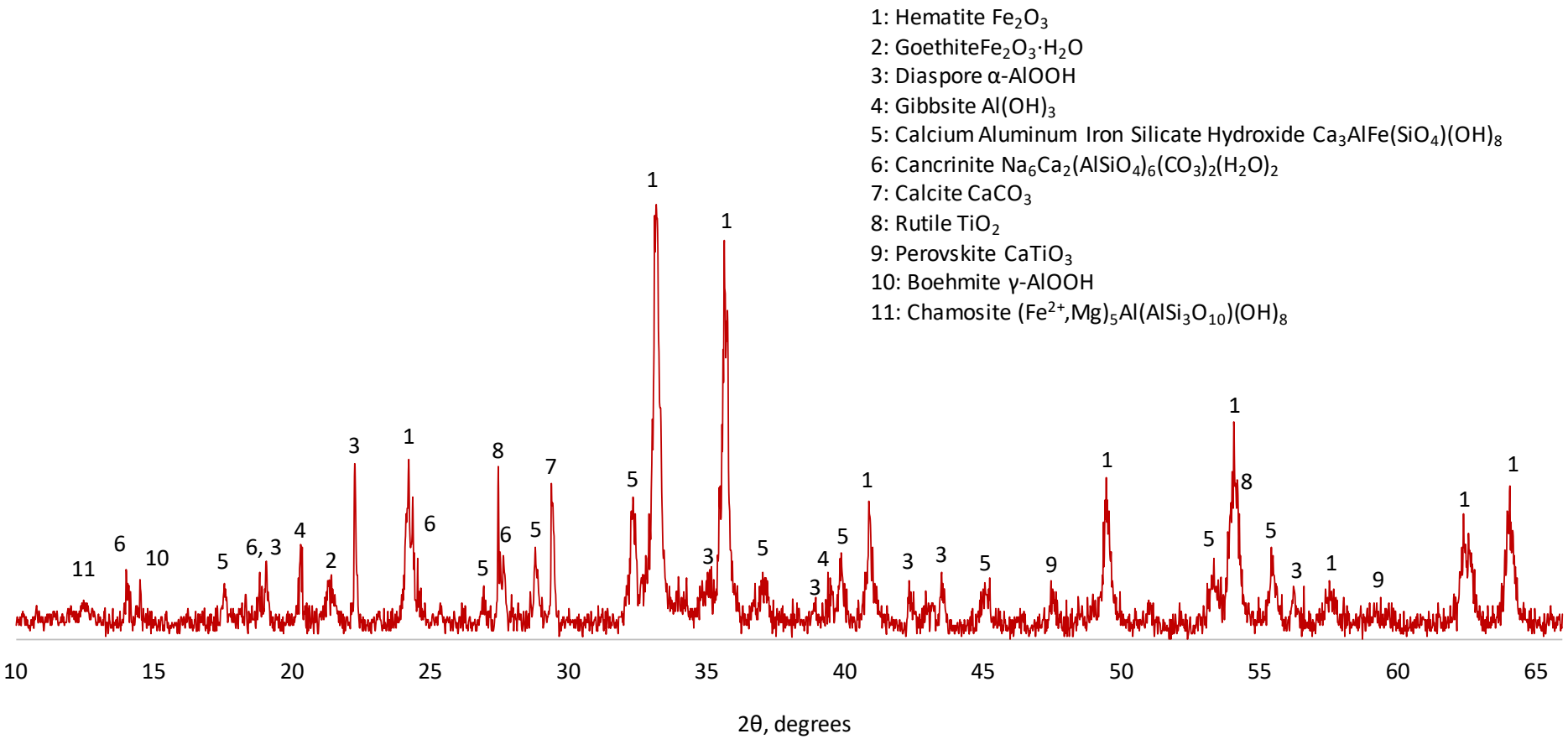

Figure 22. XRD profile of bauxite residue.

6. Reductive roasting process through conventional furnace

In BR, iron is present as oxides/oxyhydroxides, and usually it is the largest constituent (14 -45 wt. %), as already discuss in chapter **Errore. L'origine riferimento non è stata trovata.** [94]. Due to the gradual depletion of available ores and the demand for sustainable industries, several processes have been developed based on iron recovery from bauxite residue [12,19,23,99]. The present work has the scope to develop and optimize at a lab scale a reductive roasting process in a conventional tube furnace followed by wet high intensity magnetic separation (WHIMS) to recover iron from BR. The aim of the roasting process is the transformation of the non-magnetic iron phases found in BR (namely hematite and goethite), to magnetic ones such as magnetite, wüstite, and metallic iron. The magnetic iron phases in the roasting residue can be fractionated in a second stage through wet magnetic separation, forming a valuable iron concentrate and leaving a nonmagnetic residue containing rare earth elements among other constituents. Figure 23 shows the details of the experimental procedure and process diagram.

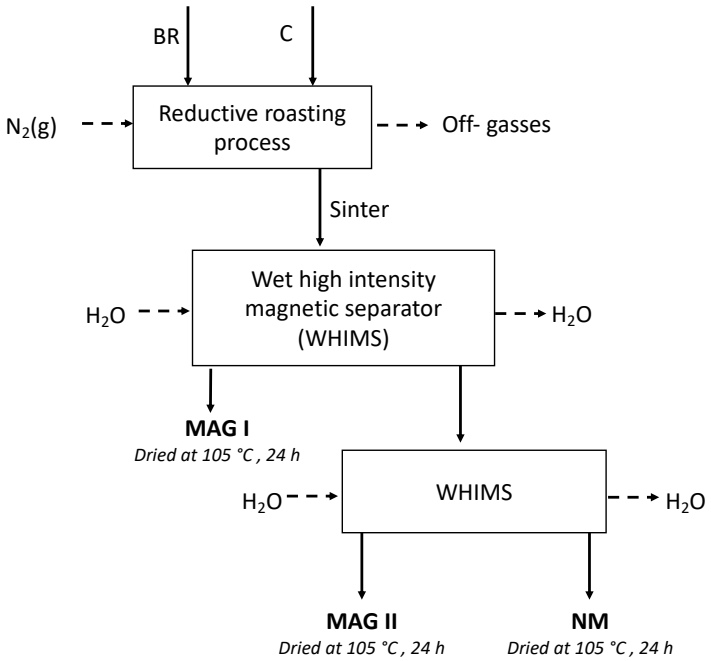

Figure 23. Experimental process flowsheet

In addition, the BR-roasting process has been modeled using a thermochemical software (FactSage 6.4^{TM}) to define process temperature, carbon/bauxite residue mass ratio (C/BR), retention time, and process atmosphere.

6.1 Thermochemical studies

The FactSage 6.4^{TM} thermochemical software was used for the thermodynamic analysis of the reductive roasting of BR in presence of C [183]. To examine the process, the databases FT- oxid, SG-TE, and FT-misc which contain all the oxides present in the system (including magnetite and wüstite), the metallic iron solution (pig iron), and the oxidic slag phase were employed. As starting point it was used the obtaining chemical analysis of BR and the additions of varying amounts of carbon for a range of temperature (25 - 1000 °C) were simulated.

The phase equilibrium diagram during the reductive roasting of pure hematite (under constant molar ratio $\frac{C}{(Fe+C)}$= 0.1 and 1 atm) as a function of process temperature and oxygen partial pressure in the system is shown in Figure 24.

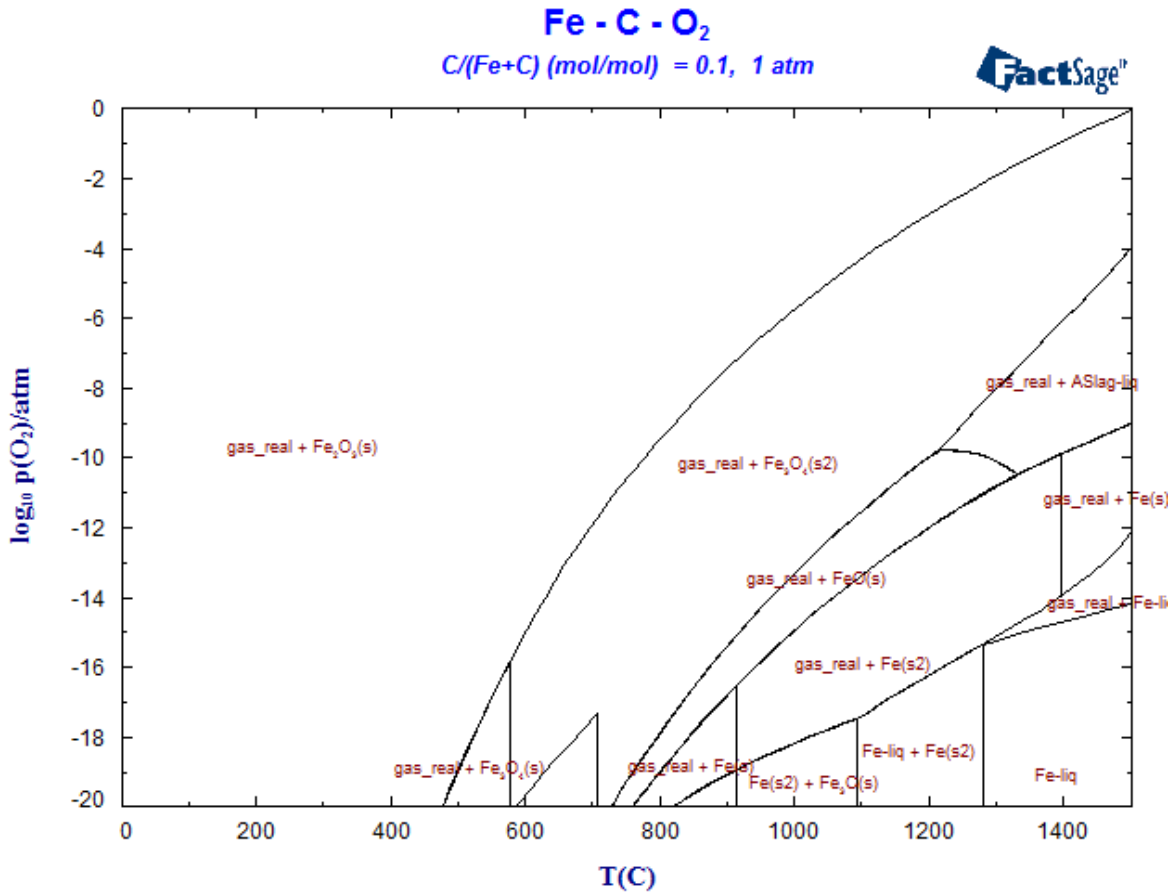

Figure 24. Fe-C-O_2 system

As it was expected, the transformation of hematite (Fe_2O_3) to magnetite (Fe_3O_4) is drastically affected by the oxygen partial pressure in the system. The transformation temperature decreases as the oxygen partial pressure decreases reaching to a value lower than 500 °C in practically an oxygen-free reaction atmosphere ($\log P_{O_2} = -20$). The increase of process temperature under low oxygen partial pressures pushes gradually the system toward the formation of wüstite (FeO) and even of metallic iron at higher temperatures.

The percentage compositions of the several mineralogical phases in the reductive roasting solid product as a function of temperature in practically an oxygen-free atmosphere with $\log \log P_{O_2} = -16$, are presented in Figure 25.

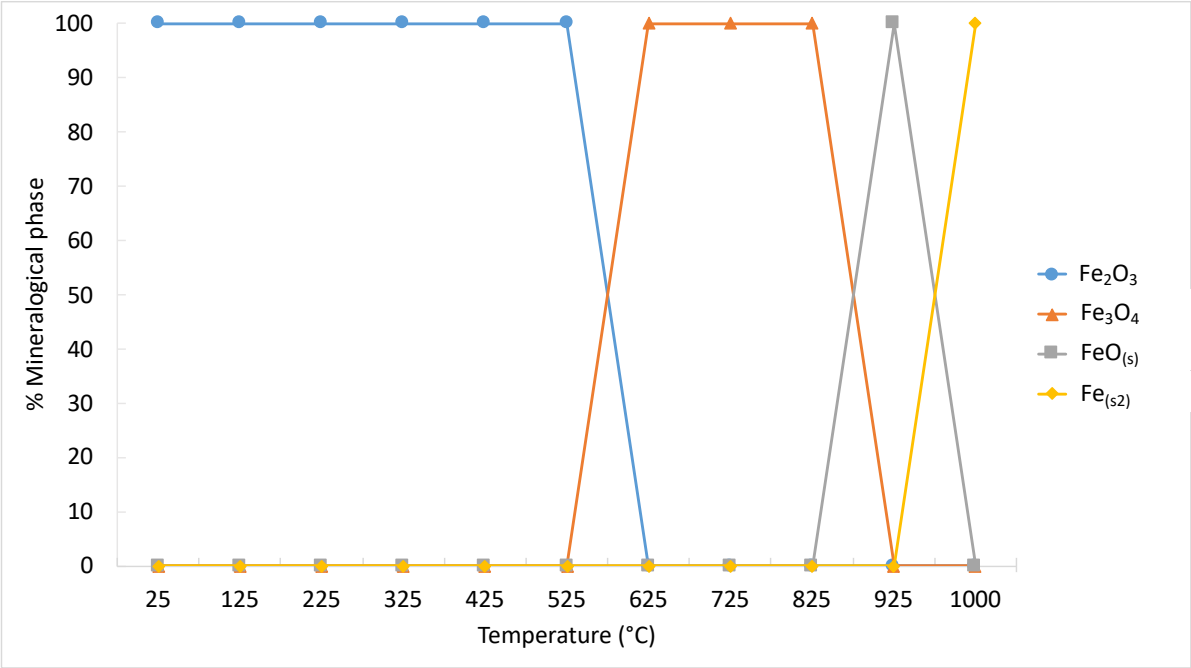

Figure 25. Percentage compositions of the several mineralogical phases in the reductive roasting solid product as a function of temperature ($\log P_{O_2} = -16$, molar ratio $\frac{C}{(Fe+C)}$ = 0.1, and P_{total} = 1 atm)

As it is seen in Figure 25, the sintered products from the reductive roasting of hematite [($\log P_{O_2} = -16$, molar ratio $\frac{C}{(Fe+C)}$ = 0.1, and P_{total} = 1 atm)] are exclusively composed of magnetite in the temperature range of 625–825 °C. The wüstite thermodynamic stability area is very narrow at the temperature range around 925 °C, while, at temperatures higher than 1000 °C, metallic iron is formed. Based on the performed thermodynamic analysis, the temperature regime between 400 and 1100 °C and an inert atmosphere were chosen as experimental parameters for the study of BR reductive roasting process.

6.2 Reductive roasting process through conventional tube furnace

The roasting process was carried out in an alumina tube furnace. Temperature in the furnace was measured using an R-type thermocouple. In Figure 26, a schematic diagram of the static tube furnace employed for the experiments is presented.

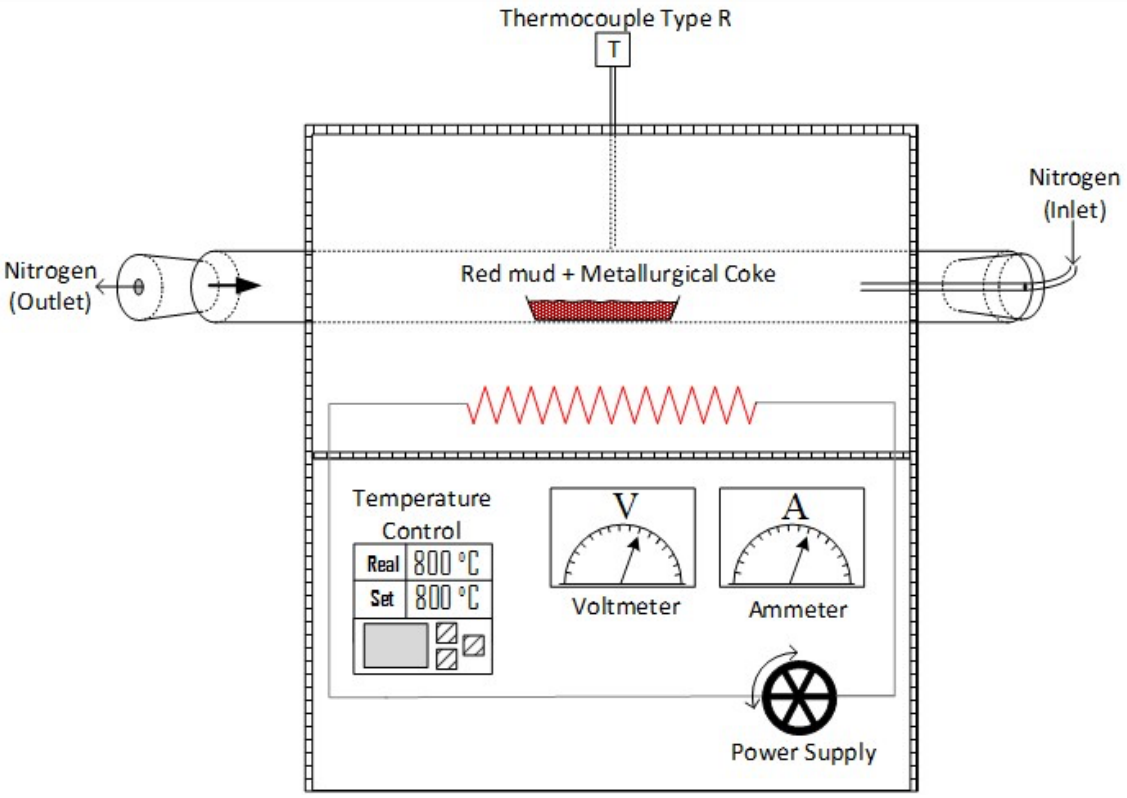

Figure 26. Schematic diagram of the static tube furnace

As a reductant agent a metallurgical coke was used. The chemical analysis results of metallurgical coke presented in Table 4 proved carbon as the main component of the sample with 80.31 wt. %. Thanks to its high fixed carbon (Fixed C) content, metallurgical coke was used as the reductant in all the experiments carried out in this work.

Table 4. Metallurgical coke chemical analysis

Component	**wt. %**
Fe_2O_3	0.83
SiO_2	3.42
CaO	1.26
MgO	0.14
Al_2O_3	1.91
TiO_2	0.10

Na_2O	0.16
Fixed C	80.31
S	0.77
P	0.03
H_2O moist.	3.31
LOI	7.38
OTHERS	0.39

Preliminary experiments were conducted to optimize the process. To evaluate the influence of temperature on the process, samples of 3.5 g possessing a metallurgical coke- to-bauxite residue mass ratio of 0.112, in the presence of N_2 flow heated at a range of temperature between 400 and 1100 °C, were reduced.

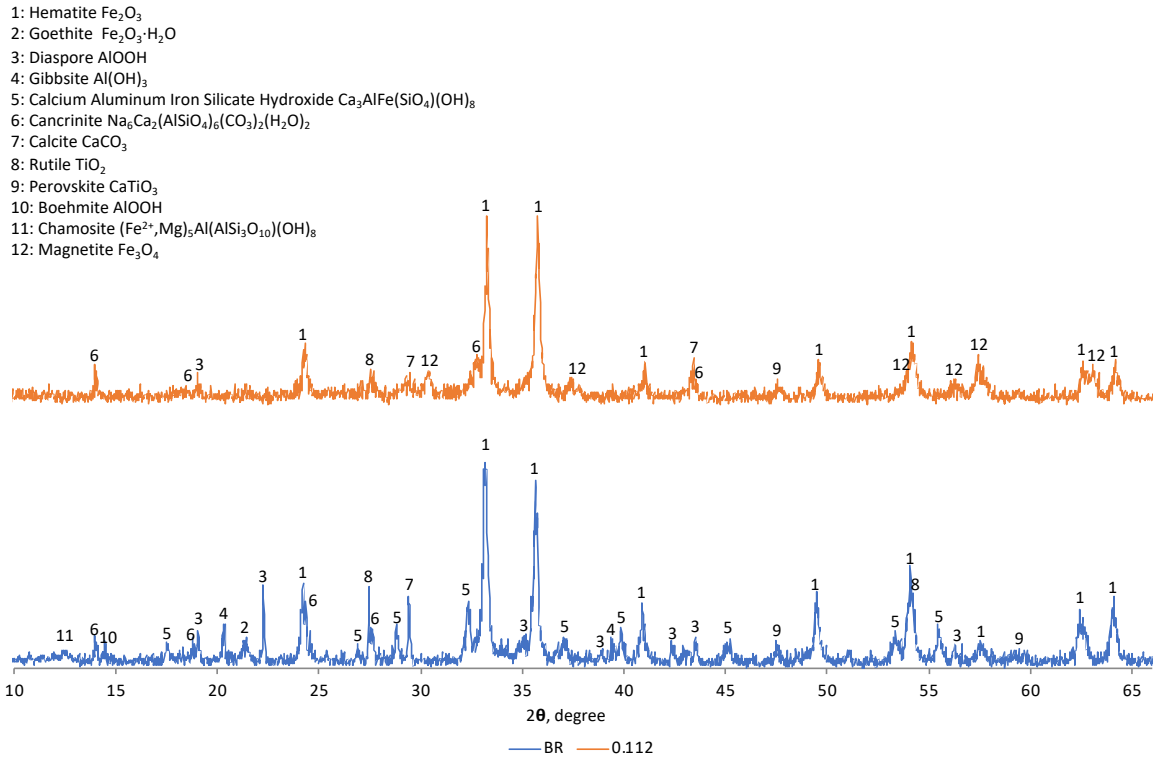

Figure 27. XRD of sinter (C/BR= 0.112 at 800 °C after 4h) compared to XRD of BR

Figure 27 shows that magnetite (Fe_3O_4) has already been formed at 800 °C as predicted by the thermochemical software. The transformation of hematite to magnetite has not been completed yet, as hematite is still the major mineralogical phase in the sinter. To achieve the complete reduction of iron phases, present in BR, several experiments, varying C/BR ratios ranging between 0.135 and 0.225, were performed. Time and temperature were kept constant at 4 h, and 800 °C, respectively, under N_2 atmosphere.

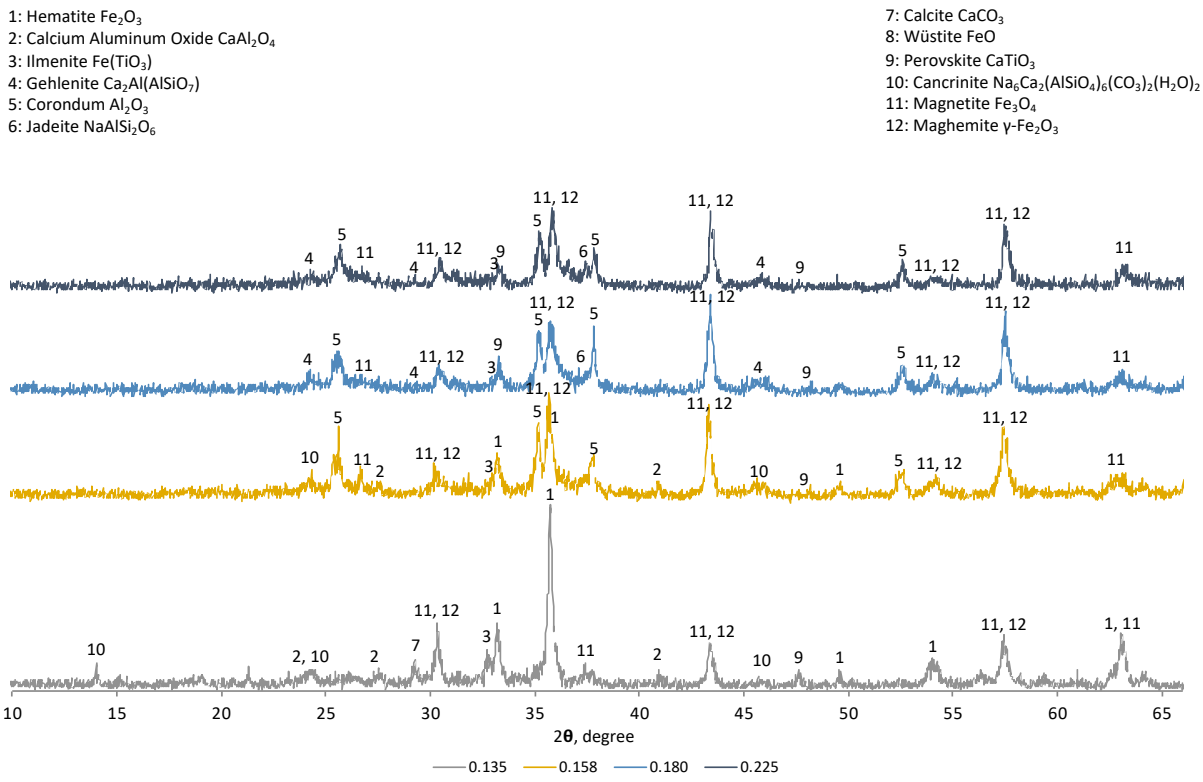

Figure 28. XRD of sinters at 800 °C under different carbon/bauxite residue ratios (between 0.135 and 0.225)

As shown in Figure 28, the transformation of trivalent iron phases of Fe_2O_3 and $Fe_2O_3{\cdot}H_2O$ into magnetic ones of Fe_3O_4 and γ-Fe_2O_3 (maghemite) is favored with the increasing carbon/bauxite residue ratio. Examining the XRD profiles of different samples, Fe_3O_4 and γ-Fe_2O_3 were the main iron mineralogical phases after 4 hours of reductive roasting reaction at 800 °C, with C/BR ratio of 0.180. At the same time, under these conditions, all alumina-containing phases in BR (gibbsite, boehmite, diaspore, cancrinite, and calcium aluminates) have been transformed to corundum and gehlenite which is a calcium aluminosilicate phase not initially existing in BR. Titanium phases have been converted to perovskite and ilmenite. The calcite peak disappeared due to its thermal decomposition

[182,184]. The result of the roasting process optimization is the production of sinter with strong magnetic properties, containing Fe_3O_4 and γ-Fe_2O_3 among the other constituents.

6.3 Wet high intensity magnetic separation

Preliminary tests were performed to understand the magnetic behavior of tube furnace sinter (at 800 °C; C/BR = 0.180; 4 h roasting time, and in the presence of N_2) using a wet high-intensity magnetic separator (WHIMS).

For the magnetic separation experimental tests, a Carpco Model MWL-3465 laboratory, high-intensity, wet magnetic separator (WHIMS) manufactured was utilized (Figure 29) [26]

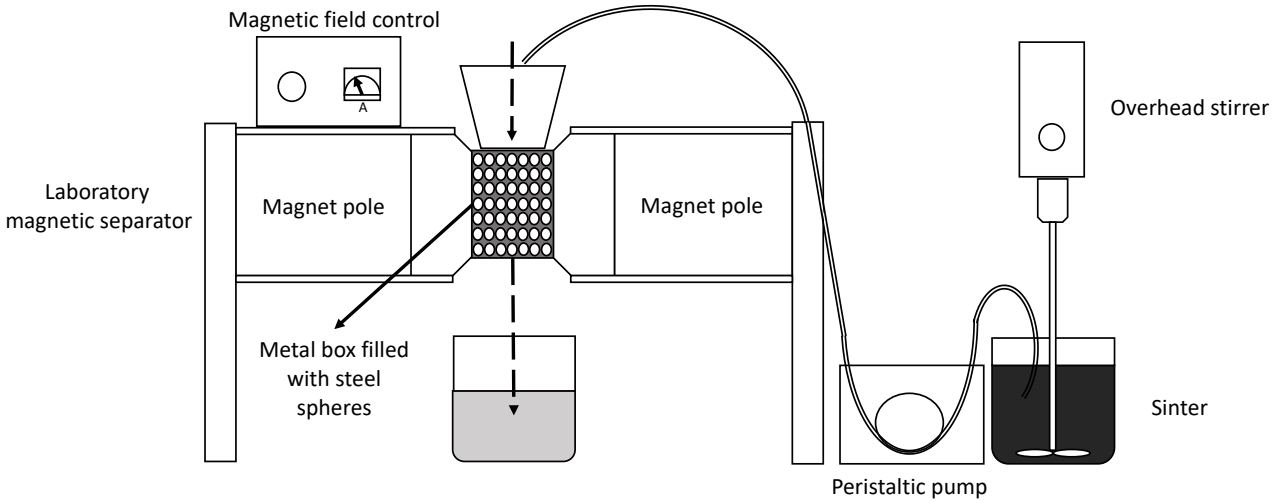

Figure 29. Carpco Model MWL-3465 laboratory, high-intensity, wet magnetic separator schematic diagram

An intensive magnetic field was generated through two magnet poles by applying a controlled electric field (0.01 A and 0.02 A).

A metal box was placed between the poles and filled with steel spheres during separations. The spheres served as induced magnetic poles and created a point with an intense magnetic field.

At the bottom of the metal box, a stainless steel slide was placed to carry the non magnetic flux in a beaker.

Magnetic separation experiments were carried out by dispersing the optimized sinter in water (50 g of sample in 800 ml of distilled water). The pulp was constantly stirred with an ES Overhead stirrer at 400 revolutions per minute (rpm) and passed throughout the metal box by using a peristaltic pump with a flow rate of 10 ml/ min. The pulp was separated into the magnetic material, which was held to the steel spheres, and the non-magnetic material that passed through the separation zone.

The main purpose of the magnetic separation was to remove the iron based components in the sinter solution and concentrate them in the magnetic product. To achieve the target, the feed was treated through the WHIMS two times.

In the first step, a magnetic fraction (MAG I) was collected by emploing a 0.01 A current intensity, while a non-magnetic fraction was run again through WHIMS. In the second pass the current intensity was increased to 0.02 A and a second magnetic fraction was gathered (MAG II).

Magnetic I, Magnetic II and Non-magnetic fractions (residue from second pass, NM) were then dried in a static furnace at 105 °C for 24 hours and characterized by using the analytical techniques above mentioned.

In Figure 30, mineralogical phases of the Magnetic I fraction are presented in comparison with BR and the tube furnace sinter.

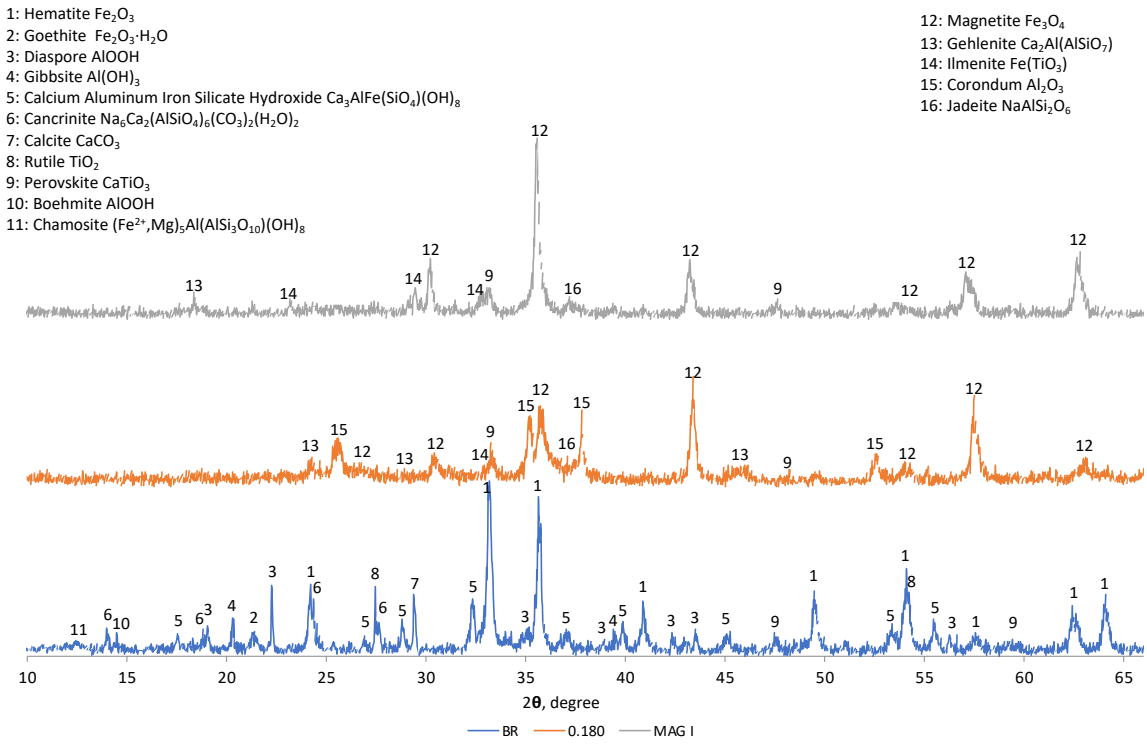

Figure 30. XRD profile of Magnetic I compared with optimized sinter and bauxite residue

Although Fe_3O_4 is the main mineralogical phases of iron, in the highest magnetic sample (Magnetic I), perovskite, ilmenite, and gehlenite also exist. Moreover, scanning electron microscope (SEM) analyses combined with EDS (Figure 31) have demonstrated the existence of Si phases together with the iron ones.

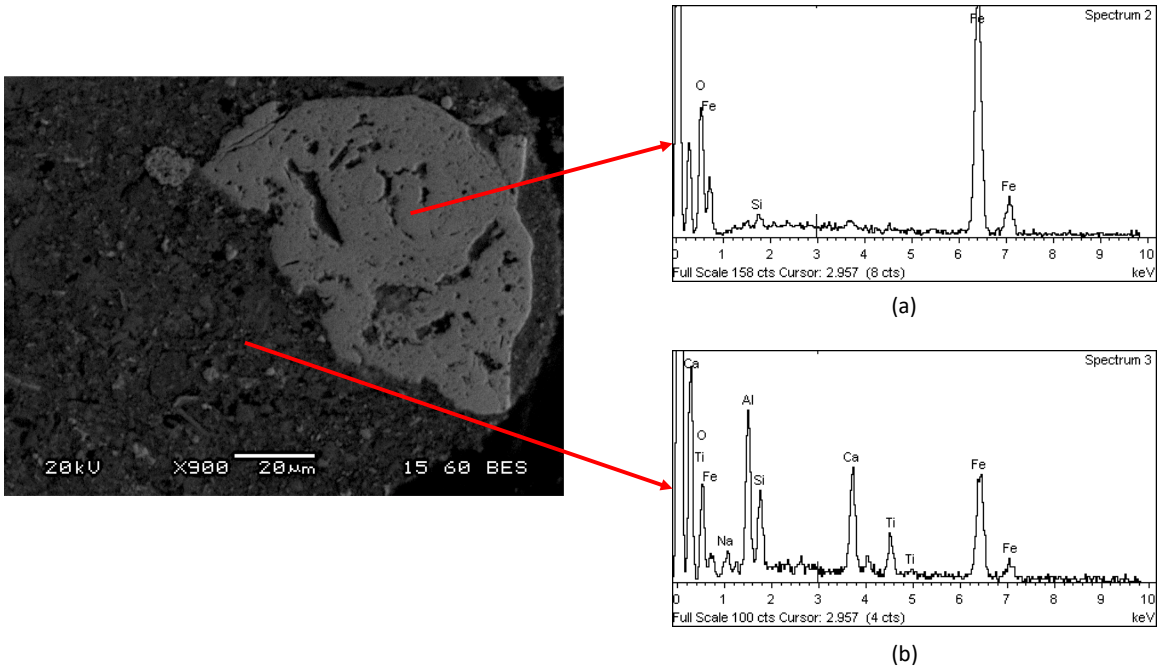

Figure 31. SEM–EDS images of Magnetic I sample

Analyzing the distribution of the elements, the white particles are composed principally of Fe_3O_4, but an amount of SiO_2 is also detected as inclusions in the scratches (black area on white particles) of the surface (Spectrum a, Figure 31). As Chao Li et al. have shown in their work [185], when iron, silicon, and calcium are finely distributed in a matrix, they are commonly complexed together. This makes their fractionation through magnetic separation a very hard issue. On the other hand, Spectrum b (Figure 31) confirms the existence of a complex matrix that entraps the iron magnetic phases.

An alternative route was then explored by performing tests at higher temperature (1100 °C) and with C/BR = 0.225, favoring metallic iron formation. The purpose of this work was the intensification of reduction conditions to produce metallic iron nuggets which could be more easily and efficiently liberated from the complex matrix by means of the magnetic separator. XRD patterns of these experiments are shown in Figure 32.

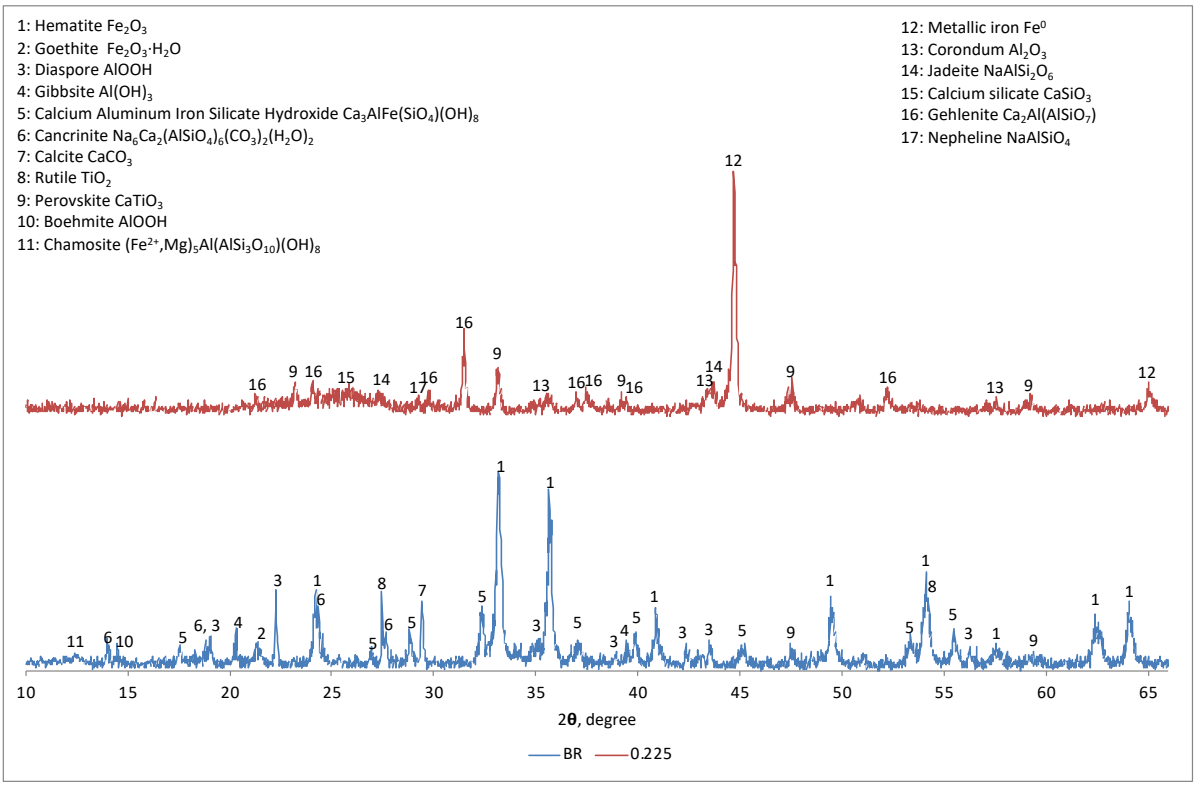

Figure 32. XRD patterns of sinter after 4 h at 1100 °C

Hematite and goethite were completely transformed into metallic iron after being roasted at 1100 °C for 4 h, while the other elements (Ca, Si, Al, Ti, and Na) are present mainly in sodium and calcium aluminosilicate phases as well as perovskite. In addition, Al is also present in the sinter as corundum.

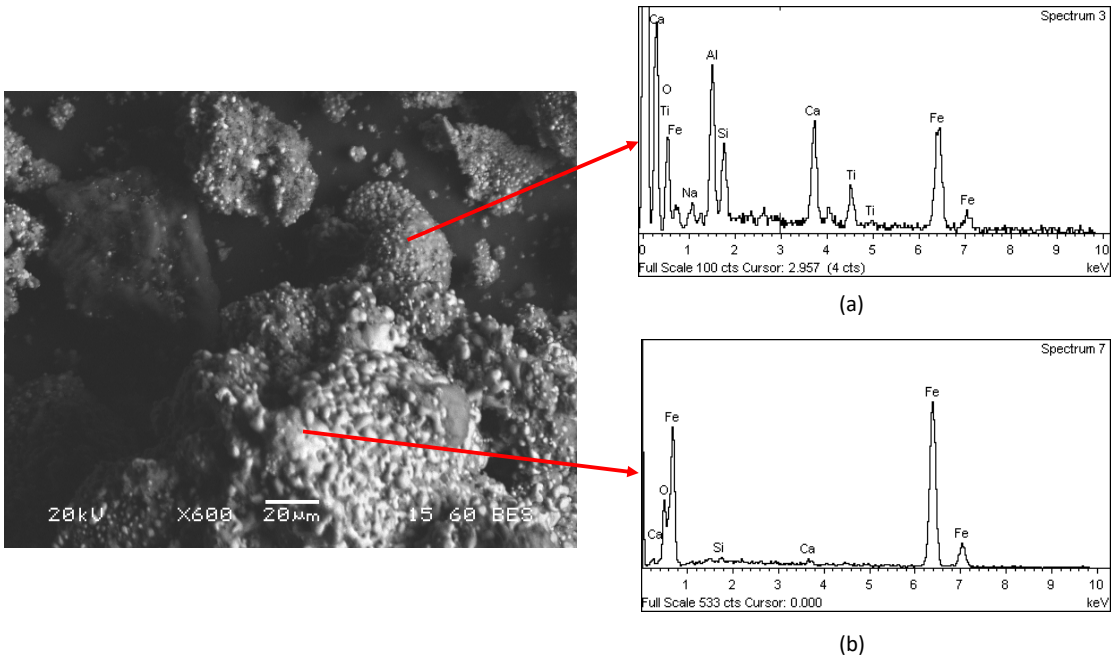

Figure 33. SEM–EDS image of sinter achieved after 1100 °C roasting process

SEM–EDS analyses have shown the presence of melted metallic iron (Spectrum b, Figure 33) concentrated in some grains of the material, entangled in a matrix mainly composed of calcium, aluminum, and silicon (Spectrum a, Figure 33).

After the reductive roasting process, the samples were ground (particle size < 90 µm) to increase the liberation of the metallic iron phase from the matrix through a planetary ball mill (Planetary Ball Mill PM 100) with a grinding time of 5 minutes and a speed a 400 rpm. The sample was treated four times with the planetary ball mill to transform the sinter into fine powder. The sample was finally separated by using WHIMS and three fractions were collected following the procedure already explained above. The chemical analysis of sinter and the three fractions is shown in Figure 34.

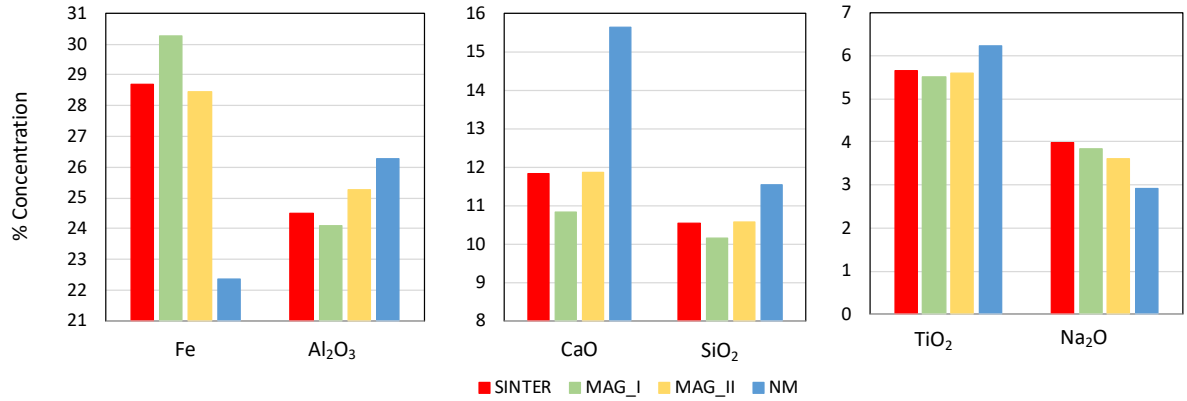

Figure 34. Main components contained in sinter (1100 °C), MAG I, MAG II and NM

As it is seen in Figure 34, metallic iron is concentrated in the MAG I fraction and diluted significantly in NM residue, although the iron content is still high. Fe occurs in NM fraction as very small, almost spherical metallic particles (< 5 µm) entrapped inside a solid matrix that contains nearly all sinter constituents (Figure 35). This can be attributed to the fact that BR contains significant amount of ceramic-forming constituents (such as SiO_2 and Al_2O_3) as well as fluxing oxides (such as Na_2O and CaO), which form a ceramic precursor that sinters the residue, during the reductive roasting process at 1100 °C. Although the roasted residue (sinter) was ground to liberate the magnetic iron particles, this proved to be an inefficient procedure for the effective magnetic separation of iron as the MAG I fraction (even though concentrated in metallic iron) contains considerable amounts of impurities.

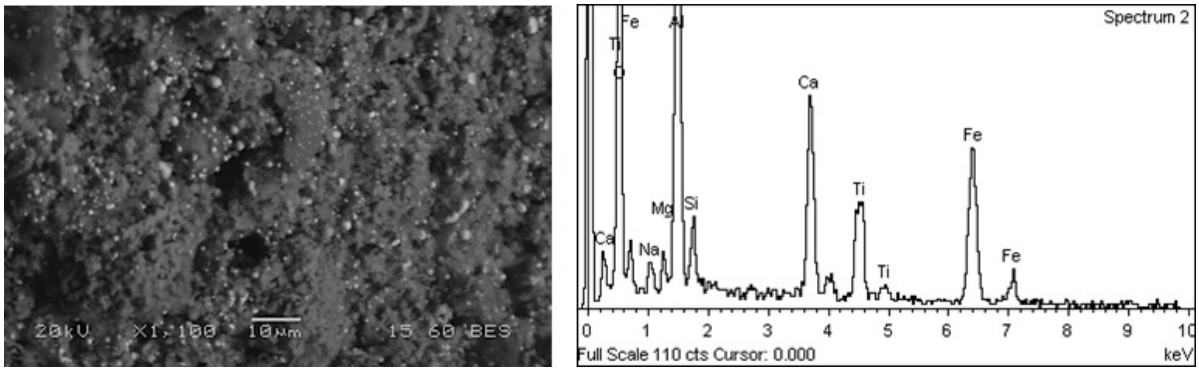

Figure 35. SEM-EDS analysis of NM fraction

By increasing the intensity of the magnetic field, a new fraction MAG II was separated, which however looks like the initial sinter as seen in Figure 36.

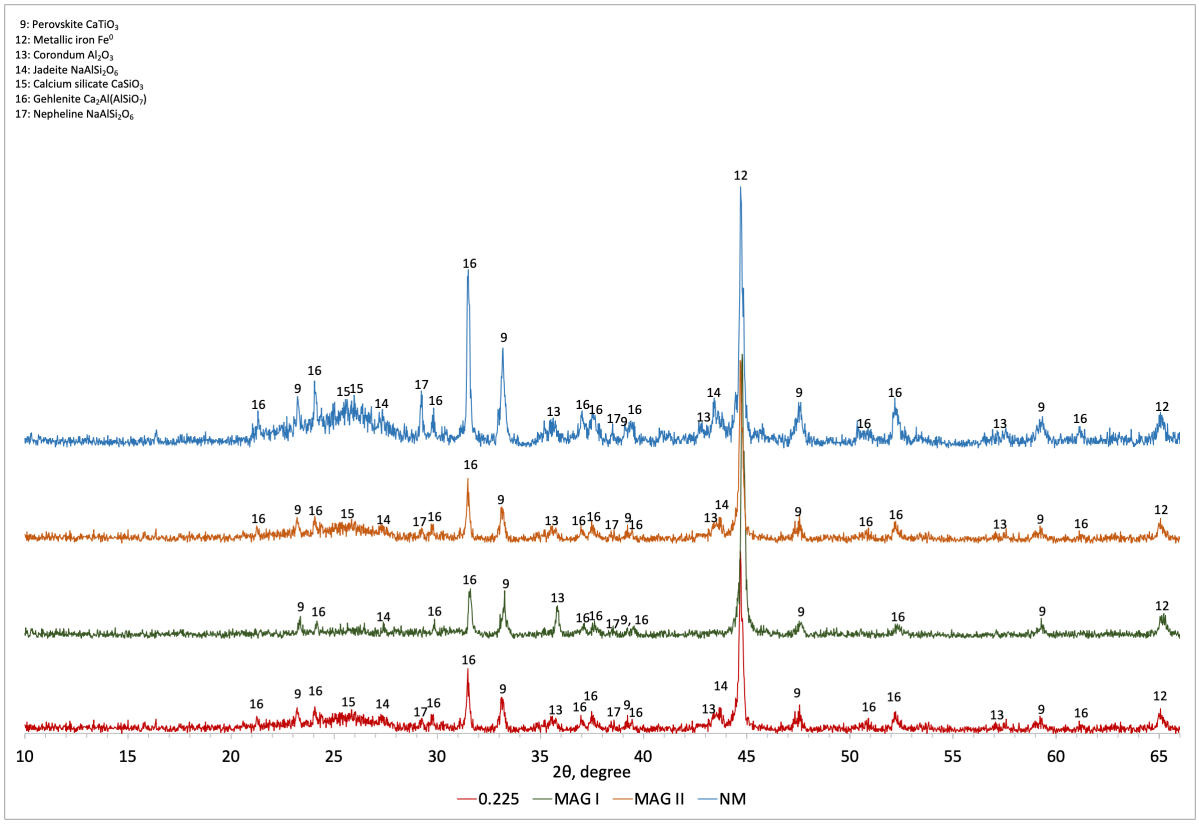

Figure 36. Comparison of the XRD profile of sinter after 4 h at 1100 °C, magnetic fraction (MAG I), weak magnetic fraction (MAG II) and non-magnetic fraction (NM).

Moreover, the produced NM fraction amounts to only the 15 % of the initial sinter material, which contains almost 78 % noniron-bearing phases (Figure 34) indicating once more, the inefficient separation of metallic iron due to its entrapment inside the ceramic matrix.

7. Microwave roasting process

A possible scenario to increase the iron recovery from BR is to utilize a microwave furnace instead of a conventional furnace. As explained in the paragraph 3.3, microwave heating has several advantages depending on the molecular interactions with the electromagnetic field generated during the process. Materials (with high dielectric loss) are internally heated up, leading to rapid heating. Since the absorption of microwave energy varies with the composition and structure of different phases, a selective heating is possible. Finally, microwaves can accelerate chemical reactions [30,34,35].

Hematite and goethite are not good microwave receptors [36], therefore a carbon (C) source (metallurgical coke) was added to BR as a reducing agent as well as microwave energy absorber. Different parameters have been studied (irradiation time, carbon/bauxite residue ratio and the influence of microwave energy on the sample) to optimize the process. The scope was to liberate the iron based components from the sinter produced matrix and concentrate them into the magnetic product by using a wet high intensity magnetic separator.

7.1 Microwave furnace

Experiments were carried out with a 2-kW microwave furnace (Fricke und Mallah Microwave Technology GmbH) and Figure 37 showed the scheme of the device employed during the carbothermic roasting process.

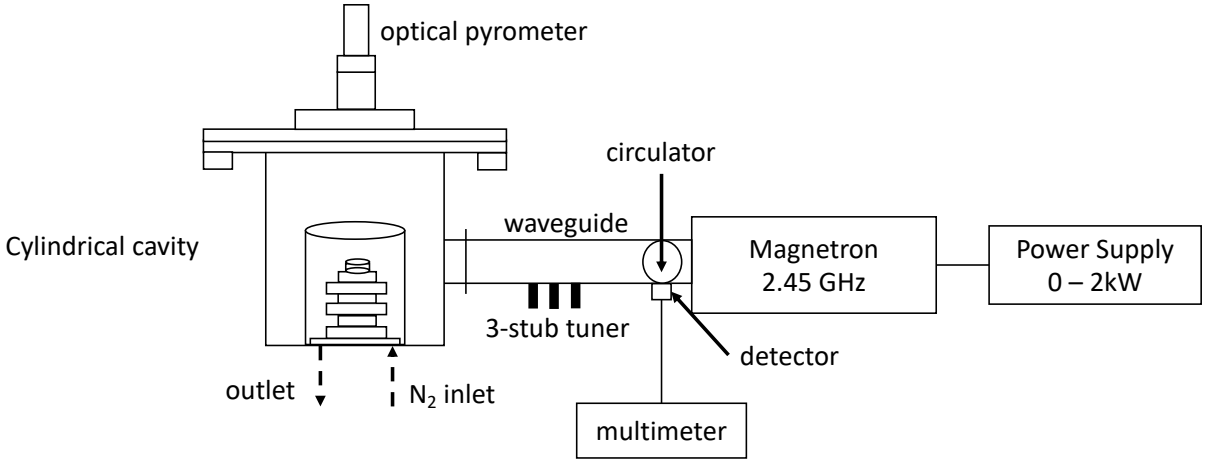

Figure 37. Schematic diagram of the microwave furnace

The above-mentioned furnace was composed by a power supply, a 2.45 GHz air-cooled magnetron, a circulator connected with a multimeter through a detector, a rectangular aluminum wave guide with 3-stub tuner and a water-cooled cylindrical aluminum cavity (diameter 150 mm and height 165 mm).

The magnetron converts electrical energy into high frequency microwaves and the power capacity can be set, from 0 kW (0 %) to 2 kW (100 %), through a potentiometer located on the switch-mode power supply. The microwave energy runs via the rectangular waveguide to the cylindrical single mode cavity, where the sample is placed.

The 3-stubs tuner present in the waveguide allowed to modify microwave energy to accomplish the highest sample absorption for the entire experimental period. The reaction occurred in accordance with the materials ability to absorb microwave.

The sample was composed by mixing BR and metallurgical coke as carbon source. The powder was transformed in tablets with dimensions of 2 cm x 2 cm x 3 mm and approximate weights of 10 g by using a manual hydraulic press.

To ensure the interaction between the modified BR and MW wavelength, the samples were settled in the furnace on the top of a tower constituted by alumina crucibles and quartz glasses with the following dimensions: 7 cm height and 3 cm length and located at the center of the cylindrical cavity. A borosilicate glass dome (Pyrex) was positioned to cover the sample and protect the cavity from the possible plasma formation during the experiment.

The optical pyrometer, IMPAC Pyrometer IGA 6/23 Advanced with a RS 485 converter LumaSense Technology, was located on the top of the chamber lid to record the temperature variation during

the whole reaction period. Nitrogen flow of 1 l/min was maintained throughout the experiments in order to ensure inert atmosphere during the reduction of Fe^{3+} oxide into Fe^{2+} oxide and metallic iron.

To determine the content of metallic iron in the samples, the Zhiyong Xu method with a tolerable error ranged below 1 wt.% was used [186].

7.2 Microwave roasting process optimization

The influence of microwave energy on the sample, the effect of irradiation time together with addition of carbon source to BR (C/BR ratio) were the parameters investigated to find the optimized combination to convert iron oxides into metallic iron, according to the sequence of $Fe_2O_3 \rightarrow Fe_3O_4 \rightarrow FeO \rightarrow Fe$ [36,186,187].

7.2.1 Influence of microwave energy

A possible approach to determine the microwaves influence on the given material, is the quantification of the absorbed power from the sample, with a laboratory-scale microwave system [132]. The power absorbed by a sample per unit volume at a specific area in the material $P_v(z)$ is given by the Equation (10) [128,131,132]

$$P_v(z) = 2\pi f \varepsilon_0 \varepsilon_r'' |E(z)|^2 \quad (20)$$

where f is the frequency of microwaves, ε_0 is the permittivity of free space, ε_r'' is the relative dielectric loss, which accounts for the conversion of microwave (MW) energy into heat. E (z) is the root mean square of the electric field strength. As it is possible to understand from the equation above, $P_v(z)$ directly depends on the dielectric properties of the sample and the electric field strength.

One of the aims of this study was to understand the behavior of BR on power conversion during the roasting process. In this perspective, the whole range of power capacity was investigated (0 - 2 kW) by performing experiments at 0.6 kW (30 %), 1.2 kW (60 %) and 1.8 kW (90 %).

BR was mixed with metallurgical coke (C/BR mass ratio 0.180) and transformed into tablets. C to BR ratio was chosen according to the optimized results obtained from a previous work [19], BR roasting process in a conventional tube furnace. Reaction time was set to 5 minutes and the nitrogen flow (N_2) of 1 l/min was maintained constant for the entire experimental period.

In order to analyze the effect of power capacity on BR, the experiments were carried out by measuring the percentage of absorbed energy (A %(t)) from the sample at a specific time and a specific power capacity as it is explained in Equation (21).

$$A\,\%(t) = [100 - \left(\frac{A_s\,(t)\cdot 100}{A_e(t)}\right)] \tag{21}$$

Where $A_e(t)$ is the absorbance value at a specific power capacity of the empty chamber collected with multimeter and $A_s\,(t)$ is the absorbance value of the sample collected with multimeter at the same power capacity employed during the empty chamber experiment. The absorbed energy from the samples was evaluated by collecting the values and combining the two series of experiments with the same power capacity.

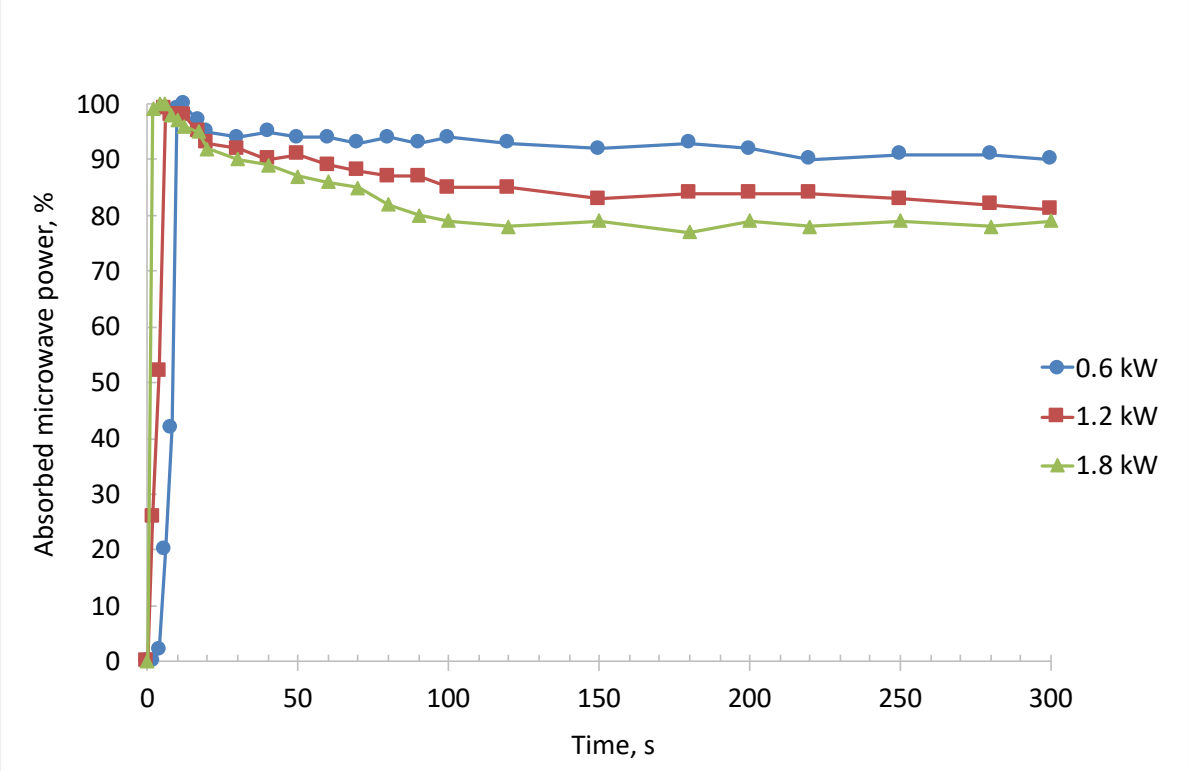

Figure 38. Percentage of the absorbed microwave power from BR, mixed with metallurgical coke (C/BR 0.180), by choosing three different power capacities, 0.6 kW, 1.2 kW and 1.8 kW at 1 l/min N_2 flow constant for 5 min

During the experiment at 0.6 kW (blue line) at the above-mentioned conditions, the modified BR absorbed 100 % microwave energy in 10 seconds. As it possible to observe in Figure 38, after 10 seconds, the absorption decreased due to the reduction of the samples and the liberation of the off

gases. To achieve the highest sample absorption, the 3-stubs tuner present in the waveguide were employed and the absorption was maintained constant around 94 % for 0.6 kW.

When the power capacity was set at 1.2 kW (red line) and successively at 1.8 kW (green line), a rapid absorption of microwave energy (5 seconds for 1.2 kW and less than 1 second for 1.8 kW) by the BR was observed. Increasing the power capacity, the electromagnetic field increased ($E(z)$ Equation (21)), and the consequence is a microwave absorption extremely fast.

On the other hand, the absorption was retained at above 85 % for the experiment at 1.2 kW and 80 % with 1.8 kW power capacity.

This behavior is attributed to the reduction of Fe^{3+} oxides into Fe^{2+} oxides and into metallic iron, as it is confirmed in the XRD profile (Figure 39). As the reaction proceeds, the matrix of material is continuously changing as well as its dielectric properties affecting the microwave energy absorption[188]. The energy absorption from the sample is then controlled by using the 3 stubs system of the furnace.

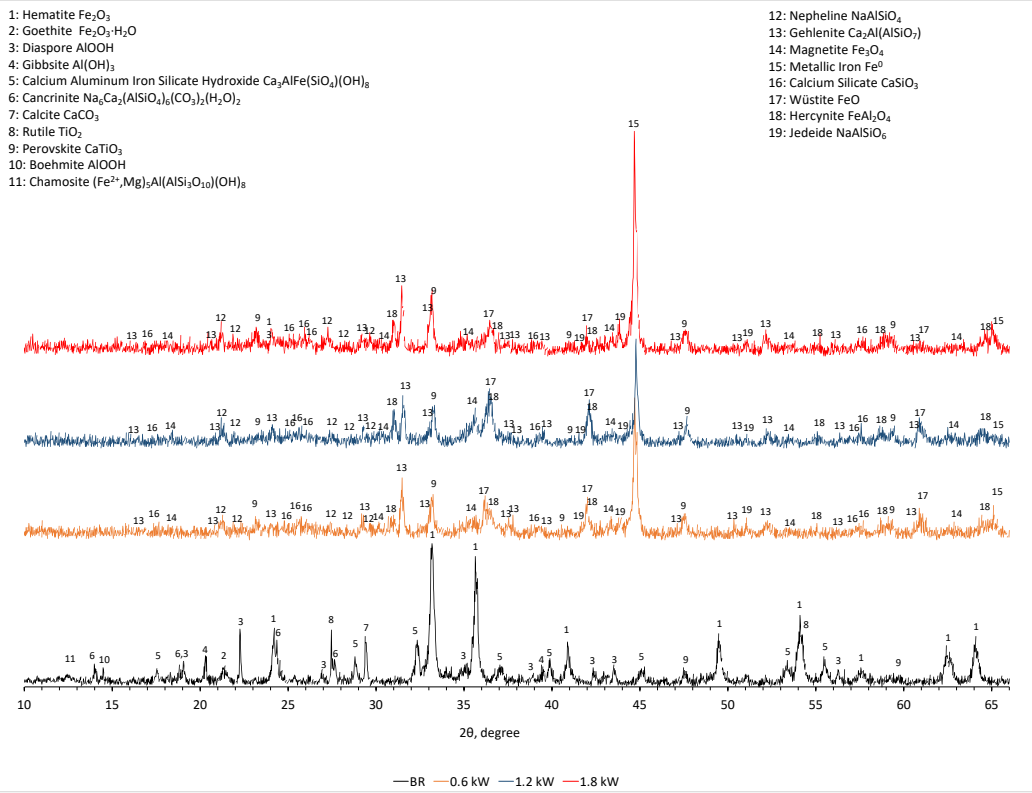

Figure 39. XRD of sinters (C/BR 0.180, and 1 l/min N_2 flow constant for 5 minutes) by changing the amount of MW energy (0.6 kW, 1.2 kW and 1.8 kW) and compared to XRD of bauxite residue

The presence of metal in the sample caused a reflection of microwave energy, due to the high material conductivity [31,34,128] that reduced the 3-stubs tuner effect.

As a consequence of the absorbed energy from the given material, sample temperature increased, and this behavior is explained by the Equation (22):

$$P_v = \rho C_p \frac{\Delta T}{\Delta t} \tag{22}$$

where ρ is the density of the material, C_p is the specific heat of the material, ΔT is the temperature variation and Δt is the time variation [133,134].

Since the effectiveness of the microwave energy absorption by the sample, is reflected on the instantaneous heating of material, temperature has been recorded during the whole duration of the tests by using an optical pyrometer which pointed the sample surface (Figure 40).

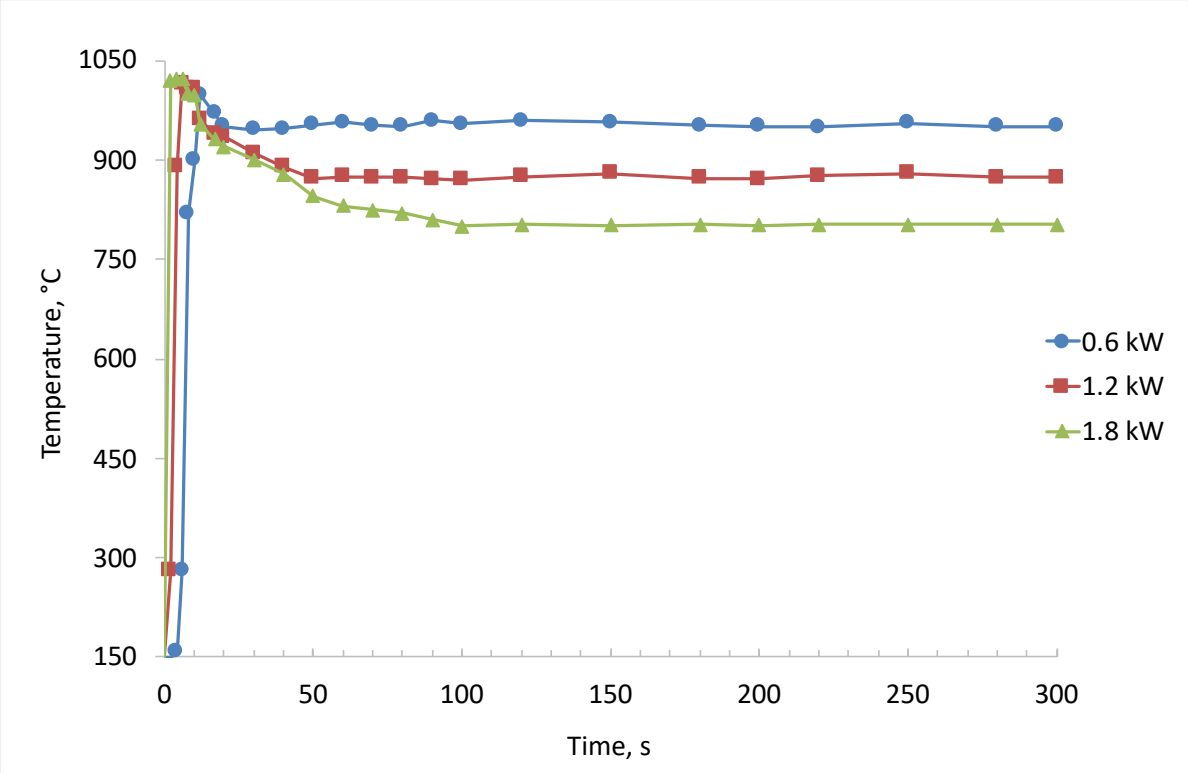

Figure 40. Heating rates of BR mixed with metallurgical coke (C/BR 0.180), by choosing three different power capacities, 0.6 kW, 1.2 kW and 1.8 kW at 1 l/min N_2 flow constant for 5 min

During the experiment at 0.6 kW, the sample has reacted at 998 °C in 10 seconds absorbing the maximum of energy. The use of 3-stub tuner had allowed to achieve a value above 950 °C.

In the case of 1.2 kW, a temperature of 1015 °C has been attained after 5 seconds and then temperature was kept constant at about 860 °C.

For the experiment at 1.8 kW, temperature exponentially rose within a second to 1020 °C. However, it is possible to observe that temperature considerably decreased at around 800 °C, due to the presence of the conductive material which defeats the effect of the 3-stubs tuner.

The results obtained from the experiments have shown the behavior of BR by using different power capacities. When power capacity was set at 0.6 kW, the iron phases present in the initial sample, were converted into magnetite (Fe_3O_4), wüstite (FeO), metallic iron (Fe^0) and hercynite ($FeAl_2O_4$) with an absorbed microwave power of 95 % and a maximum temperature of 998 °C.

7.2.2 Irradiation time

To analyze the behavior of the sample by changing the irradiation time, different sets of experiments have been performed at 180 seconds, 300 seconds and 600 seconds, while keeping constant all the other parameters at 0.6 kW, C/BR 0.180 and 1 l/min nitrogen flow.

From the comparison of the XRD spectra of BR and the sample after microwave heating treatments (

Figure **41**), it is possible to mark that the complete transformation of iron containing phases (hematite, goethite and calcium aluminum iron silicate hydroxide) present in BR, into metallic iron, wüstite, hercynite, magnetite and maghemite is favored by increasing the irradiation time. The other elements (Ca, Si, Al, Ti and Na) are present mainly in sodium and calcium aluminosilicate phases as well as perovskite and calcium silicate.

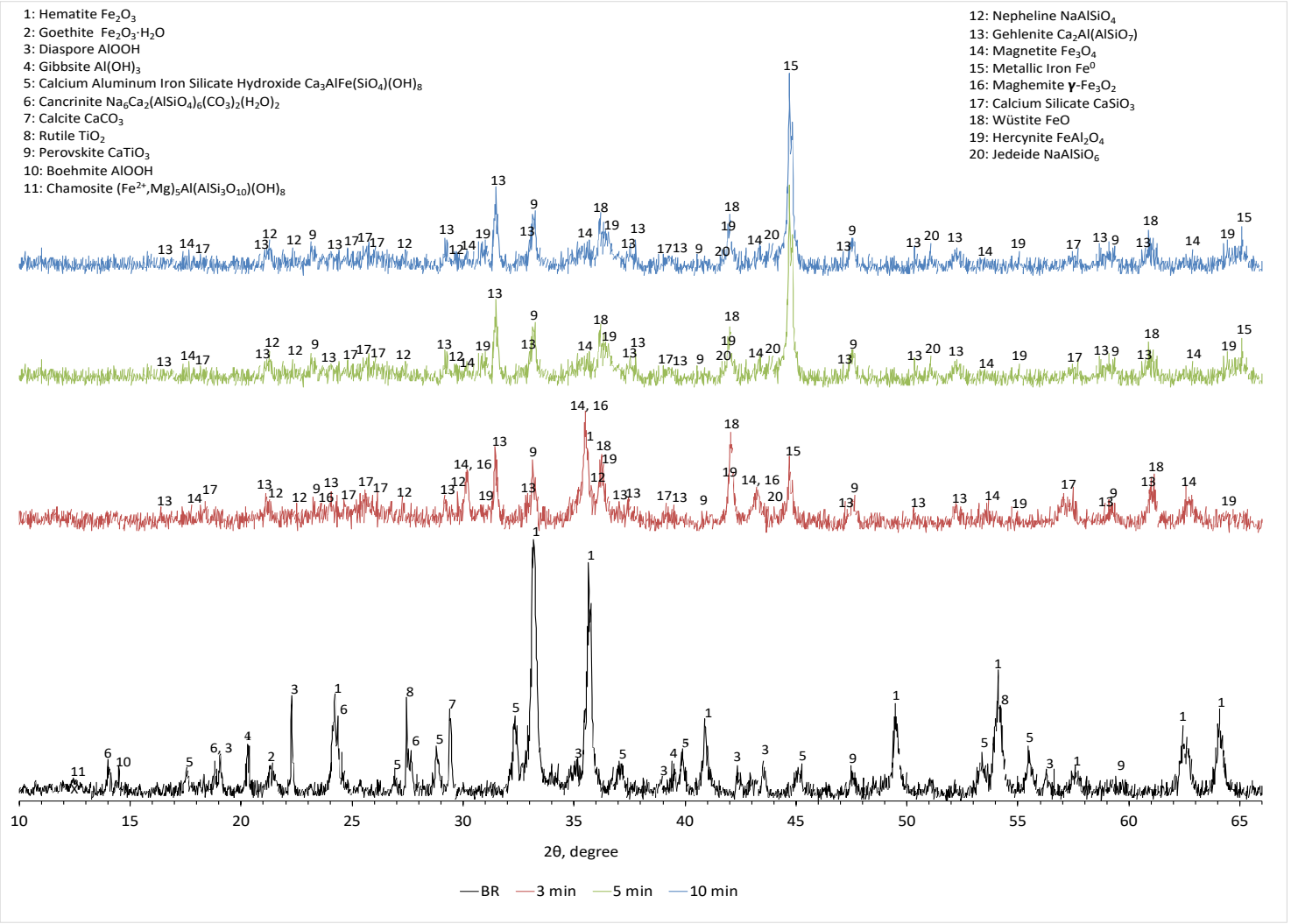

Figure 41. XRD of sinters (C/BR 0.180, 0.6 kW and 1 l/min N_2 flow) by changing the irradiation time at 180 seconds, 300 seconds and 600 seconds compared with XRD of bauxite residue

At 180 seconds, a peak of hematite is still observed. This is because the reaction was not complete, since the sample was exposed to the microwave radiation for a short period. As it can be seen in Figure 42 the tablet showed a black, partially molten state in the centre, while the outer rim of the disk remained reddish, comparable to its initial state.

Figure 42. Tablet after 180 seconds irradiation time at 0.6 kW, C/BR 0.180 and 1 l/min nitrogen flow

At 300 sand 600 seconds, hematite and maghemite peaks disappeared while magnetite, hercynite, wüstite and metallic iron were the main iron mineralogical phases among the other constituents.

Figure 43. Tablet after 300 seconds irradiation time at 0.6 kW, C/BR 0.180 and 1 l/min nitrogen flow

The above observations explain well the microwave heating behavior. The microwave radiation went through the sample, the heat was generated inside the tablet and then it was transferred to the surface of the material [132]. Therefore, at 300 seconds, the tablet resulted completely roasted (Figure 43), promoting the reduction of trivalent iron oxide into bivalent ones and metallic iron.

However, increasing the irradiation time, the presence of conductive material (such as metallic iron) caused a reflection of microwave energy. Indeed, after 300 seconds, the percentage of microwave absorption fluctuated, even though the 3-stubs tuner were employed for the entire experimental period (Figure 44).

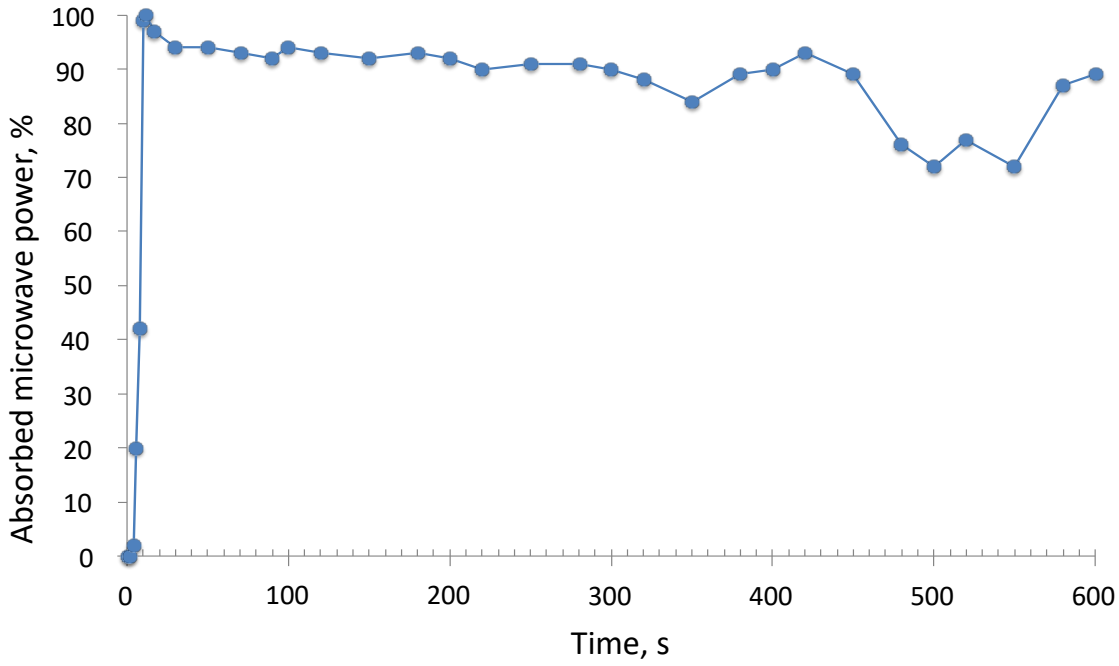

Figure 44. Percentage of the absorbed power from BR, mixed with metallurgical coke (C/BR 0.180) at 0.6 kW, 1 l/min N_2 flow constant for 600 seconds

The result of the irradiation time optimization is the production of sinter containing Fe_3O_4, FeO, Fe^0 and $FeAl_2O_4$ among the other constituents at 300 seconds.

7.2.3 Carbon source addition to BR

To clarify the role of C during the microwave roasting process and the heating behavior of BR, experiments were carried out by analyzing a BR tablet without the carbon source addition. The other parameters that were examined span the whole power capacity range (0 - 2 kW) and irradiation time between 300 and 600 seconds. The nitrogen flow remained constant at 1 l/min.

Figure 45 (a) shows the percentage of the microwave power absorbed by BR without the addition of C, at 0.6 kW, 300 seconds and 1 l/min nitrogen flow. At these conditions, it is observed that the absorbed power was negligible because the sample can be considered as a poor receptor to microwave energy. This behavior was also confirmed during the experiments at higher power capacity and irradiation time.

The above observations proved that the carbon source addition is required to facilitate the microwave absorption by the sample, in fact carbon is a good receptor of microwave energy [36]. Therefore, the heat is transferred through the BR material, promote the hematite and goethite reduction, as it was shown in the previous study [19].

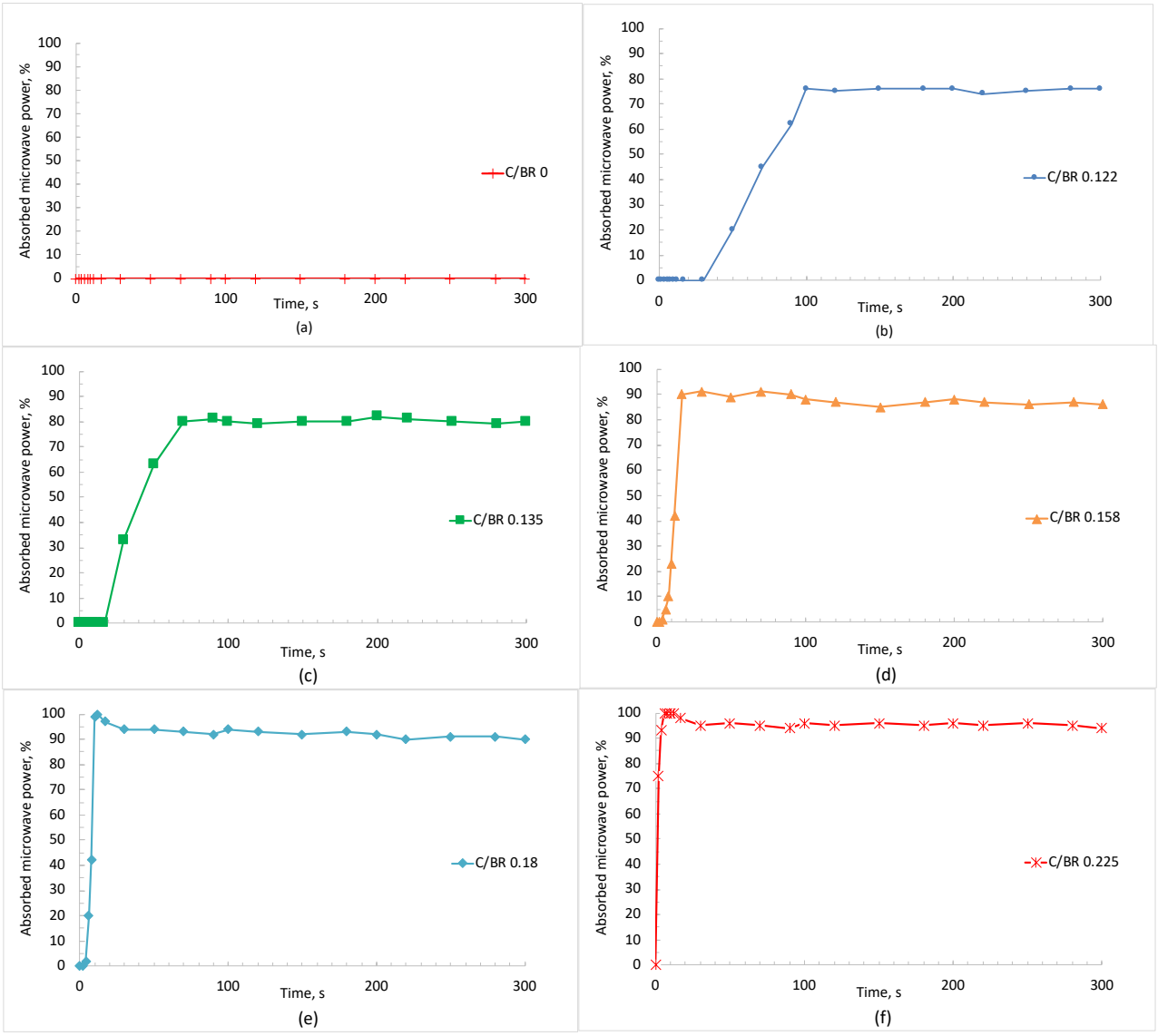

Figure 45. Percentage of absorbed microwave power from BR varying C/BR ratios ranging between 0.122 and 0.225 at 0.6 kW (30 %), 1 l/min N_2 flow constant for 300 seconds

To investigate the effect of C/BR ratio on microwave reductive roasting, several sets of experiments were performed at 0.6 kW, irradiation for 300 seconds with a constant 1 l/min N_2 flow. The following C/BR ratios were studied: 0.122, 0.135, 0.158, 0.180 and 0.225.

As it is shown in Figure 45 (b), during the microwave absorption of the sample irradiated for 300 seconds at 0.6 kW with a C/BR of 0.122, a two-step absorption sequence was observed. Up to 30 seconds of irradiation time, no absorption was registered; while after that time, the absorption rose

to 75 % and remained constant by using the 3-stubs tuner. At these conditions, the highest T recorded was at about 780 °C. Similar behavior with 0.135 C/BR was noted with 80 % microwave energy absorption and a maximum temperature of 830 °C (Figure 45 c). On the other hand, the absorption of microwave power is favored when increasing carbon/bauxite residue ratio. As it is observed for 0.158 C/BR (Figure 45 d), the energy absorption is kept almost constant at 90 % with a T around 950 °C, while for 0.180 at 95 % and a maximum T of 998 °C (Figure 45 e). Regarding C/BR 0.225 (Figure 45 f), an immediate absorption is noted and by employing the 3-stub tuner, the energy absorption was controlled at 98 % with a detected temperature of 1100 °C.

At low C/BR ratio it is possible to observe a "dead" initial period (Figure 45 b, c and d) which decreases as the C/BR ratio increases, although it is evident even at the ratio of 0.180 (Figure 45 e). This phenomenon can be attributed to the amount of heat generated per volume of material and the rate of heat transferred by conduction (q_k) which is proportional to dT/dx according to the Fourier law (Equation **Errore. L'origine riferimento non è stata trovata.**).

$$q_k = -k\,A\,\frac{dT}{dx} \tag{23}$$

where k is the thermal conductivity of the material that is temperature dependent; A is the area through which heat is transferred, T is temperature and x the direction of the heat flow [189,190].

During the MW experiment at C/BR 0.122, the initial “delay” observed depends on the small number of hot spots generated in the sample compare to the volume of the material. Consequently, the rate of heat transferred by conduction is low due to the high distance in-between a specific hot spot and its cold surround. Therefore, the sample composed with low C/BR ratio needs time to warm up net of the masses. On the other hand, when the ratio C/BR increases, the amount of heat generated per volume of material and dT/dx also increase, because more hot spots per volume are created. Therefore, time needed to disperse heat inside the given volume of material decreases and at extremely high C/BR ratio becomes practically negligible.

The mineralogical characterizations of the sinters by changing the C/BR ratio between 0.122 and 0.225 are presented in

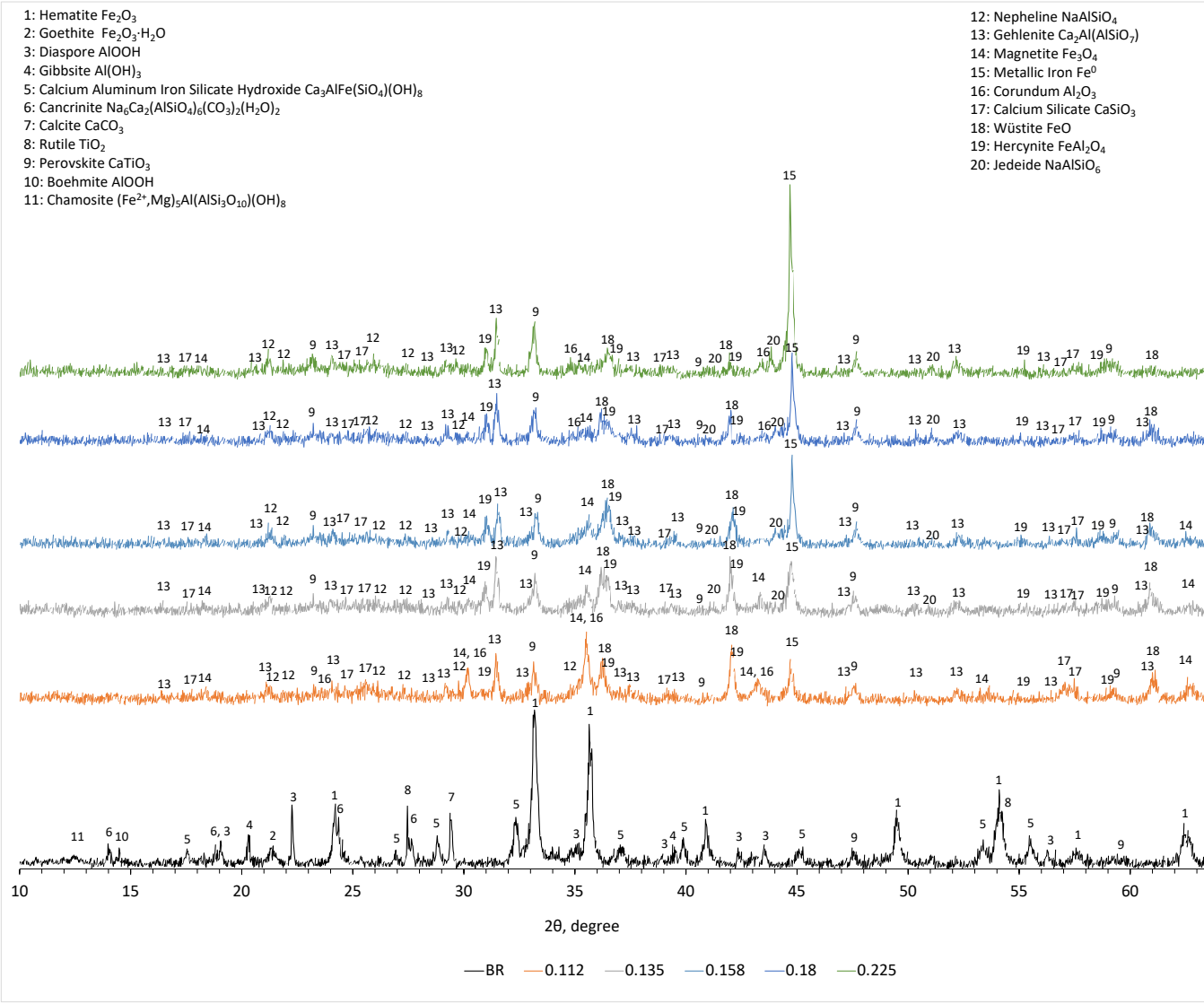

Figure **46**. The XRD analysis revealed the complete transformation of BR iron phases Fe_2O_3 and $Fe_2O_3·H_2O$ into Fe_3O_4, γ- Fe_2O_3, FeO, Fe^0 and $FeAl_2O_4$ already at 0.112 C/BR after 300 seconds and 0.6

kW (

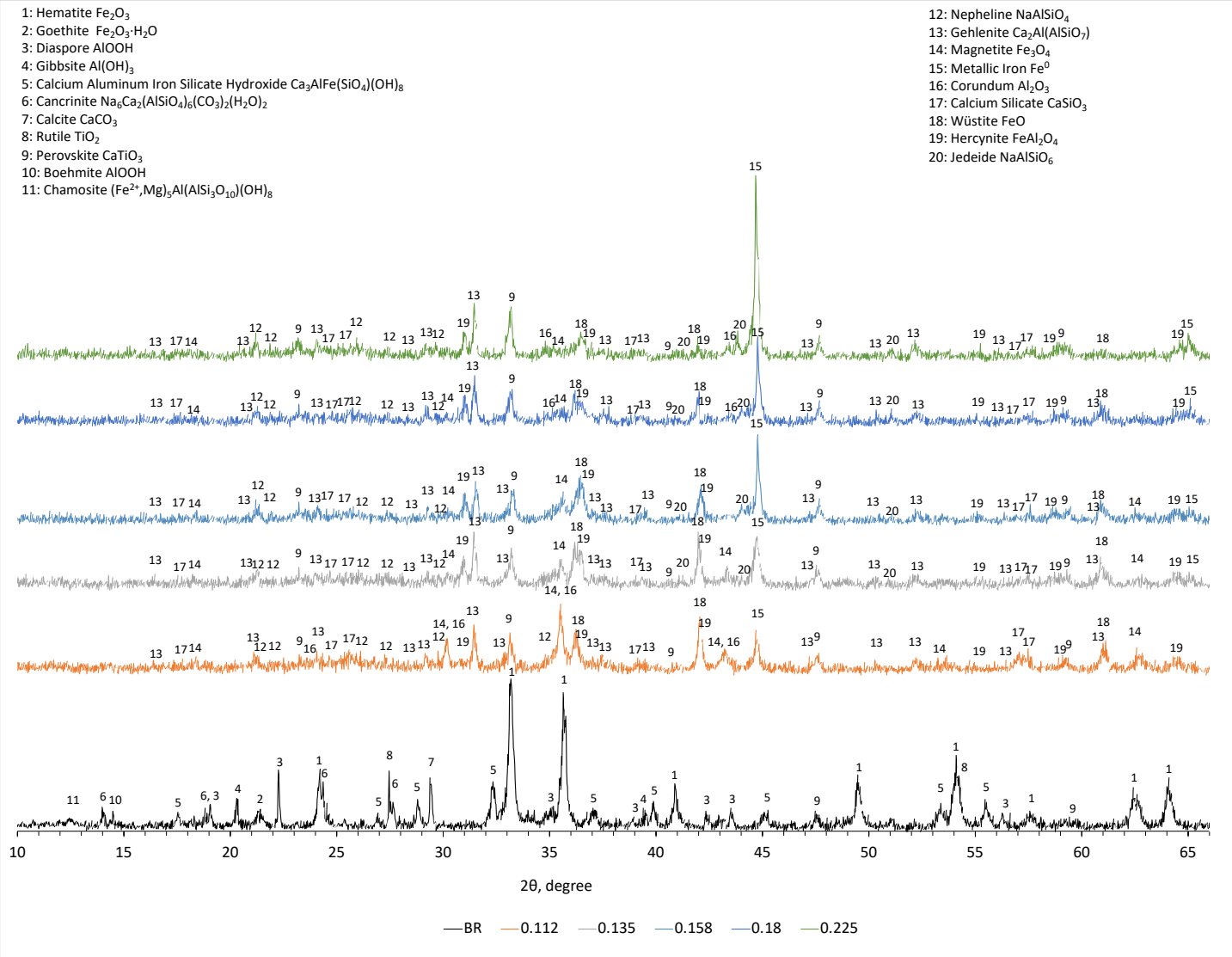

Figure **46**, orange line). At the same time, under that conditions, all alumina containing phases in BR (gibbsite, boehmite, diaspore, cancrinite and calcium aluminates) have been transformed to corundum and also into nepheline, jadeite and gehlenite which are sodium aluminosilicate and calcium aluminosilicate phases not initially existing in BR. Regarding titanium phases, these have been converted into perovskite, while the calcite peaks disappeared due to its thermal decomposition [182].

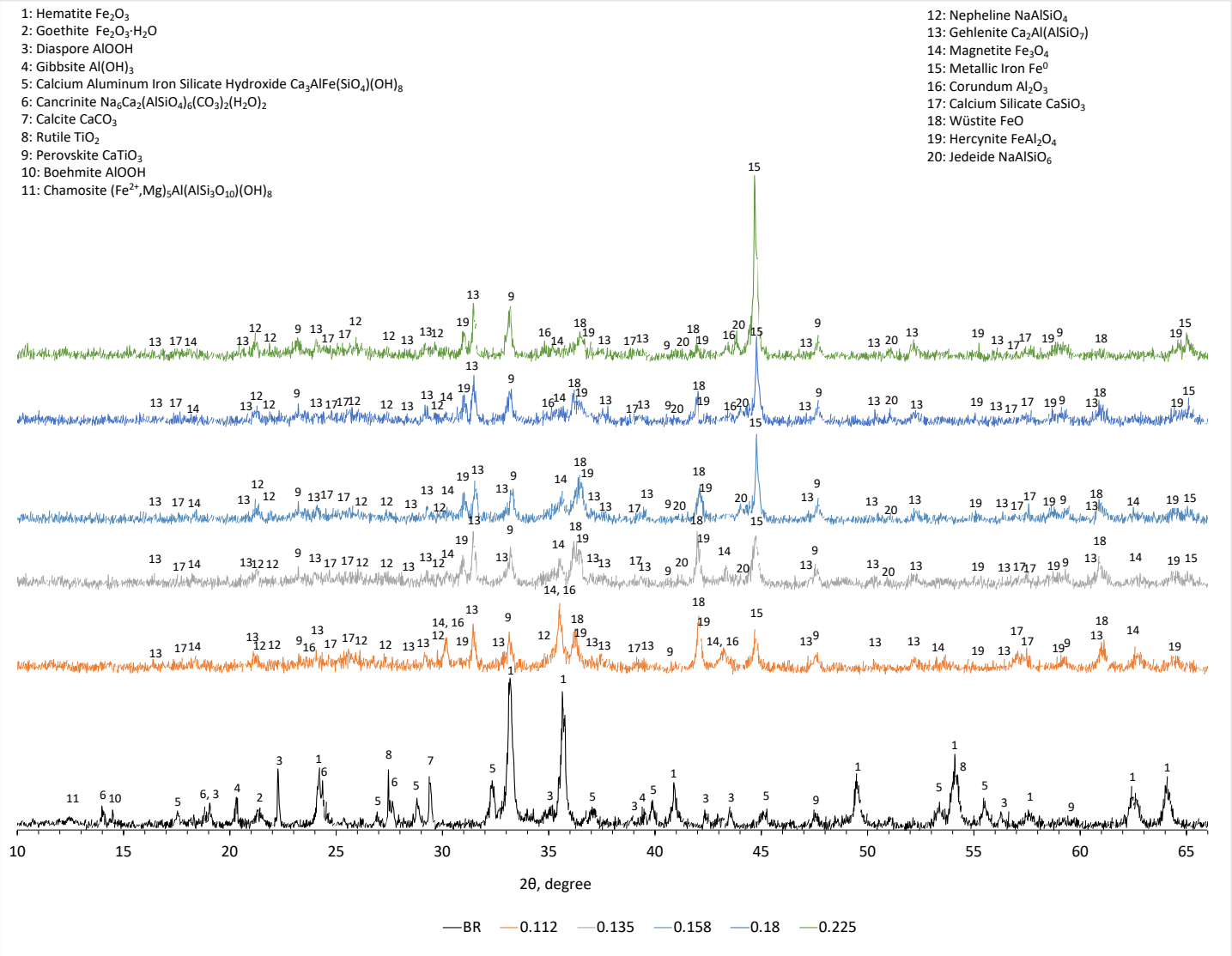

Figure 46. XRD of sinters (300 seconds, 0.6 kW and 1 l/min N_2 flow) by changing the C/BR ratio between 0.122 and 0.225 compared to XRD of bauxite residue

When increasing the C/BR ratio, an intensification of reduction conditions that foster the formation of metallic iron was observed. The Fe^0 content in the samples was determined through the Zhiyong Xu method [186] and the results shown in Table 5, confirmed the XRD profiles.

Table 5. Percentage of metallic iron / total iron content of BR and 4 different C/BR ratio sinters determined with Zhiyong Xu method [186]

Sample	% Fe^0/ Fe_{tot}
BR	0
0.122 C/BR	20
0.135 C/BR	29
0.158 C/BR	35
0.180 C/BR	57
0.225 C/BR	79

By increasing C/BR ratio from 0.122 to 0.225 C/BR, also metallic iron content increased from 20 % (0.122 C/BR) to 79 wt. % (0.225 C/BR) respectively. This is attributable to the high temperatures generated during the experiments which facilitate the conversion of trivalent iron phases, present in BR, into Fe^0.

Although 0.225 C/BR at 0.6 kW with 1 l/min N_2 flow constant for 300 seconds, can be considered the optimum conditions to obtain the best results (almost the 79 % of total Fe content present in BR, converted to Fe^0), hercynite ($FeAl_2O_4$) is still observed as the XRD analysis has shown. The backscattering electron (BES) image taken with SEM-EDS analyses confirmed the presence of $FeAl_2O_4$ Figure 47 (c) with the metallic iron which is concentrated in almost spherical particles in the matrix of material Figure 47 (b). In addition, the iron phases ($FeAl_2O_4$ and Fe^0) are entrapped in the matrix, which is mainly composed of all the other constituents Figure 47 (a).

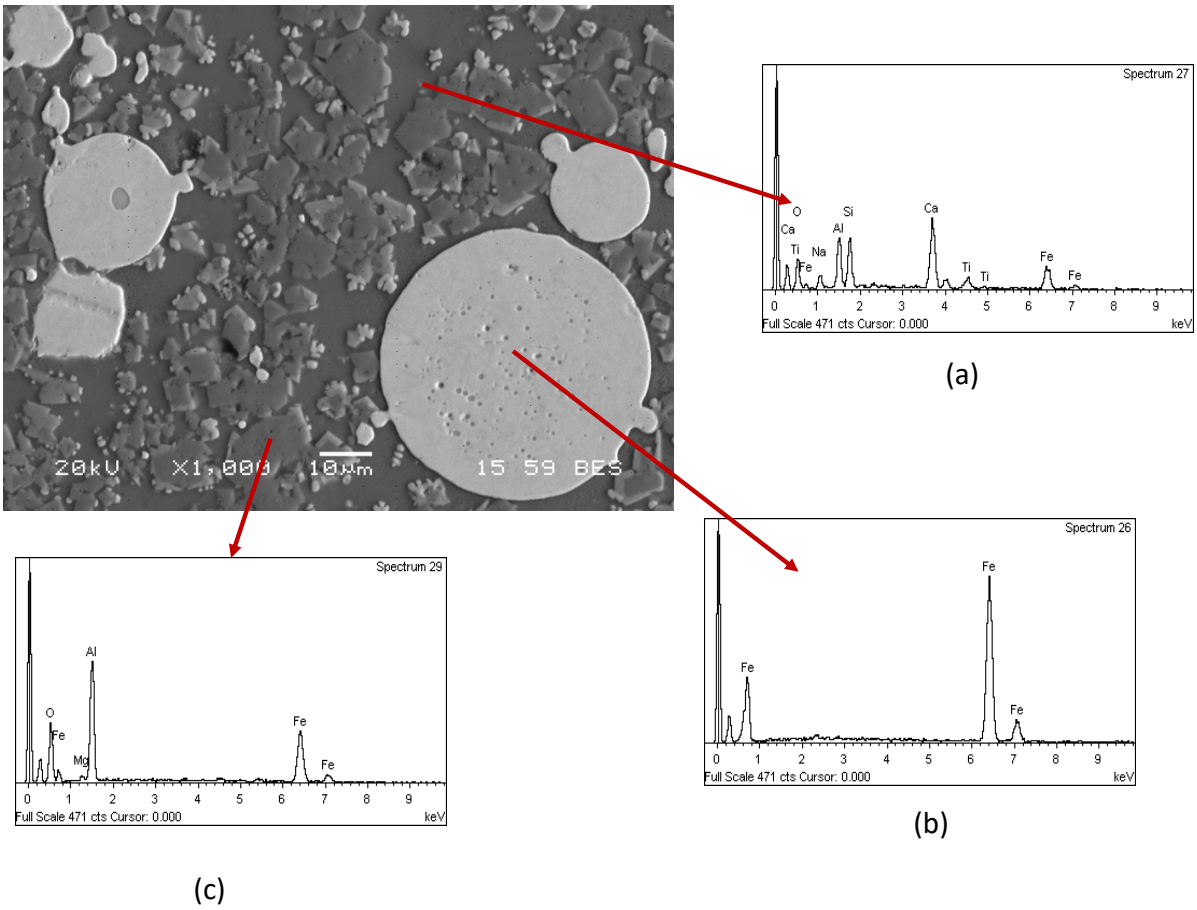

Figure 47. BES image taken with SEM-EDS analysis of 0.225 C/BR sinter

As Lu et al [158] explained in their work, the hercynite is an unavoidable product. During the roasting process, the hematite can be reduced to magnetite [19] by carbon source, but in presence of alumina can be transformed also into hercynite.

Hercynite is a normal spinel structure, where one-eighth of the tetrahedral sites are occupied by Fe^{2+} cations and one-half of the octahedral sites are occupied by Al^{3+} cations. This spinel exhibits a magnetization and can be considered as a magnetic material [191]. The presence of $FeAl_2O_4$ in the optimized sinter represents a drawback for the magnetic separation process since the magnetic fraction would be composed by oxides reducing its purity.

To avoid the presence of hercynite in the sinter, a possible scenario is to decrease Al content in BR. In fact, by adding sodium carbonate as flux all the alumina phases of BR are transformed into soluble sodium aluminates, that can be afterwards subjected to alkali leaching to recover alumina [21,109,113]. After this treatment, Fe^{+3} could be transformed into Fe^{+2} and Fe^{0} by using microwave

roasting process and the produced sinter treated with the magnetic separation process to recover iron from the other elements.

8. A combined soda sintering and microwave reductive roasting process of bauxite residue for iron recovery

In this section, an integrated process involving three stages is proposed (Figure 48) as a suitable method to transform Fe^{3+} oxides present in BR into magnetic oxides and metallic iron through a microwave roasting reduction, avoiding the formation of hercynite ($FeAl_2O_4$). Firstly, the soda roasting process of BR is taking place to transform all the alumina phases into soluble sodium aluminates which are leached out in alkaline solutions to recover alumina [21,43,192,193]. In the second stage, the leached residue is mixed with a metallurgical coke and treated in a microwave furnace at optimum conditions. After this treatment, Fe^{+3} oxides are transformed into magnetic iron oxides and Fe^0. In the final stage, the produced cinder is subjected to magnetic separation process by using a wet high intensity magnetic separator to recover iron leaving behind the other elements.

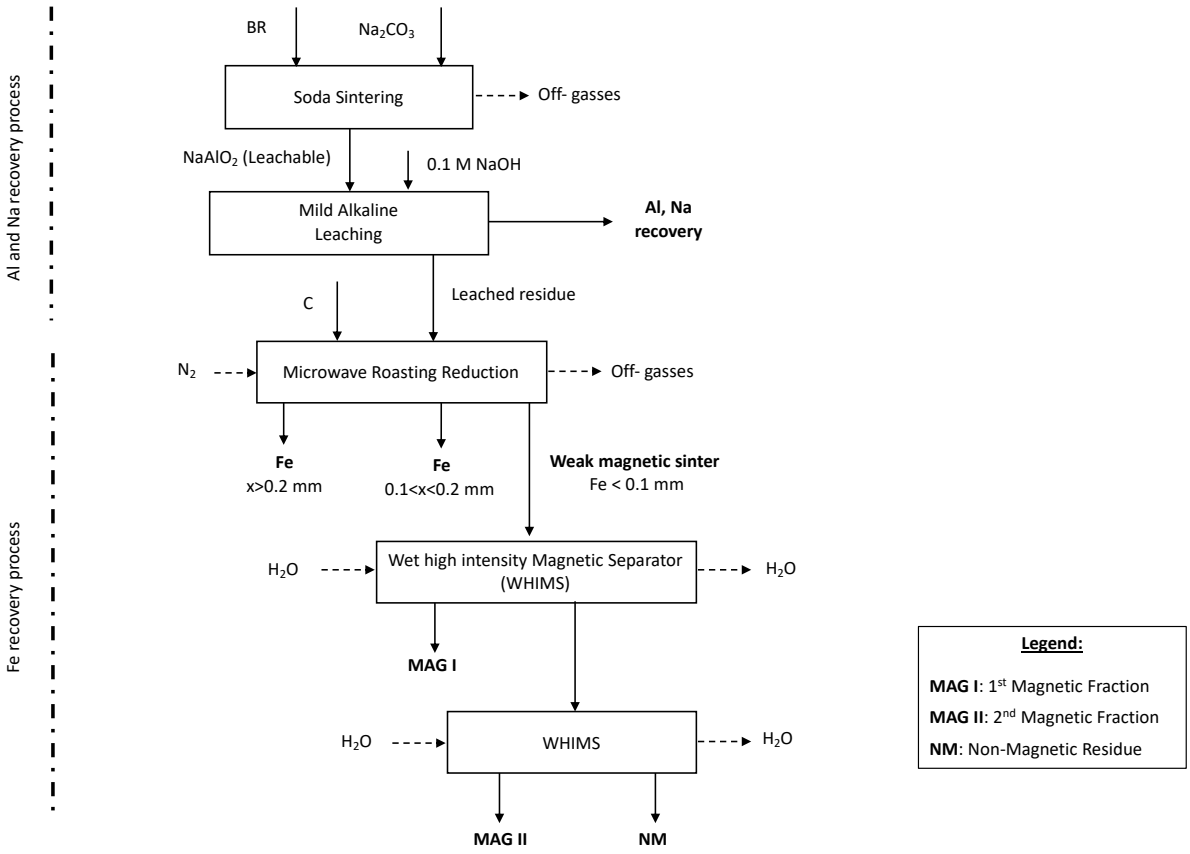

Figure 48. Conceptual flowsheet of a combined soda sintering, microwave reductive roasting process of bauxite residue and magnetic separation

8.1 Experimental devices

Experiments were carried out with a 2-kW microwave furnace mentioned in the paragraph 7.1 and the optimized setting was employed.

For the magnetic separation experimental tests, high-intensity, wet magnetic separator (WHIMS) was employed (Figure 29) [26]. An intensive magnetic field was generated through two magnet poles by applying a controlled electric field. Due to the high magnetic properties of the sinter, two current settings (0.005 A and 0.01 A) were set for the whole test duration.

Magnetic separation experiments were carried out by dispersing the optimized sinter in water (50 g of cinder in 800 ml of distilled water). The pulp was constantly stirred with an ES Overhead stirrer at 400 rpm and passed throughout the metal box by using a peristaltic pump with a flow rate of 10 ml/ min. The pulp was separated into the magnetic material, which was held to the steel spheres, and the non-magnetic material that passed through the separation zone.

The main purpose of the magnetic separation was to remove the iron-based components from the aqueous dispersion of the sinter and concentrate them in the magnetic product. To achieve the target, the feed was treated through the WHIMS two times.

In the first step, a magnetic fraction (MAG I) was collected by employing a 0.005 A current intensity, while a non-magnetic fraction was run again through WHIMS. In the second pass the current intensity was increased to 0.01 A and a second magnetic fraction was gathered (MAG II).

Magnetic I, Magnetic II and Non-magnetic fractions (residue from second pass, NM) were then dried in a static furnace at 105 °C for 24 hours and fully characterized.

8.2 Soda sintering/Leaching process

Dried homogenized bauxite residue was sintered in muffle furnace with 50 % excess of sodium carbonate (Na_2CO_3 > 99.5 % Purity) from stoichiometric amount required for sodium aluminate conversion, which amounted to 25 g Na_2CO_3 for 100 g of bauxite residue. Sintering was performed in alumina crucibles at 900 °C for 2 hours duration and left to cool overnight [43]. The sinter leaching experiments were conducted in a 1 L borosilicate glass reactor, equipped with heater, and temperature controller (thermocouple type-K) as it shown in Figure 49.

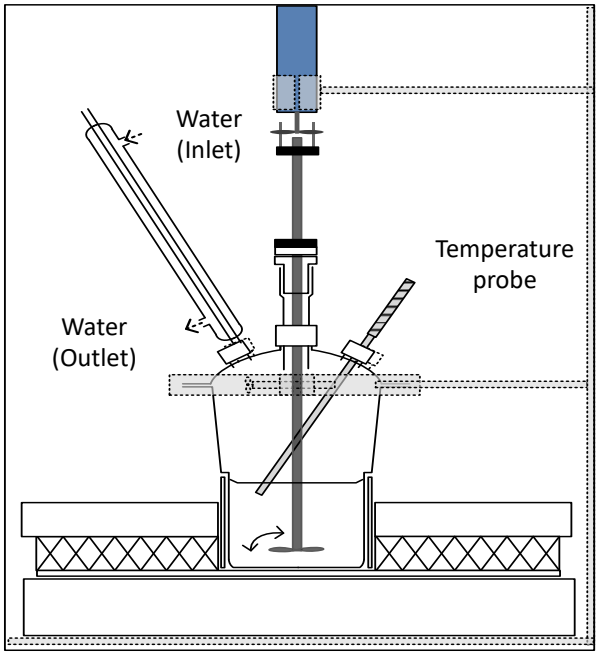

Figure 49. A schematic diagram of leaching reactor

The sinter was stirred in 0.1M NaOH solution at 80 °C for 4 hours with 1.5 % w/v pulp density at 240 rpm stirring rate. Aluminium and sodium were recovered into leachates from the leaching step, leaving solid residue that was further dried in a static oven (105 °C), which produced the modified BR (MBR) used in the next processing steps.

Figure 50 showed the mineralogical alteration of the bauxite residue after soda sintering process and mild alkaline leaching process. During the sintering step, aluminium bearing species such as boehmite, diaspore, gibbsite and complex phases such as cancrinite are transformed into sodium aluminate ($NaAlO_2$) [43]. This phase is leached out after the mild alkaline leaching step, and about 70 % of all Al is extracted from bauxite residue. Na is also co-extracted at about 85.5 %, leaving the leaching residue enriched with Fe as well as Ti for downstream processing[43]. Titanium is concentrated in the form of perovskite. Hematite is found in the leached residue and new mineralogical phases are detected in the modified BR: sodium aluminum silicate ($NaAlSiO_4$), sodium ferrotitanate ($NaFeTiO_4$) and harmunite ($CaFe_2O_4$). Table 6 shows the compositions in element wt. % basis of original bauxite residue (BR), Na_2CO_3 sintered BR and leaching residue (modified BR).

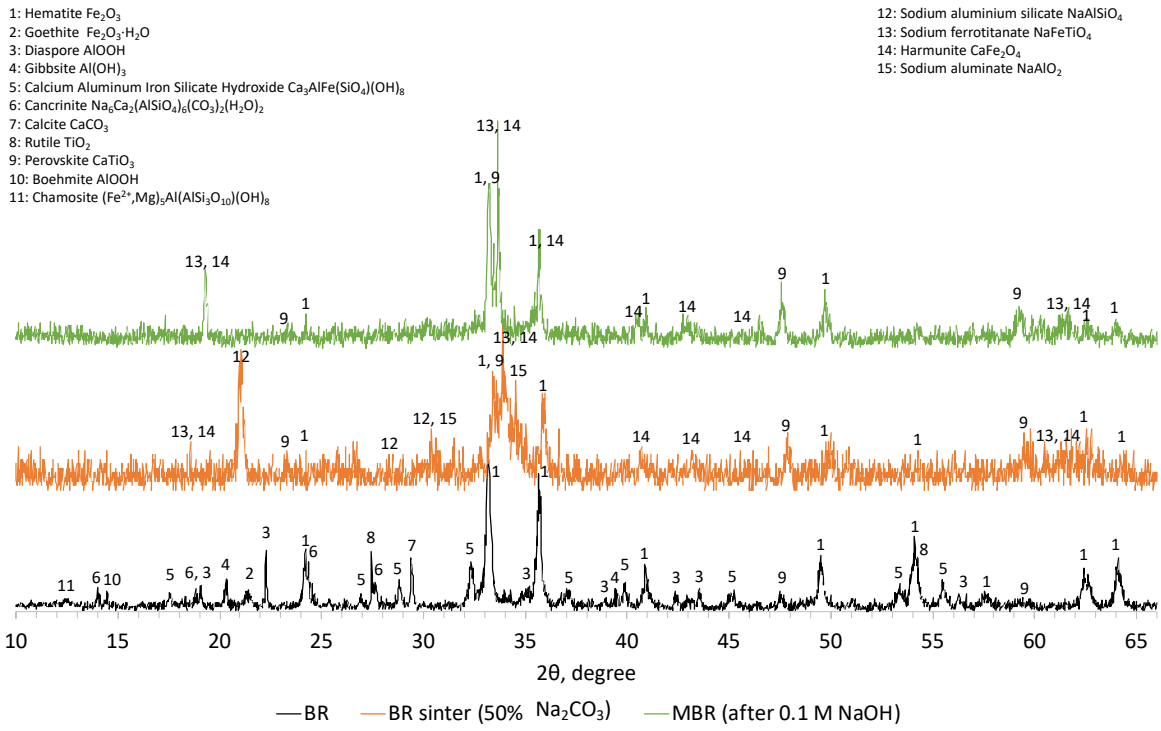

Figure 50. Comparison of the XRD profile of bauxite residue, bauxite residue sintered with sodium carbonate and leaching residue after mild alkaline leaching (0.1M NaOH)

Table 6.Chemical analysis of bauxite residue, soda sinter and leaching residue (MBR)

Sample	Fe	Al	Si	Ti	Na	Ca	OTHERS	LOI
Bauxite residue (wt. %)	30.43	10.19	3.04	3.29	2.08	6.85	0.0130	9.40
Sinter (wt. %)	27.72	9.35	2.83	2.82	14.16	6.32	0.0117	2.73
Leaching residue (wt. %)	37.47	3.83	3.25	3.64	2.86	8.53	0.0123	9.66

8.3 Microwave roasting process of modified bauxite residue

The dried modified BR (MBR) was blended with metallurgical coke (C/MBR 0.225) and it was transformed in tablets using a manual hydraulic press. The sample was treated through microwave roasting process at optimum conditions (0.6 kW, 1 l/min N_2 flow constant and 300 seconds) and then characterized via ED-XRF, XRD and SEM analyses [194].

During the microwave heating of the sample, an immediate absorption was detected, and temperature exponentially rose within some seconds to 1250 °C Figure 51.

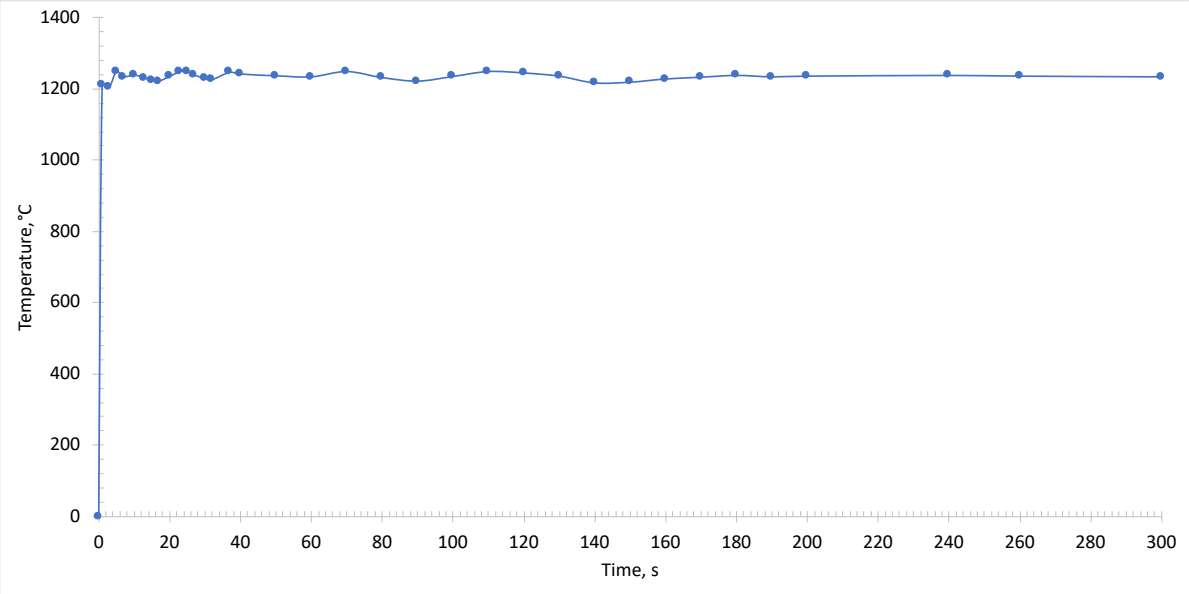

Figure 51. Heating rates of 1st MW roasting process at 0.6 kW, 1 l/min N_2 flow constant and 300 seconds

The formation of melt phases was observed through the window of the pyrometer, started from the center and propagated to the rim of the disk. In addition, at this temperature it was possible to note the reduction of iron oxide into metallic iron. In Figure 52, the cinder after the microwave roasting reduction is presented, and the presence of metallic iron nuggets is evident.

Figure 52. Cinder after 300 seconds, irradiation time at 0.6 kW, C/BR 0.225 and 1 l/min nitrogen flow

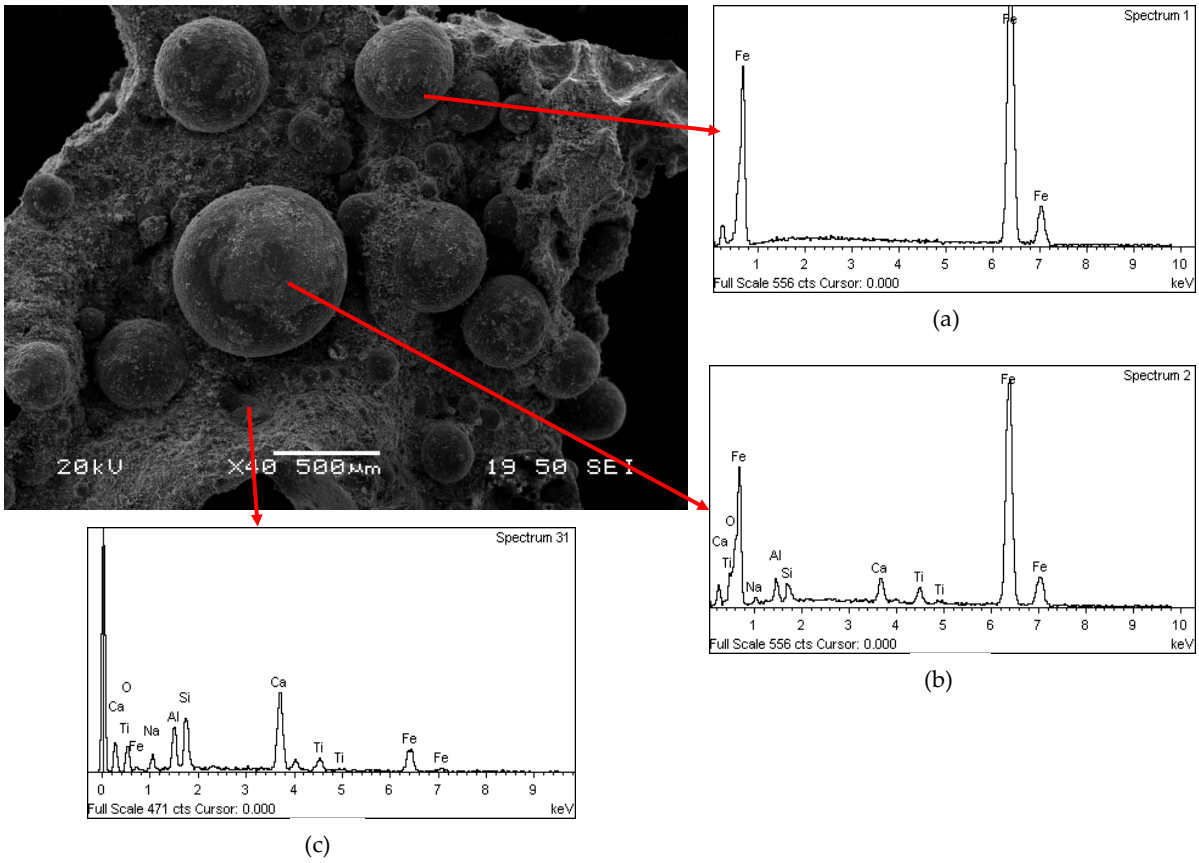

Figure 53. Second electron imaging (SEI) mode SEM-EDS analysis of sinter after the first microwave roasting reduction

SEM analysis of the cinder confirmed the presence of the spherical metallic particles which are entrapped in the matrix of the solid samples (Figure 53 a). The nuggets are covered by a layer of powder (Figure 53 b), which has the same composition of the matrix (Ca, Al, Si, Na, Ti and Fe) as it is shown in Figure 53 c.

To release the metallic iron spheres, the sample was milled through a planetary ball mill with a grinding time of 5 minutes and a speed of 400 rpm. The sample was treated four times with the planetary ball mill to transform the cinder into fine powder. The metallic iron was then separated from the matrix by employing a manual sieve. The sample was, therefore, physically separated into two fractions: the first one with a particle size higher than 0.2 mm mostly composed by Fe nuggets (around 7 wt. % of the total solid sample) and the other one with a particle size lower than 0.2 mm (around 93 wt. % of the total solid sample).

Samples were analyzed via fusion method; chemical composition of the fraction with the particle size higher than 0.2 mm and the other fraction is shown in.

Table 7. Chemical analysis of the metallic iron spheres fraction with a particle size > 0.2 mm and 1st cinder fraction with a particle size lower than 0.2 mm

Sample	Fe	Al	Si	Ti	Na	Ca	C
> 0.2 mm wt.%	95.84	0.02	1.15	0.76	0.01	1.94	-
1st cinder fraction (< 0.2 mm) wt. %	35.26	4.33	3.63	4.08	3.23	9.54	8.35

Chemical analysis confirmed (Table 7) that the main component of the fraction with particle size higher than 0.2 mm is metallic iron, being more than 95 wt. % of the total weight of the fraction. In addition, the other fraction (1st cinder fraction (< 0.2 mm)) still contains a considerable amount of iron. Analyzing the Fe mass balance, from 35.53 g of iron present in MBR, 29.59 g of Fe are present in the 1st MW cinder while 5.94 g in the > 0.2 mm fraction.

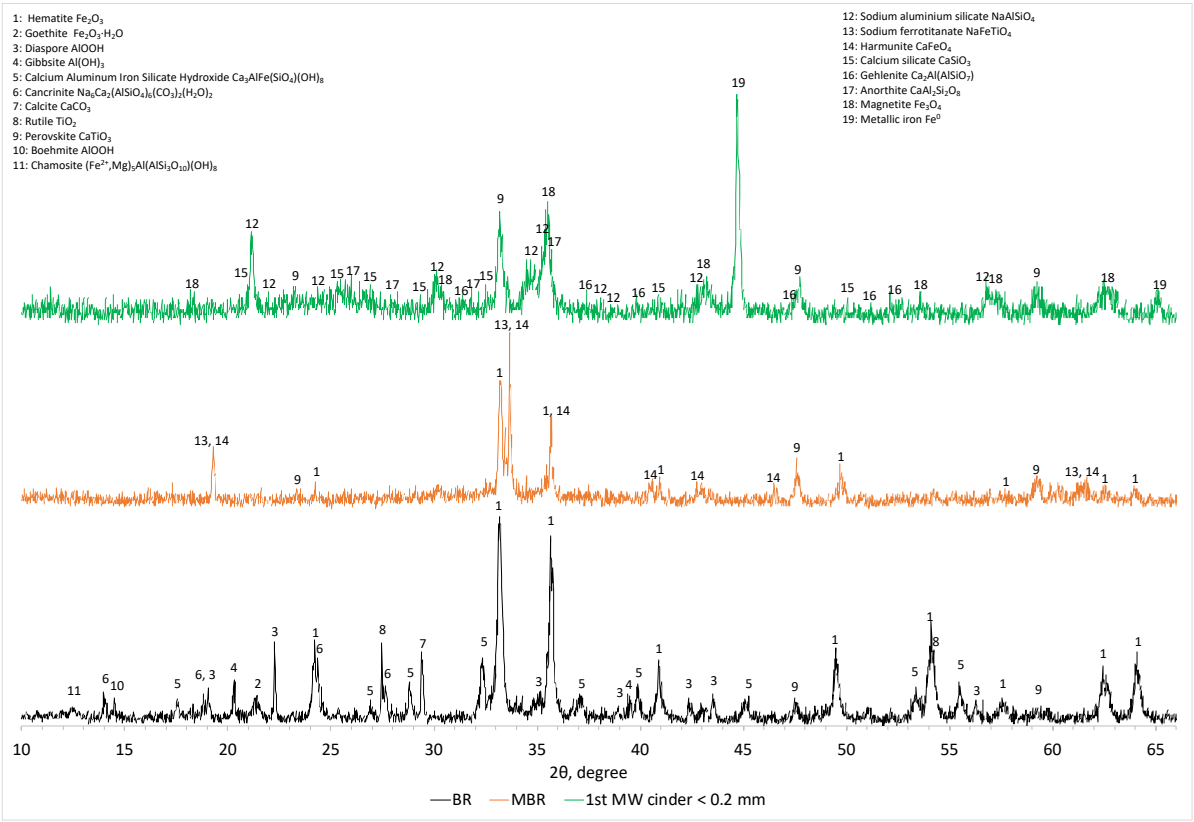

Figure 54. Comparison of XRD profiles of bauxite residue, modified BR and 1st cinder fraction with particle size < 0.2 mm

Comparing the XRD profiles of BR, leached residue and the fraction with a particle size lower than 0.2 mm (Figure 54), the results obtained with chemical and SEM analyses were confirmed. In fact, magnetite (Fe_3O_4) and metallic iron (Fe^0) are the main iron mineralogical phases after the microwave roasting reduction at the optimum conditions (C/MBR 0.225, 0.6 kW, 1 l/min N_2 flow constant and 300 seconds). Hercynite ($FeAl_2O_4$) is a mineralogical phase that is not formed during microwave reductive roasting of aluminum depleted MBR materials (Figure 54).

Decreasing the concentration of aluminum in the MBR sample, hematite and other iron-bearing phases are directly reduced into magnetite and then due to the high temperature into metallic iron. At the same time, under these conditions, small part of sodium aluminum silicate ($NaAlSiO_4$) existing initially in MBR is transformed to anorthite ($CaAl_2SiO_3$) as well as gehlenite ($Ca_2Al(AlSiO_7)$) but the major amount of aluminum in cinder remains in the form of sodium aluminum silicate ($NaAlSiO_4$) (Figure 54). In the 2-theta range of 22 to 28°, the mineralogical characterization revealed the formation of a glassy region indicated by the hump and consisting of calcium silicate ($CaSiO_3$) and anorthite. Titanium phases are converted into perovskite already from the soda roasting process and remain unchanged during the MW reductive roasting process having been beneficiated in the resulted cinder.

Since the cinder fraction with a particle size lower than 0.2 mm contained good microwave receptors (mineralogical phases such as (Fe_3O_4 and C), the sample was subjected for a second time to a microwave roasting process at the same optimum condition (0.6 kW, 1 l/min N_2 flow constant and 300 seconds), following the already described procedure.

During irradiation with microwaves, an immediate absorption from the sample was detected and the temperature exponentially rose within some seconds to 1230 °C (Figure 55).

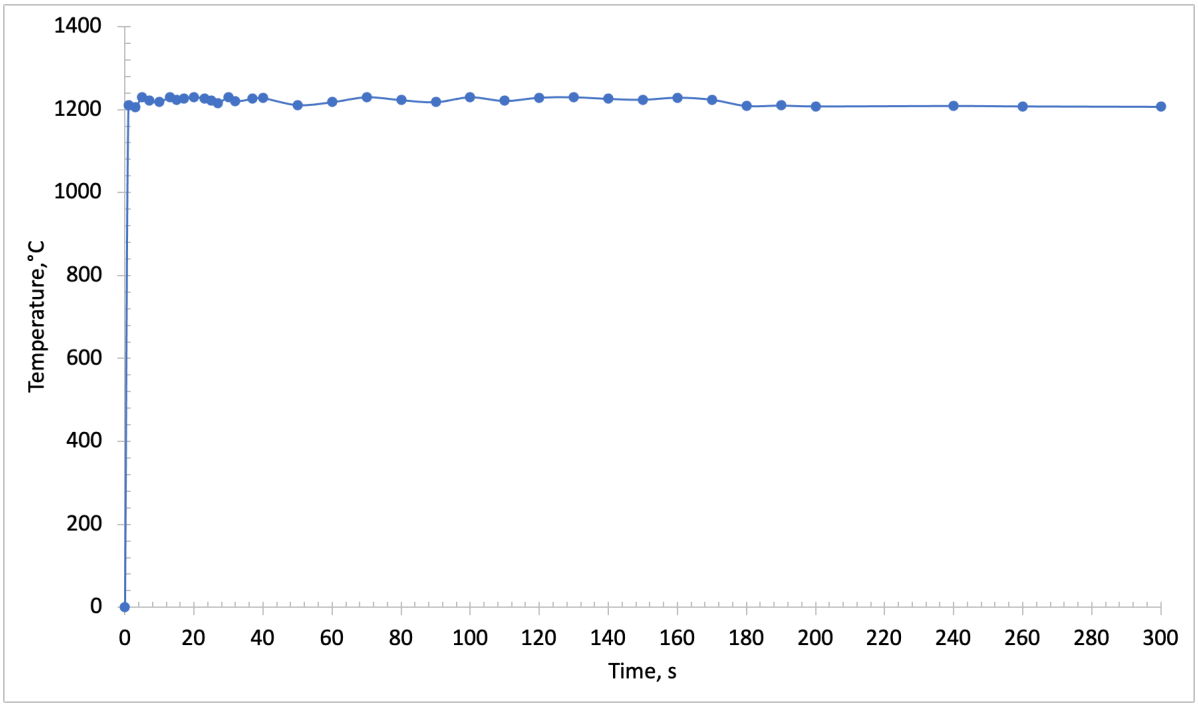

Figure 55. Heating rates of 2nd MW roasting process at 0.6 kW, 1 l/min N_2 flow constant and 180 seconds

At this temperature it was possible to note the reduction of iron oxide into metallic iron and the formation of a melt phase. Macroscopically, the 2nd cinder appeared similar to the one from the first microwave treatment, but the iron nuggets were smaller in size.

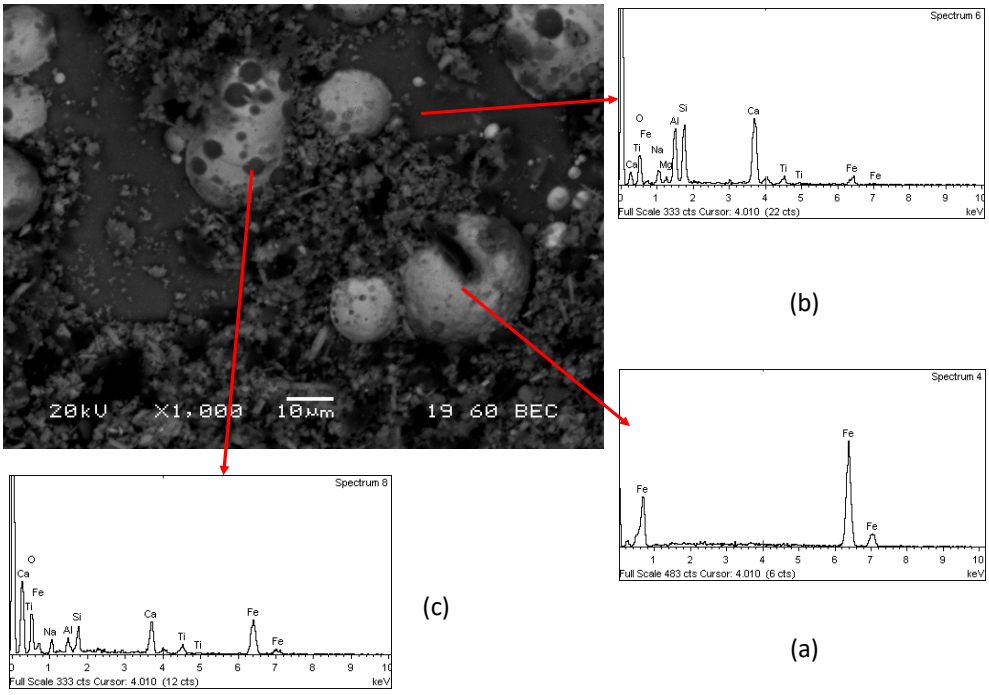

Figure 56. Back electron scattering (BEC) mode SEM-EDS analysis of the 2nd cinder after the microwave roasting reduction

In Figure 56 a back-electron scattering (BEC) picture of the 2nd cinder is shown together with EDS chemical analysis on specific components. The light gray spherical particles are metallic iron particles which are entrapped in the matrix that is mainly composed from all the other elements (Ca, Al, Si, Na, Ti and Fe) (Figure 56 b). On the top of the metallic spheres are present also some dark gray particles with the same composition of the matrix (Figure 56 c).

The 2nd cinder was grinded to release the metallic iron spheres. In this case, for the physical separation, a sieve with openings size of 0.1 mm was used. The chemical analysis of the two fractions formed are presented in Table 8.

Table 8. Chemical analysis of the metallic iron spheres fraction with a particle size > 0.1 mm and 2nd cinder fraction with a particle size lower than 0.1 mm

Sample	Fe	Al	Si	Ti	Na	Ca	C
> 0.1 mm wt.%	93.30	0.01	0.42	0.51	0.08	1.70	-
2nd cinder fraction (< 0.1 mm) wt. %	37.91	4.77	4.00	4.49	3.56	10.49	1.00

Table 8 shows that the main component of the fraction with particle size ≥ 0.1 mm, which is 1 wt. % of the total sinter weight, is metallic iron.

The other fraction is the 99 wt. % of the total sinter weight and still contains a considerable amount of iron. Analyzing the Fe mass balance, from 29.59 g of Fe present in the 1st MW cinder, 28.87 g of Fe are present in the 2nd MW cinder while 0.71 g in the >0.1 mm fraction.

The XRD analysis (Figure 57) revealed a mineralogical conformation similar to the one presented in, where magnetite (Fe_3O_4) and metallic iron (Fe^0) were the main iron mineralogical phases after the second microwave roasting reduction. The other elements are present in form of anorthite ($CaAl_2SiO_3$) gehlenite ($Ca_2Al(AlSiO_7)$) sodium aluminum silicate ($NaAlSiO_4$), calcium silicate ($CaSiO_3$) and perovskite $CaTiO_3$ as it is shown in Figure 57.

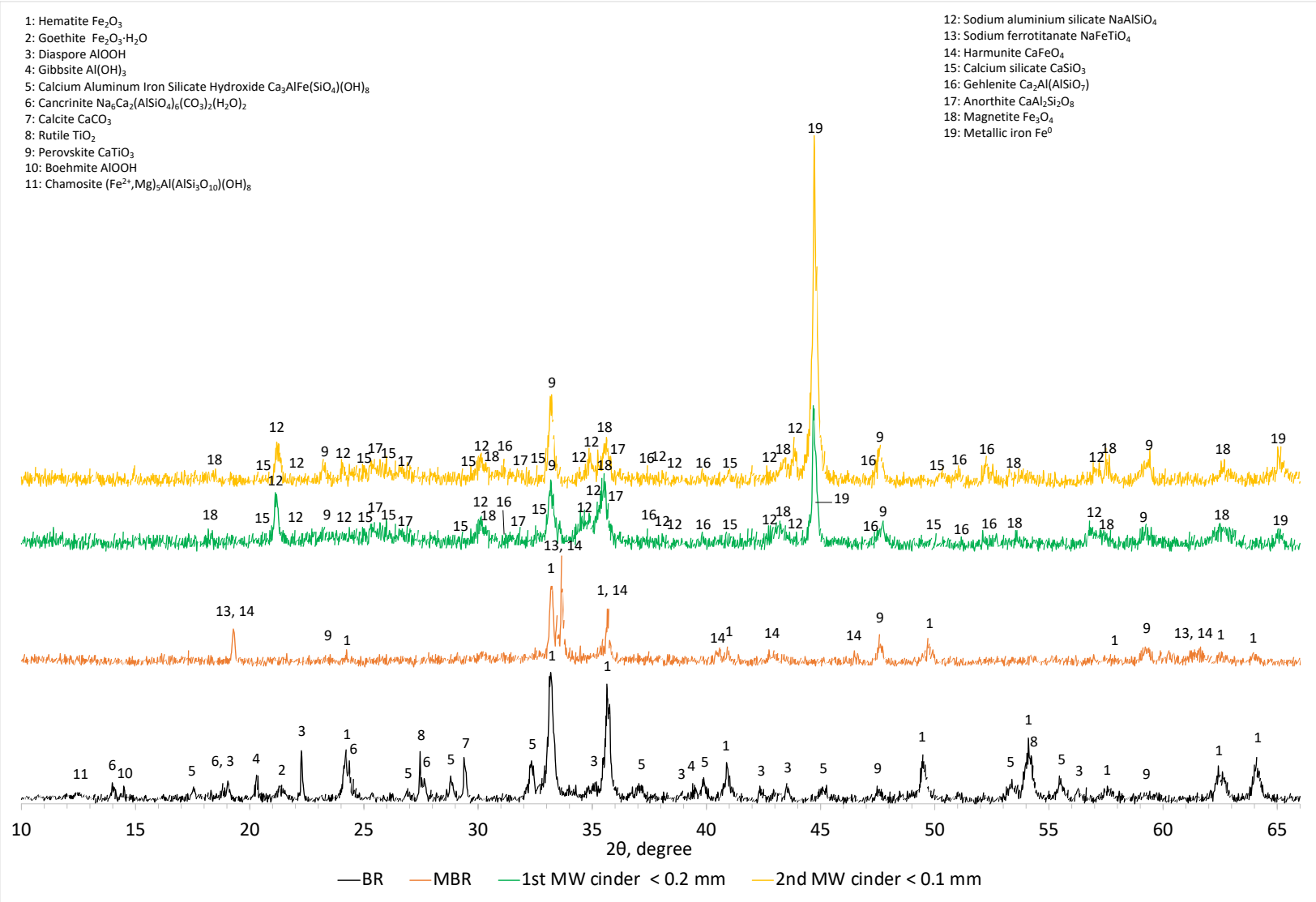

Figure 57. XRD Comparison between BR, leaching residue, cinder after 1st microwave roasting reduction and cinder after 2nd microwave roasting reduction

The experimental results from MW reductive roasting showed that although 5 minutes are enough for the full transformation of hematite to a mixture of magnetite and metallic iron, the full transformation to metallic iron necessitates more time. Even 10 minutes were not enough for this transformation. The sample was again treated at optimum conditions (0.6 kW, 1 l/min N_2 flow constant and 300 seconds) in the microwave furnace to allow the complete formation of metallic iron in the system.

The sample was transformed into tablets and placed inside the microwave furnace. As the previous microwave roasting process, an immediate absorption was detected with a consequent temperature increasing (reaching about 1250 °C). Furthermore, through the window of the pyrometer, light arcing phenomena that took place in some areas of the sample were observed. Due to these phenomena the recorded temperature locally reached around 1400 °C (Figure 58). The presence of these hot spots in the tablet depends on the interaction of metal iron, already present in the sample, with the microwave which creates a micro-arcing process [30,34,36,128,132].

After 180 seconds, a drastically reduction of T was detected from the pyrometer (Figure 58) [31,34] and the experiments were stopped as the tablet reflected the microwave energy due to the increased concentration of conductive material (such as metallic iron).

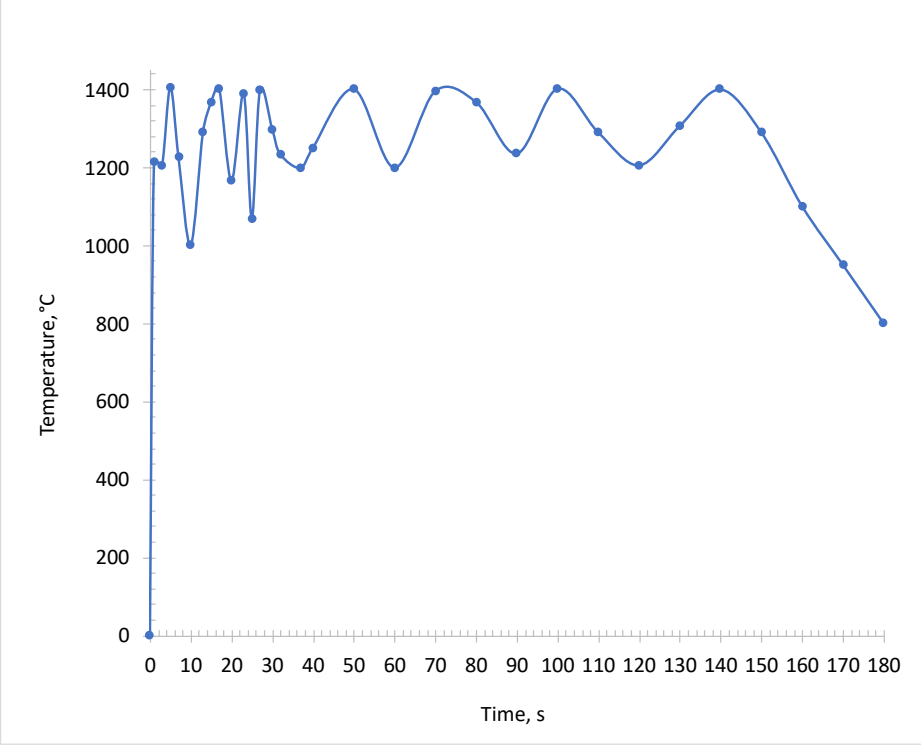

Figure 58. Heating rates of 3rd MW roasting process at 0.6 kW, 1 l/min N_2 flow constant and 180 seconds

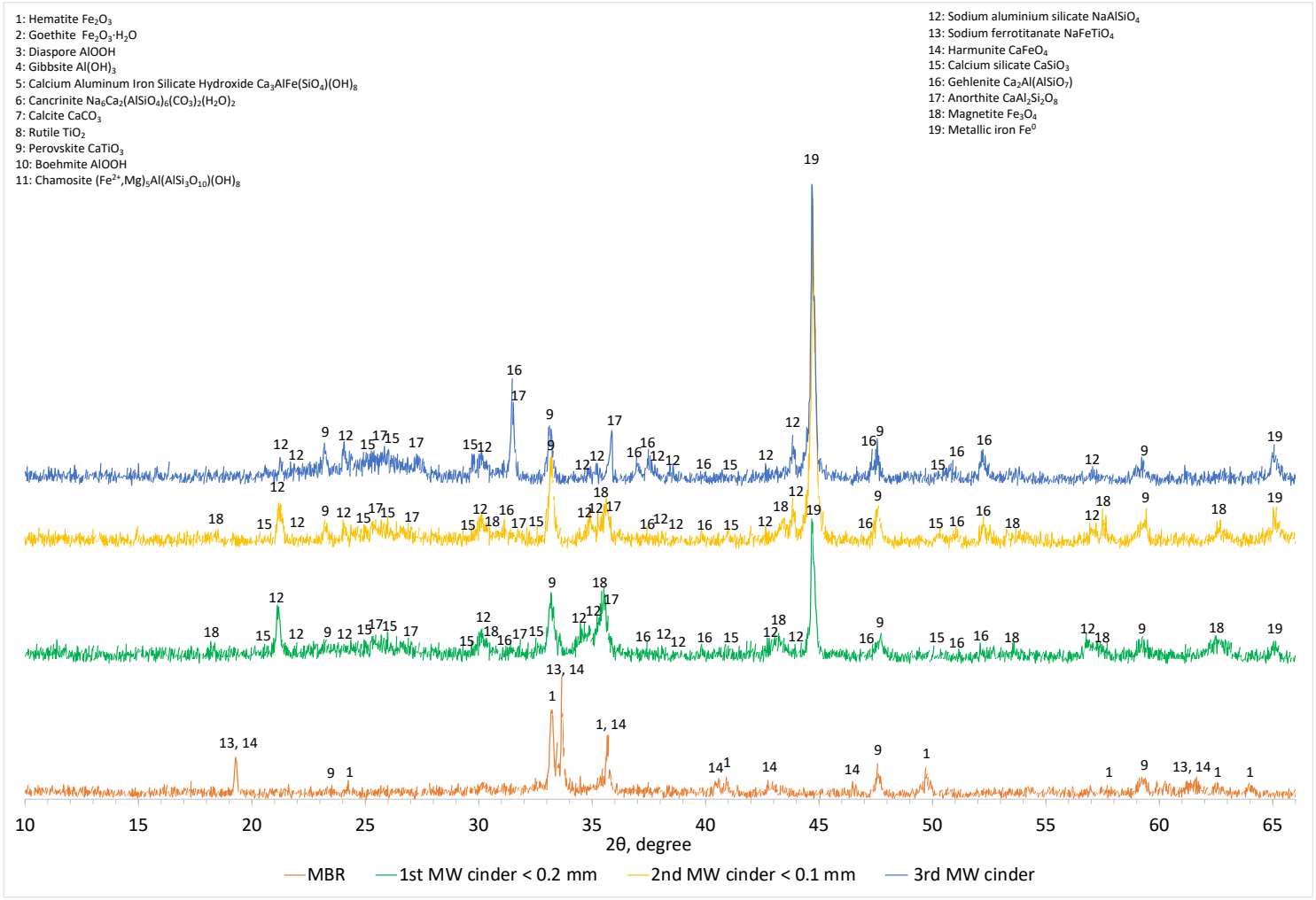

Figure 59. Comparison of the XRD spectra of MBR, cinder after 1st microwave roasting reduction, cinder after 2nd microwave roasting reduction and cinder after 3rd microwave roasting reduction

From the comparison of the XRD profile of the cinder after the 1st microwave roasting reduction (1st MW cinder < 0.2 mm), the cinder after the 2nd microwave roasting reduction (2nd MW cinder < 0.1 mm) and the cinder after the 3rd microwave roasting reduction (3rd MW cinder), it is possible to observe that metallic iron (Fe^0) is the main iron mineralogical phases in the last MW stage. In the 2-theta range of 22 to 28°, the mineralogical characterization revealed that the hump related to the formation of a glassy region consisting of calcium silicate ($CaSiO_3$) and anorthite ($CaAl_2SiO_3$), is more evident, due to the high temperature reached during the 3rd MW roasting reduction. The other elements are present in the mixed forms of gehlenite ($Ca_2Al(AlSiO_7)$), sodium aluminum silicate ($NaAlSiO_4$), and perovskite $CaTiO_3$ as it is shown in

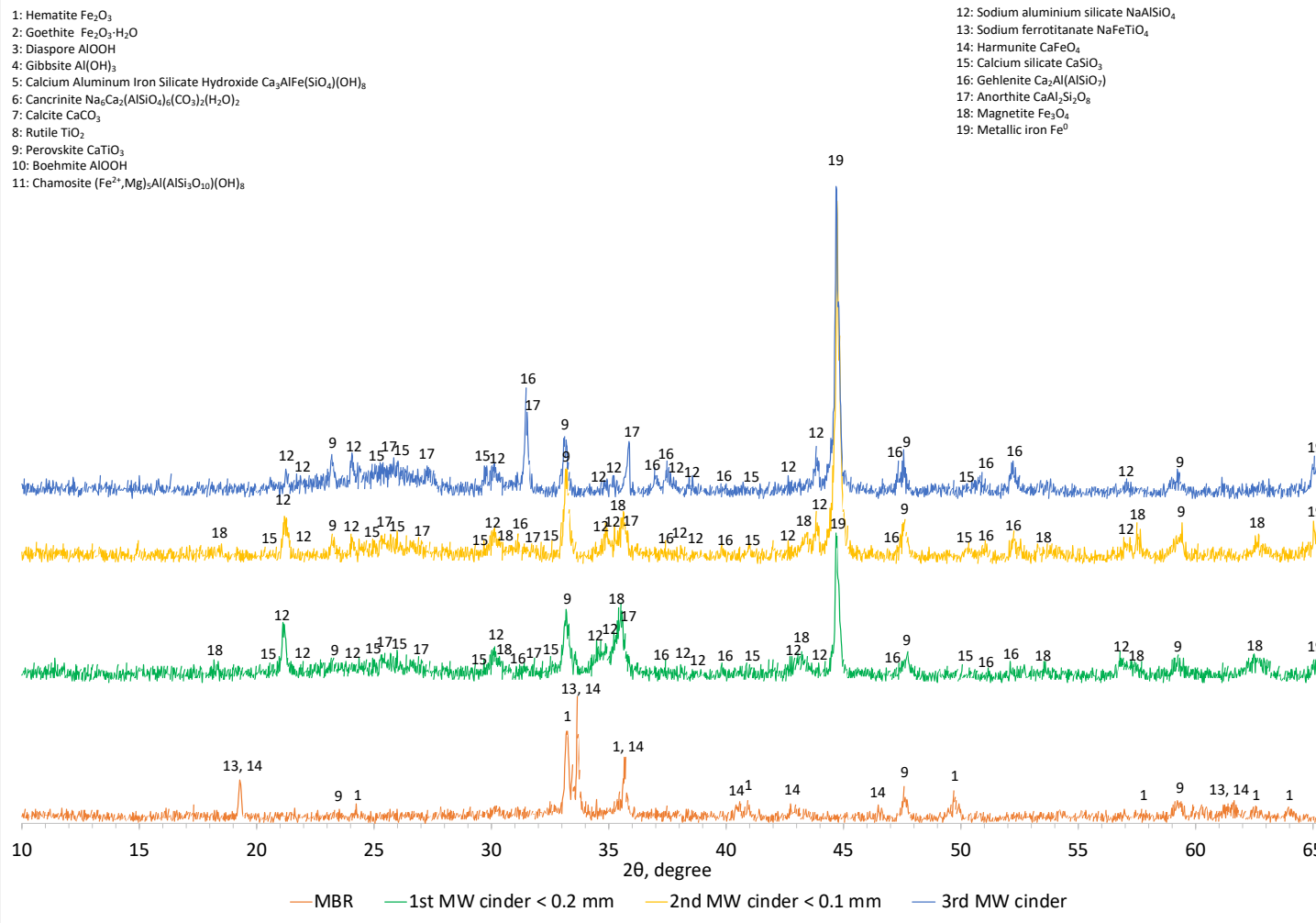

Figure **59** [180].

To confirm the increasing of the metallic iron content in each sample of the whole microwave roasting reduction (1st, 2nd and 3rd MW process), the above mentioned Zhiyong Xu method was used [186].

Table 9. Percentage of metallic iron / total iron content of leaching residue and three microwave sinters determined with Zhiyong Xu method

Sample	% Fe^0/ Fe_{tot}
Leaching residue	0.2
1st MW sinter	69
2nd MW sinter	85
3rd MW sinter	98

As it can be seen from the results shown in Table 9, after each microwave roasting reduction the percentage of the metallic iron present in the sample increased, comparing with the total amount of Fe.

The 3rd MW cinder was collected due to its strong magnetic properties and was treated through a Carpco™ Wet High Intensity Magnetic Separator (WHIMS).

8.4 Magnetic separation process

The purposes of the magnetic separation are to liberate from the cinder the iron based components from the matrix and to concentrate them in the magnetic product.

To achieve these aims, the cinder was dispersed in water and was treated through the WHIMS two times following the procedure described in paragraph 6.3.

Three different products (MAG I, MAG II and NM) were collected and representative samples were analyzed. MAG I represented the 62 wt. % of the 3rd MW cinder whereas MAG II was the 17 wt. % and NM the 21 wt. %

The three fractions were treated with Zhiyong Xu method to investigate the percentage of metallic iron in the sample comparing with the total amount of Fe. The results showed that in all the magnetic fractions, the iron analyzed was almost completely in form of metallic iron (about 98 %).

As it can be seen from the chemical analysis shown in Figure 60, the MAG I is mainly concentrated in iron, while calcium, silicon, titanium are present in minor amount. Aluminum is around 2 wt. % and Na content is negligible. On the other hand, in the NM fraction, metallic iron is still present (4 wt. %), whereas the concentration of the other elements that composed the matrix is higher.

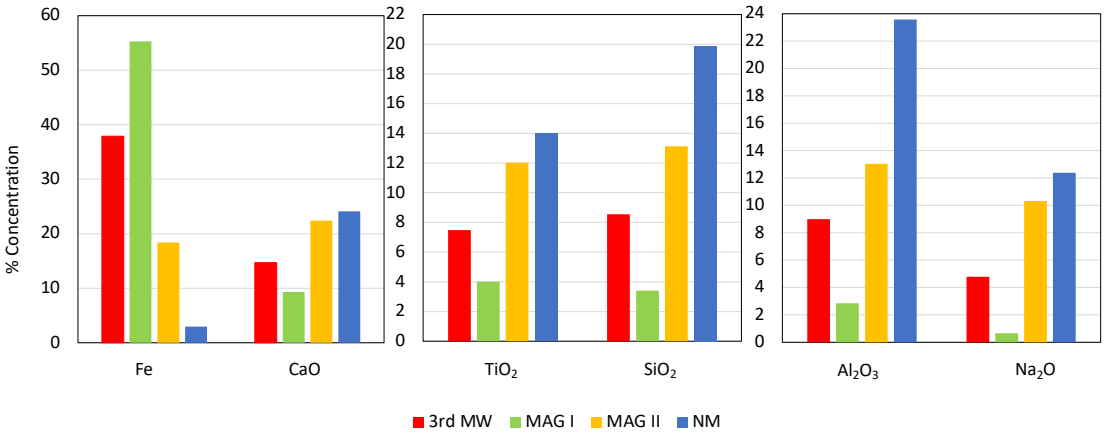

Figure 60. Chemical analysis of the sinter (3rd MW) and the three fractions (MAG I, MAG II and NM) after the magnetic separation

The XRD comparison of 3rd MW cinder, MAG I, MAG II and NM is presented in Figure 61. In MAG I the main peak is related to metallic iron, while the other mineralogical phases (gehlenite, calcium titanate, and anorthite) are detected with low intensity. Moreover, between 22 to 28°, the characteristic hump associated to calcium silicate and anorthite is not visible and the peaks attributed to sodium aluminum silicate disappear.

XRD analysis of NM fraction showed a different profile comparing with the one of MAG I. As it can be seen, the peak related to metallic iron (about 45°) is drastically reduced in intensity, while the hump associated to calcium silicate and anorthite is noticeable. Gehlenite and sodium aluminum silicate are detected with high intensity peaks.

Regarding MAG II, it is possible to notice that its mineralogical characterization is comparable to the initial cinder (3rd MW cinder).

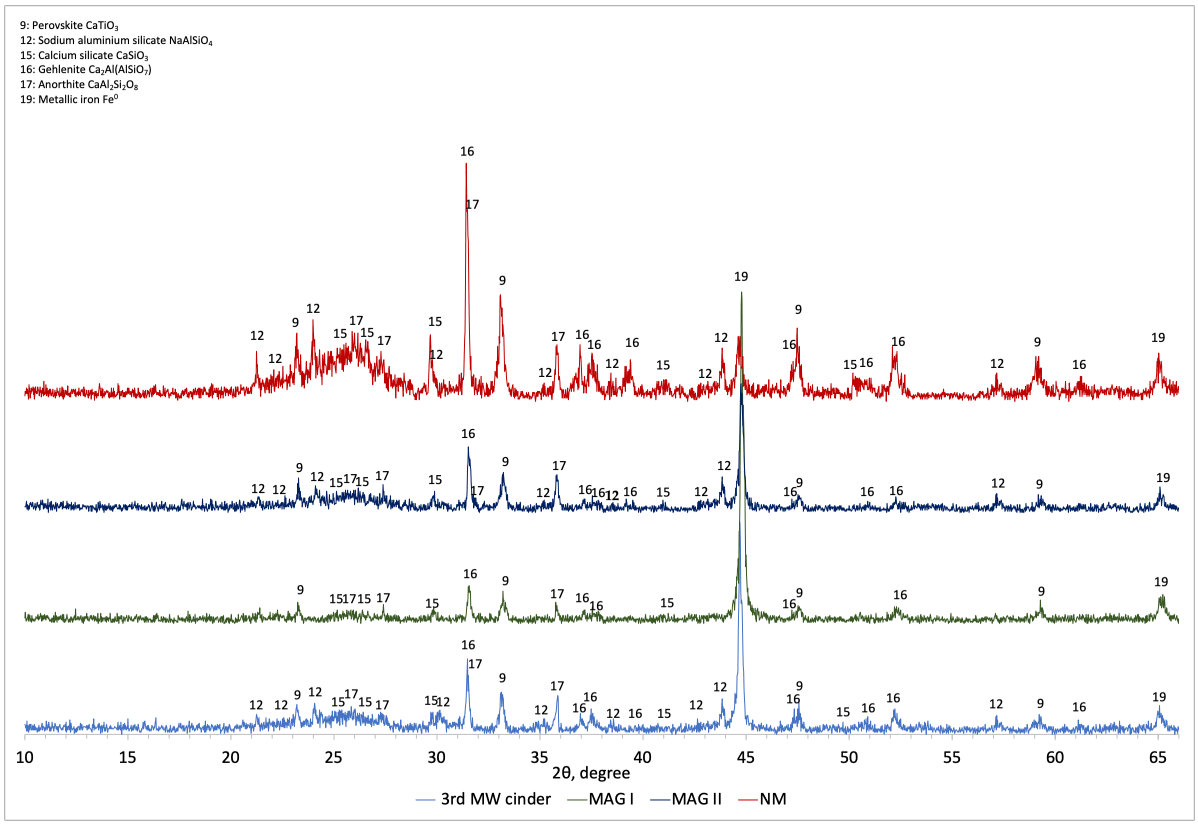

Figure 61. Comparison of the XRD profile of cinder after 3rd MW roasting process, magnetic fraction (MAG I), weak magnetic fraction (MAG II) and non-magnetic fraction (NM)

SEM-EDS analysis of the three magnetic fractions confirmed the results of chemical and XRD analyses. The back electron scattering (BEC) macrograph of MAG I fraction (Figure 62) showed that the sample is composed by a melted metallic iron (Figure 62, a) which has entrapped due to imperfect separation a solid matrix containing all the cinder constituents (Figure 62, c). In addition, small particles with calcium titanate were detected, also entrapped inside the metallic iron phase (Figure 62, b).

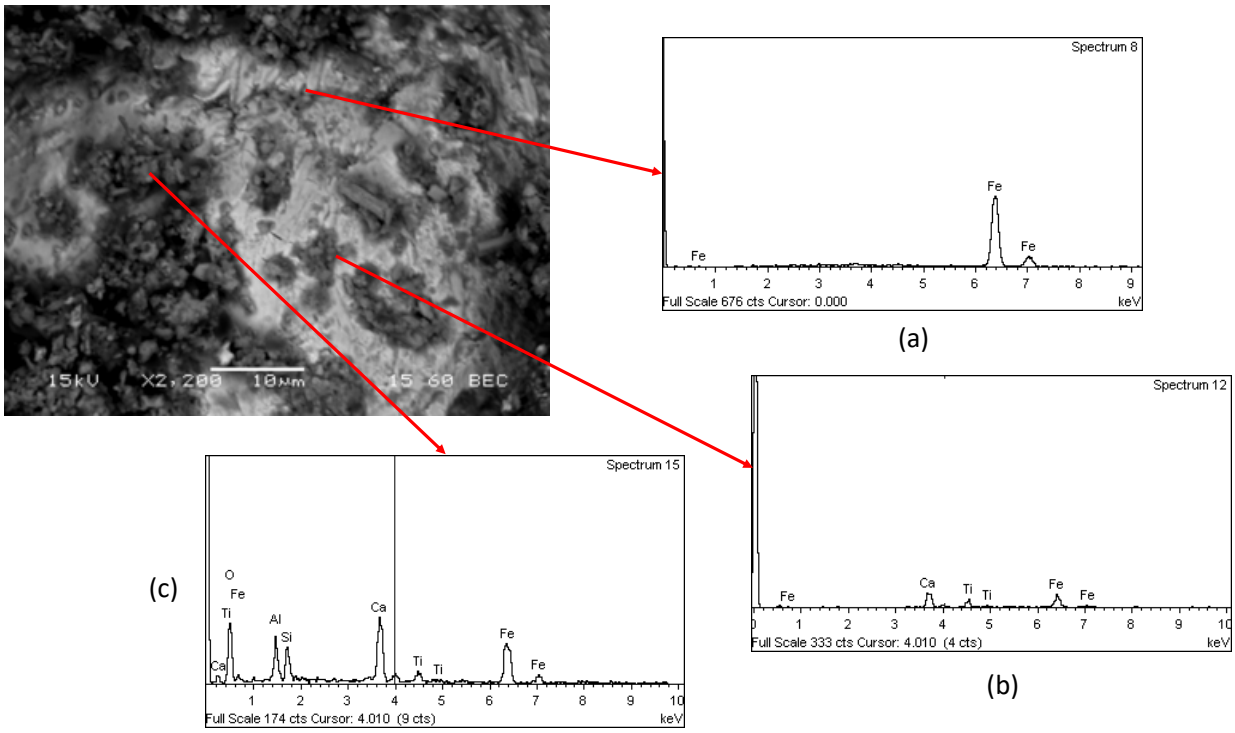

Figure 62. Back electron scattering (BEC) mode SEM-EDS analysis of MAG I fraction

To understand the stratification of the different constituents of the sample, the area of sample shown in Figure 63 was studied through second electron imaging (SEI) mode. As it is possible to observe the particles containing the elements of the matrix are embedded on the melted metallic iron (dark substrate, Figure 63, a) forming aggregates. Some particles were identified as calcium aluminum silicon oxide (Figure 63, b), while some others were composed of Si, Ca and Ti oxide mixture (Figure 63, c).

The presence of Fe in the spectrum 1 (Figure 63, c) is attributed to interferences from the metallic substrate, due the high magnification.

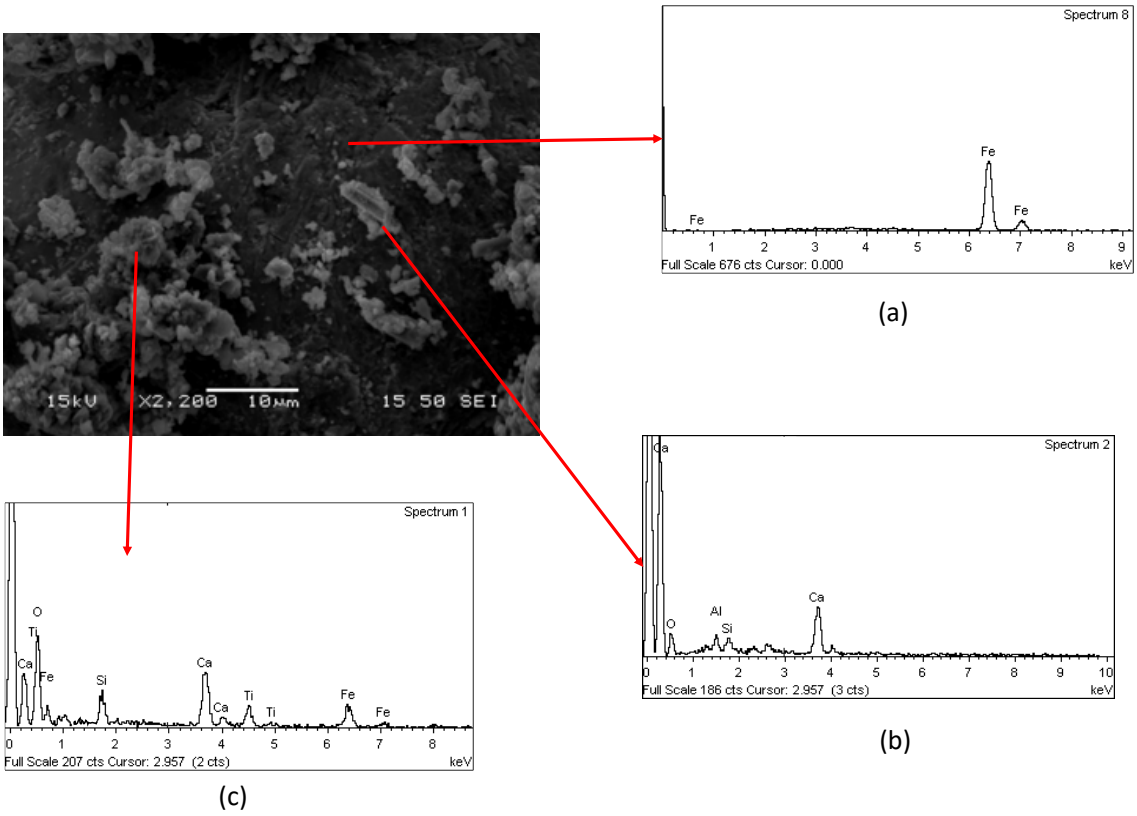

Figure 63. Secondary electron imaging (SEI) mode SEM-EDS analysis of MAG I fraction

In Figure 64 the SEM analysis of the NM fraction with back electron scattering mode is shown. The image shows the presence of small metallic iron (Figure 64, a) particles surrounded by light gray particles (calcium aluminum silicon oxide) (Figure 64, b) and entrapped into dark gray area which was mainly composed by all the cinder constituents (Na, Al, Ca, Si, Ti and Fe) (Figure 64, c). Also, in this case, the presence of Fe in the spectra 3 and 4 (Figure 64, b and c) is due to the interference from the metallic particles close to the detected area.

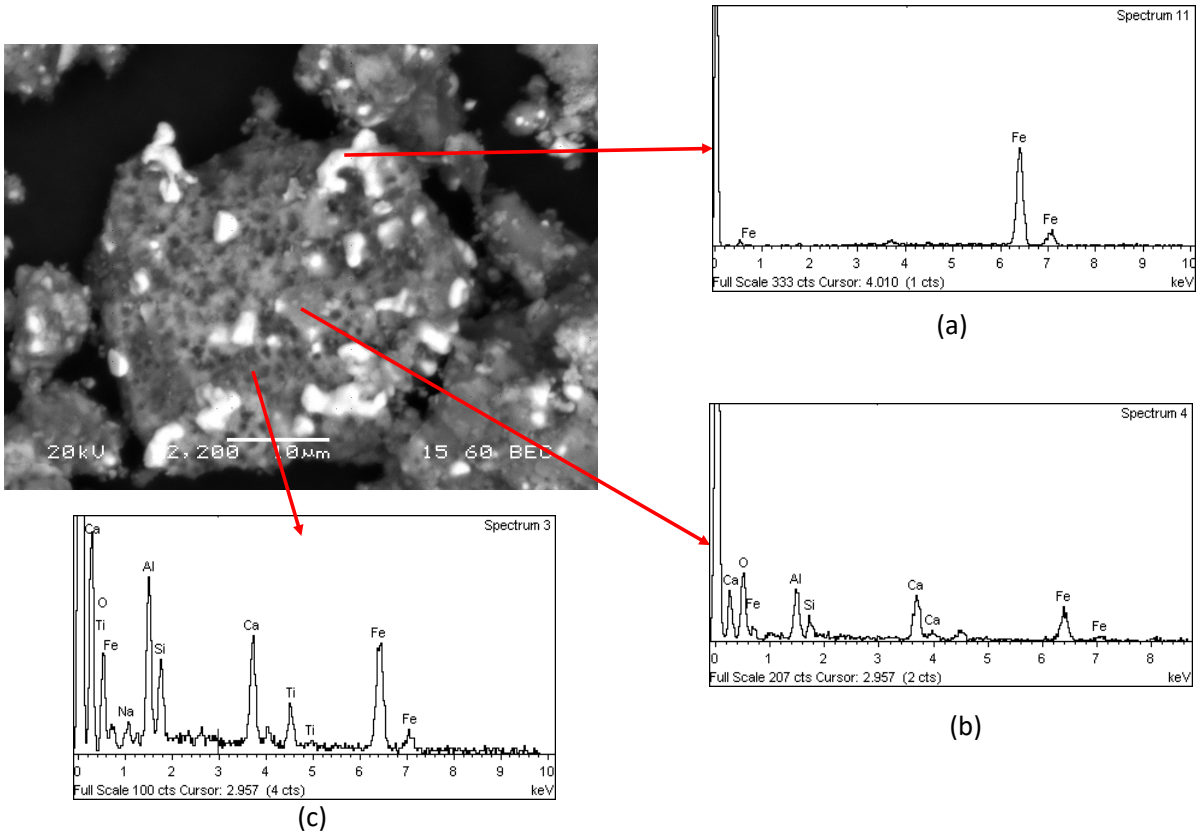

Figure 64. Back electron scattering (BEC) mode SEM-EDS analysis of NM fraction

Furthermore, the NM fraction was analyzed by employing a secondary electron imaging mode to comprehend the existing different mineralogical phases (Figure 65).**Errore. L'origine riferimento**

non è stata trovata.

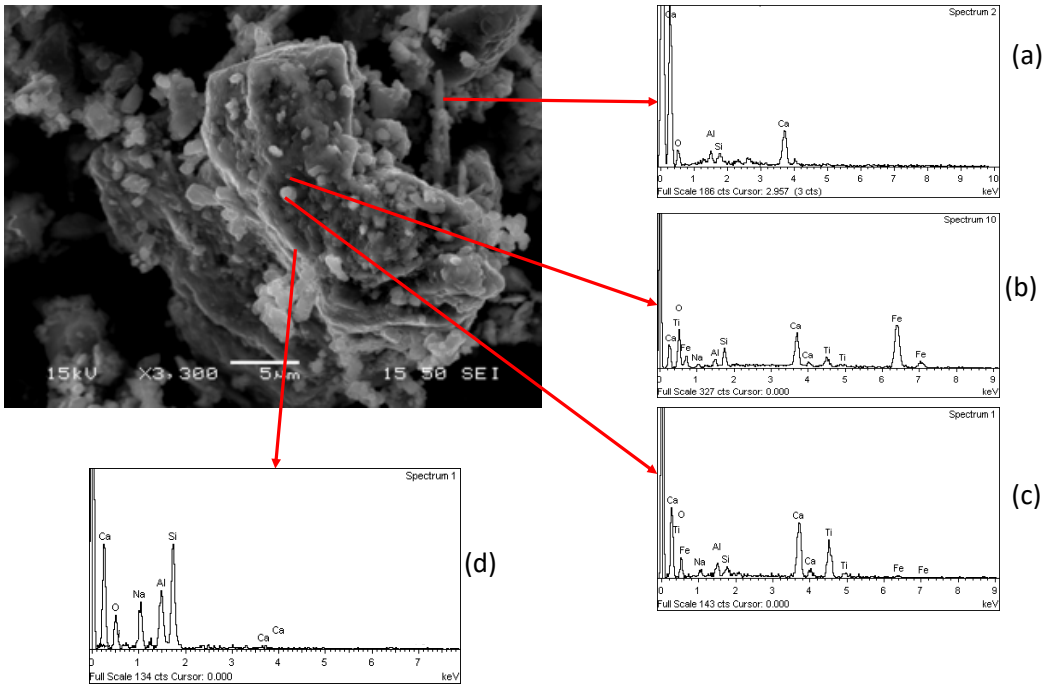

Figure 65. Secondary electron imaging (SEI) mode SEM-EDS analysis of NM fraction

Big particles composed with sodium aluminum silicate were identified (Figure 65, d), in this grain also a calcium titanium phase (Figure 65, c) and iron (Figure 65, b) were detected. The presence of the other elements in the EDS-spectra depends on the proximity interference of the other mineralogical phases. Calcium aluminum silicate were found in a specific area of the sample (Figure 65, a).

In conclusion, in terms of Fe partition within the different phases formed during the complex treatment of BR; after the 1st and 2nd microwave roasting reduction, nuggets were produced with high purity in Fe (Table 7 and Table 8), overall extracting about 16 % in the metallic Fe spheres fraction with particle size > 0.2 mm and 2 % in the spheres with a particle size > 0.1 mm of the total Fe content of BR. Moreover, Fe was recovered through a magnetic separation process. Three fractions (MAG I, MAG II and NM) were produced and analyzed. The Fe recovery from BR attested to 69 % in MAG I, while it was 6 % in MAG II and 1 % in NM. The losses in the soda sintering stage and in the mild alkaline stage are attributed to within experimental error margin of 5-10 %.

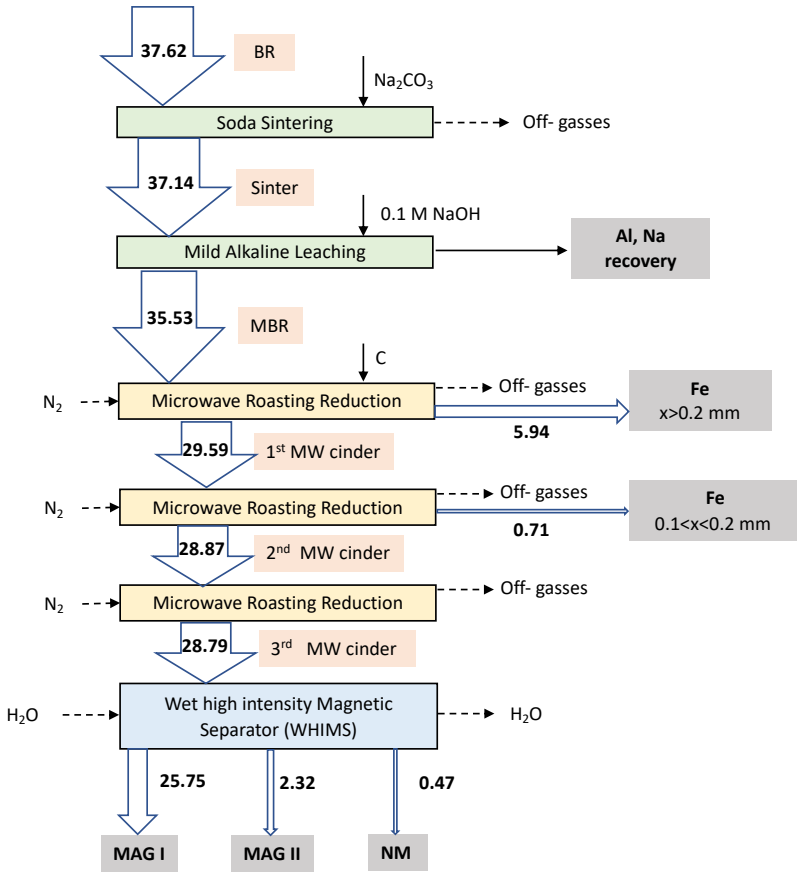

Figure 66. Mass distribution of Fe (g) based on chemical analysis data

9. Conclusions

Bauxite residue is the hydrometallurgical by-product generated from the digestion of bauxite ore in NaOH solution. The aluminum hydroxide is the precursor to alumina and the production of 1 metric ton of alumina normally creates between 0.8 and 1.5 metric tons of residue, although the range can be somewhat broader, depending on the composition of initial bauxite ore and the processing conditions [7,63]. The massive volume of BR produced, which exceeds 160 million metric tons per year worldwide [2], is causing drastic scarcity of available storage areas [2,6]. However, the main waste product of alumina production, is a potential secondary resource, since it contains valuable metals (i.e. REEs, Sc, Fe, Ti). Iron oxide, in the form of hematite and goethite, is the largest constituent of BR with concentrations range between 14-45 wt. %. Although iron content in bauxite residue is not as high as in average iron ores (60 wt. %) used in the iron industry [6], the gradual depletion of available ores and the demand for sustainable industrial processing have encouraged technology development based on secondary raw materials with almost zero-waste production [98]. In this perspective, processes for recovering iron from BR have been studied within the framework of this PhD thesis. In particular, the aim of this research work was to develop an optimal process for reduction of hematite (Fe_2O_3) and goethite ($Fe_2O_3 \cdot H_2O$) into magnetite (Fe_3O_4) in BR using a carbon source (metallurgical coke) as a reducing agent. This research study was focused on the recovery of Fe from bauxite residue through reductive roasting processes following by wet high intensity magnetic separation.

The bauxite residue was provided by Aluminum of Greece (Mytilineos S.A.) and fully characterized. The main iron minerals were hematite (Fe_2O_3), goethite ($Fe_2O_3 \cdot H_2O$), calcium aluminum iron silicate hydroxide ($Ca_3AlFe(SiO_4)(OH)_8$) and chamosite ($(Fe^{2+},Mg)_5Al(AlSi_3O_{10})(OH)_8$. In addition, iron oxide was the major constituent in the bauxite residue accounting for about 42 wt. %. It was followed by aluminum oxide with 16 wt. %, while titanium oxide was 4 wt. % and total rare earth oxides (REO) assessed to 0.2 wt. %. All the reductive roasting experiments were carried out in presence of metallurgical coke its C_{fix} amount attested around 80 wt. %.

Firstly, an electrical tube furnace was employed in the BR roasting process to investigate the transformation of the nonmagnetic iron phases found in BR (namely hematite and goethite), to magnetic ones such as magnetite, wüstite, and metallic iron. Based on the performed thermodynamic analysis, the temperature regime between 400 and 1100 °C and an inert atmosphere were chosen as experimental parameters for the study of BR reductive roasting process. Iron oxides contained in bauxite residue have been transformed into magnetite and maghemite after roasting process with a C/BR ratio = 0.180 at 800 °C. The result was the production of sinter with high-intensity magnetic properties. Following wet magnetic separation, SEM and XRD analyses of the magnetic fraction revealed the existence of calcium aluminum silica oxides on the surface of iron grains that reduced Fe enrichment in the magnetic concentrate.

Successively, other experiments were performed with high temperature (1100 °C) and C/BR ratio (0.225) to intensify reducing conditions and produce metallic iron. Results of magnetic separation again have shown the same problems with calcium aluminum silica phases attached to metallic iron. The presence of nonmagnetic BR oxides reduced the purity of the magnetic fraction.

As possible scenario a microwave furnace instead of a conventional furnace was employed to increase the iron recovery from BR.

In this study, it was demonstrated that microwave-assisted heating is a suitable method to transform Fe^{3+} oxide contained in bauxite residue into Fe^{2+} oxide and metallic iron, within a short processing time. Experiments have been carried out in a 2-kW microwave furnace with 3-stub tuner present in the waveguide that allowed modification of the microwave energy to accomplish the highest sample absorption for the entire experimental period. The quantification of the absorbed power by the sample as a possible approach to determine the microwaves influence on the given material, the effect of irradiation time together with addition of carbon source to BR (C/BR mass ratio) were the parameters investigated to optimize the carbothermic roasting process. At 0.6 kW and 0.225 C/BR with 1 l/min N_2 flow constant for 300 seconds, Fe^{3+} oxides reduction into Fe^{2+} oxides and metallic iron

was facilitated by the high temperature reached during the experiment (1100 °C). In particular, the result was the production of sinter with 79 % of metallic iron, while the rest of iron mineralogical phases were attributed to Fe_3O_4, FeO, and $FeAl_2O_4$.

The formation of hercynite ($FeAl_2O_4$) was unavoidable during the microwave roasting process [158] and the presence of this iron aluminum oxide mineralogical phase is considered a drawback for the magnetic separation process, due to its paramagnetic properties.

An integrated process to transform Fe^{3+} oxides contained in bauxite residue (hematite and goethite) into Fe^{2+} oxides (magnetite and wüstite) and metallic iron it was presented, avoiding the formation of hercynite.

In soda roasting process bauxite residue was mixed with 50 % excess of sodium carbonate as flux and heated at 900 °C for 2 hours, to transform all the alumina phases of BR into soluble sodium aluminates followed by alkaline leaching to recover alumina.

Subsequently, the leached residue was mixed with carbon and treated in the microwave furnace at optimum conditions (0.6 kW and 0.225 C/MBR with 1 l/min N_2 flow constant for 300 seconds).

At these conditions, the temperature reached was 1250 °C within some seconds. The cinder resulted to be rich of spherical metallic particles entrapped in the matrix; magnetite (Fe_3O_4) and metallic iron (Fe^0) were the main iron mineralogical phases after the microwave roasting reduction, hercynite was not detected.

The cinder after MW reductive roasting was firstly milled and then separated by employing a manual sieve to release the spheres. Two fractions received and fully characterized: the first one with a particle size > 0.2 mm, was mostly composed by Fe nuggets (around 7 wt. % of the total solid sample) and the other one with a particle size < 0.2 mm (around 93 wt. % of the total solid sample).

Since the fraction with a particle size < than 0.2 mm still contained a considerable amount of iron, accounting for 51 wt. %, in form of magnetite and metallic iron and due to the presence of an unreacted C source (8 wt. %), the cinder was transformed into a tablet and treated again in the microwave furnace. During this experiment, temperature immediately reached 1230 °C and metallic iron particles with a particle size > 0.1 mm were formed. Milling and sieving separation was used again to separate metallic iron. Analyzing the results, the main component of the fraction with particle size < 0.1 mm was metallic iron (1 wt. % of the total solid sample), while the other fraction still contained a considerable amount of iron oxide, accounting for 55 wt. % (99 wt. % of the total solid sample).

Thanks to the presence of a considerable amount of microwave absorbing material (magnetite and metallic iron) as well as of still unreacted small amount of carbon the sample was treated at the optimum conditions to push the system towards the complete reduction into metallic iron and promote the magnetic separation. In contrast with the previous experiments, the roasting process was stopped after 180 seconds. This was attributed to the increased concentration of conductive material (metallic iron) that reflected the microwave energy. The result of the 3rd MW roasting reduction was the production of a cinder with high magnetic properties.

After the wet high intensity magnetic separation, three different products (MAG I, MAG II and NM) were collected. MAG I represented the 62 wt.% of the 3rd MW roasting cinder, MAG II was the 17 wt.% and NM the 21 wt.%.

Results of magnetic separation have shown that the higher concentration of metallic iron was detected in MAG I (56 wt.%), even though calcium, silicon and titanium were still present in minor amount. SEM and XRD analysis of the non-magnetic fraction (NM) revealed the existence of metallic iron particles (about 4 wt. %) embedded on the ceramic matrix.

It can be concluded that the combined process presented is a favorable approach to recover iron comparing with a previous works [18,19]. In addition, an added value of this process is also the recovery of aluminum (70 % of aluminum recovered) after the alkali leaching in the first step.

In terms of Fe recovery, after the 1st and 2nd MW roasting reduction, nuggets were produced with high purity in Fe, overall extracting about 16 % in the fraction with a particle size > 0.2 mm and 2 % in the fraction with a particle size > 0.1 mm of the total Fe content of BR. Moreover, an advantage of this procedure is that Fe nuggets are easily recoverable through physical separation. Thereafter the 3rd MW roasting reduction, Fe was recovered through the magnetic separation process and attested to 69 % in MAG I, while it was 6 % in MAG II and 1 % in NM.

MAG I contains almost 55 % metallic iron and have as impurities calcium aluminosilicates as well as perovskite. It is an upgraded material in comparison with BR and can be added in the electric arc furnaces of secondary steel production as a raw material together with scrap. The impurities can play the role of fluxes for formation of the $CaO\text{-}SiO_2\text{-}Al_2O_3$ type slag. In addition to MAG I, the Fe nuggets separated from the first two MW treatments can be also added in EAF for iron recovery. The nuggets have a purity in metallic iron higher than 93 % and the impurities are also aluminosilicates. Therefore, with the combine soda roasting and MW carbothermic roasting process almost 87 % of iron contained in BR is recovered as impure metallic iron and 70 % of contained aluminum is recovered in

the form of a sodium aluminate solution which can be recycled in the Bayer process for alumina production.

As a final conclusion the combined soda roasting and MW carbothermic roasting process could be potentially developed into a high throughput continuous process to valorize BR and make it a secondary raw material resource.

9.1 Future work

In this PhD thesis a conceptual flowsheet for recovering metals from bauxite residue was proposed. Bauxite residue was mixed with metallurgical coke and treated through a reductive roasting process to reduce Fe^{+3} oxides into Fe^{+2} oxides and Fe^{0} and allow the magnetic separation process. However, some aspects of this work need to be studied more in details. Furthermore, energy and cost calculations need to be performed for evaluating the economic feasibility at higher scale.

Bauxite residue mixed with carbon was treated in a single mode microwave cavity which do not have a uniform, and predictable, electromagnetic field distribution. This cavity is used for laboratory-scale experiments to study the interaction between material and microwave. However, single mode applicators could not scale-up to industrial application due to geometric limitation and a non-uniform field. The transformation process can potentially take place continuously at a high throughput, turning the suggested modification into a realistic valorization scenario. To scale up the process a multi-mode applicator is suggested since it is more versatile comparing to single mode.

The utilization of a carbon source is fundamental during the experiment to transform hematite (Fe_2O_3) and goethite ($Fe_2O_3 \cdot H_2O$) present in BR into magnetite (Fe_3O_4), wüstite (FeO) and metallic iron (Fe^0) according to the iron reduction pathway $Fe_2O_3 \rightarrow Fe_3O_4 \rightarrow FeO \rightarrow Fe$. However, the production of carbon oxides emissions are an intrinsic part of the extraction processes and cannot realistically be avoided or abated [195] and could be a drawback related to the European “zero waste” policy. A possible solution is to use alternative reducing agents as biomass pyrolysis biochar [195,196] or carbon capture and storage (CCS) could represent a future option for managing emissions from chemical processes [195].

Moreover, the magnetic iron phases in the roasting residue can be fractionated through wet high intensity magnetic separation, forming an iron concentrate and leaving a nonmagnetic residue containing other constituents. However, further work required on magnetic separation process is to study in detail the magnetic properties of the sinter to find the suitable method to efficiently separate the magnetic iron phases from the nonmagnetic matrix.

In the last two decades the microwave techniques have been developed in mineral processing and extractive metallurgy [32,34,197–199], thanks to several advantages to conventional heat treatment methods as: non-contact heating; energy transfer; rapid heating rate; material selective heating; volumetric heating; clean energy and instantaneous control[34].

On the other hand, the microwave metal extraction remains essentially a laboratory technique due to some disadvantages as the complexity of the interaction between the electromagnetic field and the material, the not-uniform temperature and the higher capital cost installation [198]. However, a scale-up reactor for microwave process is presented in Figure 67 to illustrate a possible scenario.

The scale up is based on the industrial continuous-type reactor. In industrial applications the frequency utilized is 912 MHz with the maximum power capacity of 100 kW [198].

Multimode applicator is the common processing system employed in the industrial applications thanks to its large location range in the cavity. However, the presence of different modes results in multiple hot spots and the consequence is the not uniform heating of the sample. To reduce the effect of hot spots and uniform the material heating, it is necessary to move the sample in the field and/or use a multiple magnetron [128]. Besides to a conveyor belt, presented in Figure 67, it is possible to employ a rotate tube which is the set up chosen for the microwave furnace in the RemovAL project [200].

The most used devices in pyrometallurgical processes for measuring temperature (thermocouple and optical pyrometer) have some issues. In particular, in the case of the thermocouple, the main drawbacks are related to the direct contact with the sample and the interaction with the field. On the other hand, the optical pyrometer could detect only the surface temperature, while the highest temperature is generated within the sample. In addition, both the devices can detect temperature only in one point. To compensate all these drawbacks, modelling techniques can be utilized to predict the temperature distribution in the material [198].

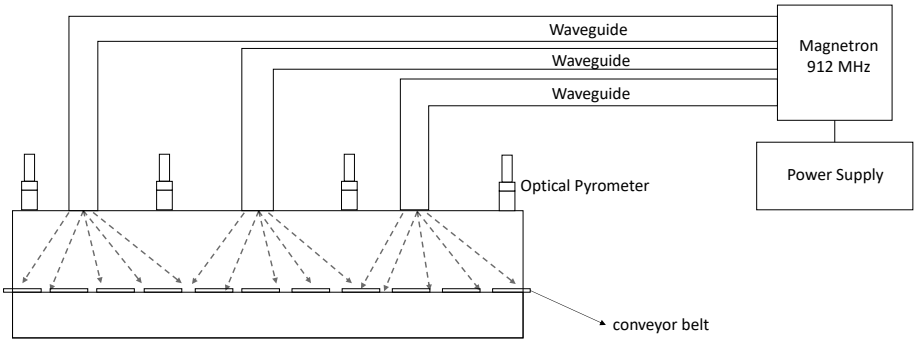

Figure 67. A possible scale-up of the microwave reactor

References

1. Sutar, H. Progress of Red Mud Utilization: An Overview. *Am. Chem. Sci. J.* **2014**, *4*, 255–279, doi:10.9734/acsj/2014/7258.

2. International Aluminium Institute (IAI) and European Aluminium (EA) *Bauxite Residue Management: Best Practice*; 2015;

3. Habashi, F. *Textbook of Hydrometallurgy*; 1999;

4. PARAMGURU, R. K.; RATH, P. C.; MISRA, V. N. TRENDS IN RED MUD UTILIZATION – A REVIEW. *Miner. Process. Extr. Metall. Rev.* **2004**, *26*, 1–29, doi:10.1080/08827500490477603.

5. Gräfe, M.; Power, G.; Klauber, C. Bauxite residue issues: III. Alkalinity and associated chemistry. *Hydrometallurgy* **2011**, *108*, 60–79, doi:10.1016/j.hydromet.2011.02.004.

6. Kumar, R.; Alex, T. C.; Mishra, C. R.; Mehrotra, S. P.; Company, N. A. TOWARDS SUSTAINABLE ALUMINA PRODUCTION. *Envicon* **2007**, 45–51.

7. Evans, K. The History, Challenges, and New Developments in the Management and Use of Bauxite Residue. *J. Sustain. Metall.* **2016**, *2*, 316–331, doi:10.1007/s40831-016-0060-x.

8. Mishra, B.; Gostu, S. Materials sustainability for environment: Red-mud treatment. *Front. Chem. Sci. Eng.* **2017**, *11*, 483–496, doi:10.1007/s11705-017-1653-z.

9. Bánvölgyi, G.; Huan, T. M. De-watering , disposal and utilization of red mud : state of the art and emerging technologies. *Proc. XVII Int. Symp. ICSOBA* **2010**, *35*, 431–443.

10. Liu, Y.; Lin, C.; Wu, Y. Characterization of red mud derived from a combined Bayer process and bauxite calcination method. *J. Hazard. Mater.* **2007**, *146*, 255–261.

11. Klauber, C.; Gräfe, M.; Power, G. Bauxite residue issues: II. options for residue utilization. *Hydrometallurgy* **2011**, *108*, 11–32, doi:10.1016/j.hydromet.2011.02.007.

12. Liu, Y.; Naidu, R. Hidden values in bauxite residue (red mud): Recovery of metals. *Waste Manag.* **2014**, *34*, 2662–2673, doi:10.1016/J.WASMAN.2014.09.003.

13. Borra, C. R.; Blanpain, B.; Pontikes, Y.; Binnemans, K.; Van Gerven, T. Recovery of Rare Earths and Major Metals from Bauxite Residue (Red Mud) by Alkali Roasting, Smelting, and Leaching. *J. Sustain. Metall.* **2017**, *3*, 393–404, doi:10.1007/s40831-016-0103-3.

14. Liu, Z.; Li, H. Metallurgical process for valuable elements recovery from red mud—A review. *Hydrometallurgy* **2015**, *155*, 29–43, doi:10.1016/J.HYDROMET.2015.03.018.

15. Kumar, S.; Kumar, R.; Bandopadhyay, A. Innovative methodologies for the utilisation of wastes from metallurgical and allied industries. *Resour. Conserv. Recycl.* **2006**, *48*, 301–314, doi:10.1016/j.resconrec.2006.03.003.

16. Xenidis, A.; Zografidis, C.; Kotsis, I.; Boufounos, D. Reductive Smelting of Greek Bauxite Residues for Iron Production. *Light Met. 2011* **2011**, 113–117, doi:10.1002/9781118061992.ch20.

17. Agrawal, S.; Dhawan, N. Investigation of carbothermic microwave reduction followed by acid leaching for recovery of iron and aluminum values from Indian red mud. *Miner. Eng.* **2020**, *159*, 106653, doi:10.1016/j.mineng.2020.106653.

18. Cardenia, C.; Xakalashe, B.; Balomenos, E.; Panias, D.; Friedrich, B. Reductive Roasting Process for the Recovery of Iron Oxides from Bauxite Residue through Rotary Kiln Furnace and Magnetic Separation. *35th Int. ICSOBA Conf. Hamburg, Ger. 2 – 5 October, 2017* **2017**, 595–602.

19. Cardenia, C.; Balomenos, E.; Panias, D. Iron Recovery from Bauxite Residue Through Reductive Roasting and Wet Magnetic Separation. *J. Sustain. Metall.* **2018**, *5*, doi:10.1007/s40831-018-0181-5.

20. Xenidis, A.; Zografidis, C.; Kotsis, I.; Boufounos, D. Reductive roasting and magnetic separation of Greek bauxite residue for its utilization in iron ore industry. *TMS Light Met.* **2009**, 63–67.

21. Zhu, D.; Chun, T.; Pan, J.; He, Z. Recovery of Iron From High-Iron Red Mud by Reduction Roasting With Adding Sodium Salt. *J. Iron Steel Res. Int.* **2012**, *19*, 1–5, doi:10.1016/S1006-706X(12)60131-9.

22. Jayshankar, K.; Mukherjee, P.; Bhoi, B.; Mishra, C. Production of pig iron and Portland slag cement from red mud by application of Novel Thermal Plasma Technique. In *IBAAS-CHALIECO 2013 international sympo- sium. Nanning, Guangxi*; 2013.

23. Borra, C. R.; Blanpain, B.; Pontikes, Y.; Binnemans, K.; Van Gerven, T. Smelting of Bauxite Residue (Red Mud) in View of Iron and Selective Rare Earths Recovery. *J. Sustain. Metall.* **2016**, *2*, 28–37, doi:10.1007/s40831-015-0026-4.

24. Balomenos, E.; Kemper, C.; Diamantopoulos, P.; Panias, D.; Paspaliaris, I.; Friedrich, B. Novel technologies for enhanced energy and exergy efficiencies in primary aluminium production industry. In *First Metallurgical & Materials Engineering Congress of South-East Europe*; 2013; pp. 85–91.

25. Ning, G.; Zhang, B.; Liu, C.; Li, S.; Ye, Y.; Jiang, M. Large-Scale Consumption and Zero-Waste Recycling Method of Red Mud in Steel Making Process. *Minerals* **2018**, *8*, 102, doi:10.3390/min8030102.

26. Samouhos, M.; Taxiarchou, M.; Tsakiridis, P. E.; Potiriadis, K. Greek “red mud” residue: A study of microwave reductive roasting followed by magnetic separation for a metallic iron recovery process. *J. Hazard. Mater.* **2013**, *254–255*, 193–205, doi:10.1016/j.jhazmat.2013.03.059.

27. El Khaled, D.; Novas, N.; Gazquez, J. A.; Manzano-Agugliaro, F. Microwave dielectric heating: Applications on metals processing. *Renew. Sustain. Energy Rev.* **2018**, *82*, 2880–2892, doi:10.1016/j.rser.2017.10.043.

28. Agrawal, S.; Rayapudi, V.; Dhawan, N. Comparison of microwave and conventional carbothermal reduction of red mud for recovery of iron values. *Miner. Eng.* **2019**, *132*, 202–210, doi:10.1016/j.mineng.2018.12.012.

29. Agrawal, S.; Rayapudi, V.; Dhawan, N. Microwave Reduction of Red Mud for Recovery of Iron Values. *J. Sustain. Metall.* **2018**, *4*, 427–436, doi:10.1007/s40831-018-0183-3.

30. Pickles, C. A. Microwaves in extractive metallurgy: Part 2 – A review of applications. *Miner. Eng.* **2009**, *22*, 1112–1118, doi:10.1016/j.mineng.2009.02.014.

31. Meredith, R. J. Engineers' Handbook of Industrial Microwave Heating. *IEE London UK ISBN* 1998, 382.

32. Jones, D. a.; Lelyveld, T. P.; Mavrofidis, S. D.; Kingman, S. W.; Miles, N. J. Microwave heating applications in environmental engineering—a review. *Resour. Conserv. Recycl.* **2002**, *34*, 75–90, doi:10.1016/S0921-3449(01)00088-X.

33. Lovas, M.; Znamenackova, I.; Zubrik, M.; Kovacova, M.; Dolinska, S. The application of microwave energy in mineral processing – a review. *Rocnik* **2011**, *16*, 137–148.

34. Haque, K. E. Microwave energy for mineral treatment processes—a brief review. *Int. J. Miner. Process.* **1999**, *57*, 1–24, doi:10.1016/S0301-7516(99)00009-5.

35. Pickles, C. A. A. Microwaves in extractive metallurgy: Part 1 – Review of fundamentals. *Miner. Eng.* **2009**, *22*, 1102–1111, doi:10.1016/j.mineng.2009.02.015.

36. Standish, N.; Worner, H. Microwave application in the reduction of metal oxides with carbon. *J. Microw. Power Electromagn. Energy* **1990**, *25*, 177–180, doi:10.1080/08327823.1990.11688126.

37. Kaußen, F. M.; Friedrich, B. Methods for Alkaline Recovery of Aluminum from Bauxite Residue. *J. Sustain. Metall.* **2016**, *2*, 353–364, doi:10.1007/s40831-016-0059-3.

38. Kaußen, F. M.; Sofras, I.; Friedrich, B. Carbothermic reduction of red mud in an EAF and subsequent recovery of aluminum from the slag by pressure leaching in caustic solution. In *In Proceedings of the Bauxite Residue Valorisation and Best Practices (BR 2015),*; Leuven, Belgium, 2015; pp. 185–189.

39. Zheng, K.; Gerson, A. R.; Addai-Mensah, J.; Smart, R. S. C. The influence of sodium carbonate on sodium aluminosilicate crystallisation and solubility in sodium aluminate solutions. *J. Cryst. Growth* **1997**, *171*, 197–208, doi:10.1016/S0022-0248(96)00480-0.

40. Alp, A.; Aydin, A. O. The Investigation of Efficient Conditions for Alumina Production from Diasporic Bauxites. *Can. Metall. Q.* **2002**, *41*, 41–46, doi:10.1179/cmq.2002.41.1.41.

41. Meher, S. N.; Rout, A. K.; Padhi, B. K. Extraction of Alumina from Red Mud by Divalent Alkaline Earth Metal Soda Ash Sinter Process. In *Light Metals 2011*; John Wiley & Sons, Inc.: Hoboken, NJ, USA, 2011; pp. 231–236.

42. Meher, S. N.; Padhi, B. A novel method for extraction of alumina from red mud by divalent alkaline earth metal oxide and soda ash sinter process. *Int. J. Environ. Waste Manag.* **2014**, *13*, 231, doi:10.1504/IJEWM.2014.059932.

43. Tam; Panias; Vassiliadou Sintering Optimisation and Recovery of Aluminum and Sodium from Greek Bauxite Residue. *Minerals* **2019**, *9*, 571, doi:10.3390/min9100571.

44. Zinoveev, D.; Grudinsky, P.; Zakunov, A.; Semenov, A.; Panova, M.; Valeev, D.; Kondratiev, A.; Dyubanov, V.; Petelin, A. Influence of Na2CO3 and K2CO3 Addition on Iron Grain Growth during Carbothermic Reduction of Red Mud. *Metals (Basel).* **2019**, *9*, 1313, doi:10.3390/met9121313.

45. Kaußen, F.; Friedrich, B. Reductive Smelting of Red Mud for Iron Recovery. *Chemie Ing. Tech.* **2015**, *87*, 1535–1542, doi:10.1002/cite.201500067.

46. Kaußen, F. M.; Friedrich, B. Phase characterization and thermochemical simulation of (landfilled) bauxite residue ("red mud") in different alkaline processes optimized for aluminum recovery. *Hydrometallurgy* **2018**, *176*, 49–61, doi:10.1016/j.hydromet.2018.01.006.

47. Anisonyan, K. G.; Kopyev, D. Y.; Goncharov, K. V.; Sadykhov, G. B. An investigation of a single-stage red mud reducing roasting process with the cast iron and aluminate slag production. *Non-ferrous Met.* **2018**, 18–23, doi:10.17580/nfm.2018.01.04.

48. Tam, P. W. Y.; Cardenia, C.; Xakalashe, B.; Vassiliadou, V.; Panias, D.; Friedrich, B. Conceptual flowsheets for combined recovery of Fe and Al from bauxite resi-due. In *2nd International Bauxite Residue Valorisation and Best Practices Conference.*; 2018.

49. Tam, P.; Yin, W.; Xakalashe, B.; Friedrich, B.; Panias, D. Carbothermic Reduction of Bauxite Residue for Iron Recovery and Subsequent Aluminium Recovery from Slag Leaching. *35th Int. ICSOBA Conf. Hamburg, Ger. 2 – 5 October, 2017* **2017**, 603–614.

50. Liu, W.; Yang, J.; Xiao, B. Review on treatment and utilization of bauxite residues in China. *Int. J. Miner. Process.* **2009**, *93*, 220–231, doi:10.1016/j.minpro.2009.08.005.

51. Vind, J.; Malfliet, A.; Bonomi, C.; Paiste, P.; Sajó, I. E.; Blanpain, B.; Tkaczyk, A. H.; Vassiliadou, V.; Panias, D. Modes of occurrences of scandium in Greek bauxite and bauxite residue. *Miner. Eng.* **2018**, *123*, 35–48, doi:10.1016/J.MINENG.2018.04.025.

52. Vind, J.; Malfliet, A.; Blanpain, B.; Tsakiridis, P. E.; Tkaczyk, A. H.; Vassiliadou, V.; Panias, D. Rare earth element phases in bauxite residue. *Minerals* **2018**, *8*, doi:10.3390/min8020077.

53. Vind, J.; Alexandri, A.; Vassiliadou, V.; Panias, D. Distribution of selected trace elements in the bayer process. *Metals (Basel).* **2018**, *8*, 1–21, doi:10.3390/met8050327.

54. Bardossy, G. Classification of Bauxite Deposits. In *Developments in Economic Geology*; 1982; Vol. 14, pp. 16–22.

55. Bardossy, G.; Aleva, G. Lateritic Bauxites. In *Developments in Economic Geology*; Elsevier Scientific Publication Co., Ed.; 1990; pp. 2–624 ISBN 0444988114.

56. Meyer, F. M. Availability of Bauxite Reserves. *Nat. Resour. Res.* **2004**, *13*, 161–172, doi:10.1023/B:NARR.0000046918.50121.2e.

57. Kaußen, F. M.; Friedrich, B. Methods for Alkaline Recovery of Aluminum from Bauxite Residue. *J. Sustain. Metall.* **2016**, *2*, 353–364, doi:10.1007/s40831-016-0059-3.

58. Jamieson, E.; van Riessen, A.; McLellan, B.; Penna, B.; Kealley, C.; Nikraz, H. Chapter 8 - Introducing Bayer Liquor–Derived Geopolymers. In *Handbook of Low Carbon Concrete*; Nazari, A., Sanjayan, J. G., Eds.; Butterworth-Heinemann, 2017; pp. 159–193 ISBN 978-0-12-804524-4.

59. Power, G.; Gräfe, M.; Klauber, C. Bauxite residue issues: I. Current management, disposal and storage practices. *Hydrometallurgy* **2011**, *108*, 33–45, doi:10.1016/J.HYDROMET.2011.02.006.

60. Adamson, A. N.; Bloore, E. J.; Carr, A. R. Basic Principles of Bayer Process Design. In *Essential Readings in Light Metals*; Cham; pp. 100–117 ISBN 9781118647868.

61. Bray, E. L. National Minerals Information Center Available online: https://www.usgs.gov/centers/nmic/bauxite-and-alumina-statistics-and-information?qt-science_support_page_related_con=0#qt-science_support_page_related_con.

62. L. Sidrak, Y. Dynamic Simulation and Control of the Bayer Process. A Review. *Ind. & Eng. Chem. Res.* **2001**, *40*, 1146–1156, doi:10.1021/ie000522n.

63. Balomenos, E.; Panias, D.; Paspaliaris, I. Energy and exergy analysis of the primary aluminum production processes: A review on current and future sustainability. *Miner. Process. Extr. Metall. Rev.* **2011**, *32*, 69–89, doi:10.1080/08827508.2010.530721.

64. Pontikes, Y. Red Mud Project Available online: http://redmud.org/.

65. Paramguru, R. K.; Rath, P. C.; Misra, V. N. Trends in red mud utilization - A review. *Miner. Process. Extr. Metall. Rev.* **2005**, *26*, 1–29, doi:10.1080/08827500490477603.

66. Hudson, L. K.; Misra, C.; Perrotta, A. J.; Wefers, K.; Williams, F. S. Aluminum Oxide. In *Ullmann's Encyclopedia of Industrial Chemistry*; Wiley-VCH Verlag GmbH & Co. KGaA: Weinheim, Germany, 2000.

67. Authier-Martin, M.; Forte, G.; Ostap, S.; See, J. The mineralogy of bauxite for producing smelter-grade alumina. *JOM* **2001**, *53*, 36–40, doi:10.1007/s11837-001-0011-1.

68. Whelan, T. J.; Ellis, A.; Kannangara, G. S. K.; Marshall, C. P.; Smeulders, D.; Wilson, M. A. Macromolecules in the Bayer process. *Rev. Chem. Eng.* 2003, *19*, 431–471.

69. Senaputra, A.; Fawell, P.; Jones, F.; Smith, P. The impact of desilication product on Bauxite

Residue flocculation. In *Proceedings of the 9th International Alumina Quality Workshop*; 2012; pp. 186–192.

70. Gerson, A. R.; Zheng, K. Bayer process plant scale: transformation of sodalite to cancrinite. *J. Cryst. Growth* **1997**, *171*, 209–218, doi:10.1016/S0022-0248(96)00482-4.

71. Balomenos, E.; Kastritis, D.; Panias, D.; Paspaliaris, I.; Boufounos, D. The Enexal Bauxite Residue Treatment Process: Industrial Scale Pilot Plant Results. *Light Met. 2014* **2014**, *9781118889*, 141–147, doi:10.1002/9781118888438.ch25.

72. USGS 2015 Minerals Yearbook, Greece. *United States Geol. Surv.* **2018**, 1–8.

73. USGS *Mineral Commodity Summaries*; 2018; ISBN 9781411341999.

74. World Aluminium — Alumina Production Available online: http://www.world-aluminium.org/statistics/alumina-production/#histogram.

75. Tabereaux, A. Hungarian red mud disaster: Addressing environmental liabilities of alumina residue storage & disposal. *Light Met. Age* **2010**, *68*, 22–24.

76. Balomenos, E. *EU MSCA-ETN REDMUD Policy Brief*; 2018;

77. Bánvölgyi, G. The red mud pond dam failure at Ajka (Hungary) and subsequent developments György (George) Bánvölgyi. In *Bauxite residue seminar, ICSOBA 2011*; Goa, India, 2011.

78. Ruyters, S.; Mertens, J.; Vassilieva, E.; Dehandschutter, B.; Poffijn, A. A. A.; Smolders, E. The Red Mud Accident in Ajka (Hungary): Plant Toxicity and Trace Metal Bioavailability in Red Mud Contaminated Soil. *Environ. Sci. Technol.* **2011**, *45*, 1616–1622, doi:10.1021/es104000m.

79. Evans, K.; Nordheim, E.; Tsesmelis, K. Bauxite Residue Management. In *Light Metals 2012*; Springer International Publishing: Cham, 2012; pp. 63–66.

80. Klauber, C.; Gräfe, M.; Power, G. Bauxite Residue Utilization and the Lack Thereof. In *In The Bauxite Residue Seminar, ICSOBA 2011,Goa, India,*; Goa, India, 2011; pp. 188–195.

81. Erçağ, E.; Apak, R. Furnace smelting and extractive metallurgy of red mud: recovery of TiO2, Al2O3 and pig iron. *J. Chem. Technol. Biotechnol.* **1997**, *70*, 241–246, doi:10.1002/(SICI)1097-4660(199711)70:3<241::AID-JCTB769>3.0.CO;2-X.

82. Yagmurlu, B.; Alkan, G.; Xakalashe, B. S.; Friedrich, B. *Combined SAF Smelting and Hydrometallurgical Treatment of Bauxite Residue for enhanced Valuable Metal Recovery Electronic Scrap Recycling View project Circular economy (recycling processes) for batteries View project*; 2017;

83. Bonomi, C.; Alexandri, A.; Vind, J.; Panagiotopoulou, A.; Tsakiridis, P.; Panias, D. Scandium and Titanium Recovery from Bauxite Residue by Direct Leaching with a Brønsted Acidic Ionic Liquid. **2018**, doi:10.3390/met8100834.

84. Alkan, G.; Yagmurlu, B.; Cakmakoglu, S.; Hertel, T.; Kaya, Ş.; Gronen, L.; Stopic, S.; Friedrich, B. Novel Approach for Enhanced Scandium and Titanium Leaching Efficiency from Bauxite Residue with Suppressed Silica Gel Formation. *Sci. Rep.* **2018**, *8*, 5676, doi:10.1038/s41598-018-24077-9.

85. Maria Th. Ochsenkühn-Petropoulou, *,†; Konstantinos S. Hatzilyberis, ‡; Leonidas N. Mendrinos, † and; Salmas‡, C. E. Pilot-Plant Investigation of the Leaching Process for the Recovery of Scandium from Red Mud. **2002**, doi:10.1021/IE011047B.

86. Ochsenkühn-Petropulu, M.; Lyberopulu, T.; Ochsenkühn, K. M.; Parissakis, G. Recovery of lanthanides and yttrium from red mud by selective leaching. *Anal. Chim. Acta* **1996**, *319*, 249–254, doi:10.1016/0003-2670(95)00486-6.

87. Hertel, T.; Blanpain, B.; Pontikes, Y. A Proposal for a 100 % Use of Bauxite Residue Towards Inorganic Polymer Mortar. *J. Sustain. Metall.* **2016**, *2*, 394–404, doi:10.1007/s40831-016-0080-6.

88. Pontikes, Y.; Angelopoulos, G. N. Bauxite residue in cement and cementitious applications: Current status and a possible way forward. *Resour. Conserv. Recycl.* **2013**, *73*, 53–63, doi:10.1016/J.RESCONREC.2013.01.005.

89. Pontikes, Y.; Rathossi, C.; Nikolopoulos, P.; Angelopoulos, G. N.; Jayaseelan, D. D.; Lee, W. E. Effect of firing temperature and atmosphere on sintering of ceramics made from Bayer process bauxite residue. *Ceram. Int.* **2009**, *35*, 401–407, doi:10.1016/j.ceramint.2007.11.013.

90. McConchie, D. .; Clark, M. .; Hanahan, C. .; Davies-McConchie, F. The Use of Seawater-neutralised Bauxite Refinery Residues in the Management of Acid Sulphate Soils, Sulphidic Mine Tailings and Acid Mine Drainage. In *3rd Queensland Environmental Conference: Sustainable Solutions or Industry and Government*; Environmental Engineering Society, 2000; pp. 201–208.

91. Biswas, W. K.; Cooling, D. Sustainability Assessment of Red Sand as a Substitute for Virgin Sand and Crushed Limestone. *J. Ind. Ecol.* **2013**, *17*, n/a-n/a, doi:10.1111/jiec.12030.

92. Bonomi, C.; Cardenia, C.; Yin, P. T. W.; Panias, D.; Tam, P.; Panias, D. Review of technologies in the recovery of iron, aluminium, titanium and rare earth elements from bauxite residue (red mud). *Proc. 3rd Int. Symp. Enhanc. Landfill Min. (ELFM III)* **2016**, 259–276, doi:10.5281/zenodo.571694.

93. Balomenos, E.; Davris, P.; Pontikes, Y.; Panias, D. Mud2Metal: Lessons Learned on the Path for Complete Utilization of Bauxite Residue Through Industrial Symbiosis. *J. Sustain. Metall.* **2017**, *3*, 551–560, doi:10.1007/s40831-016-0110-4.

94. Kumar, R.; Premchand, J. Utilization of iron values of red mud for metallurgical applications. *Environ. Waste Manag. (ISSN 0971-9407)* **1998**, doi:10.13140/RG.2.1.2077.7446.

95. Binnemans, K.; Jones, P.; Blanpain, B.; Van Gerven, T.; Yang, Y.; Walton, A.; Bucher, M. Recycling of rare earths: a critical review. *J. Clean Prod* **2013**, *51*, 1–22, doi:doi:10.1016/j.jclepro.2012. 12.037.

96. Avdibegović, D.; Yagmurlu, B.; Dittrich, C.; Regadío, M.; Friedrich, B.; Binnemans, K. Combined multi-step precipitation and supported ionic liquid phase chromatography for the recovery of rare earths from leach solutions of bauxite residues. *Hydrometallurgy* **2018**, *180*, 229–235, doi:10.1016/J.HYDROMET.2018.07.023.

97. Avdibegović, D.; Regadío, M.; Binnemans, K. Recovery of scandium(iii) from diluted aqueous solutions by a supported ionic liquid phase (SILP). *RSC Adv.* **2017**, *7*, 49664–49674, doi:10.1039/C7RA07957E.

98. Binnemans, K.; Jones, P. T.; Blanpain, B.; Van Gerven, T.; Pontikes, Y. Towards zero-waste valorisation of rare-earth-containing industrial process residues: a critical review. *J. Clean. Prod.* **2015**, *99*, 17–38, doi:10.1016/J.JCLEPRO.2015.02.089.

99. Balomenos, E.; Gianopoulou, I.; Panias, D.; Paspaliaris, I.; Perry, K.; Boufounos, D. Efficient and Complete Exploitation of the Bauxite Residue (Red Mud) Produced in the Bayer Process. *Proc. EMC 2011* **2011**, 745–758.

100. Alkan, G.; Schier, C.; Gronen, L.; Stopic, S.; Friedrich, B.; Alkan, G.; Schier, C.; Gronen, L.; Stopic, S.; Friedrich, B. A Mineralogical Assessment on Residues after Acidic Leaching of Bauxite Residue (Red Mud) for Titanium Recovery. *Metals (Basel).* **2017**, *7*, 458, doi:10.3390/met7110458.

101. Alkan, G.; Yagmurlu, B.; Ma, Y.; Xakalashe, B.; Stopic, S. Combining pyrometallurgical conditioning and dry acid digestion of red mud for selective Sc extraction and TiO2 enrichment in mineral phase. In *2nd International Bauxite Residue Valorisation and Best Practices Conference, Athens, Greece*; 2018; pp. 215–222.

102. Yagmurlu, B.; Dittrich, C.; Friedrich, B. Precipitation Trends of Scandium in Synthetic Red Mud Solutions with Different Precipitation Agents. *J. Sustain. Metall.* **2017**, *3*, 90–98, doi:10.1007/s40831-016-0098-9.

103. Rudnick, R. L.; Gao, S. Composition of the Continental Crust. *In Treatise on Geochemistry; Elsevier* **2003**, 1–64.

104. Commission, E.; European Commission Study on the Review of the List of Critical Raw Materials.

105. Khairul, M. A.; Zanganeh, J.; Moghtaderi, B. The composition, recycling and utilisation of Bayer red mud. *Resour. Conserv. Recycl.* **2019**, *141*, 483–498, doi:10.1016/j.resconrec.2018.11.006.

106. Stickney, W. A.; Butler, M. O.; Mauser, J. E.; Fursman, O. C. Utilization of red mud residues from alumina production. *U.S. Dept. Inter. Bur. Mines* **1970**.

107. Li, Y.; Wang, J.; Wang, X.; Wang, B.; Luan, Z. Feasibility study of iron mineral separation from red mud by high gradient superconducting magnetic separation. *Phys. C Supercond.* **2011**, *471*, 91–96, doi:10.1016/j.physc.2010.12.003.

108. Peng, X.; Huang, G. Method for recovering iron concentrates from alumina red mud 2011.

109. LI, X. bin; XIAO, W.; LIU, W.; LIU, G. hua; PENG, Z. hong; ZHOU, Q. sheng; QI, T. gui Recovery of alumina and ferric oxide from Bayer red mud rich in iron by reduction sintering. *Trans. Nonferrous Met. Soc. China* **2009**, *19*, 1342–1347, doi:10.1016/S1003-6326(08)60447-1.

110. Liu, W.; Yang, J.; Xiao, B. Application of Bayer red mud for iron recovery and building material production from alumosilicate residues. *J. Hazard. Mater.* **2009**, *161*, 474–478, doi:10.1016/j.jhazmat.2008.03.122.

111. Raspopov, N. A.; Korneev, V. P.; Averin, V. V.; Lainer, Y. A.; Zinoveev, D. V.; Dyubanov, V. G. Reduction of iron oxides during the pyrometallurgical processing of red mud. *Russ. Metall.* **2013**, *2013*, 33–37, doi:10.1134/S0036029513010114.

112. Jayasankar, K.; Ray, P. K.; Chaubey, A. K.; Padhi, A.; Satapathy, B. K.; Mukherjee, P. S. Production of pig iron from red mud waste fines using thermal plasma technology. *Int. J. Miner. Metall. Mater.* **2012**, *19*, 679–684, doi:10.1007/s12613-012-0613-3.

113. Liu, W.; Sun, S.; Zhang, L.; Jahanshahi, S.; Yang, J. Experimental and simulative study on phase transformation in Bayer red mud soda-lime roasting system and recovery of Al, Na and Fe. *Miner. Eng.* **2012**, *39*, 213–218, doi:http://dx.doi.org/10.1016/j.mineng.2012.05.021.

114. Rath, S. S.; Pany, A.; Jayasankar, K.; Mitra, A. K.; Kumar, C. S.; Mukherjee, P. S.; Mishra, B. K. Statistical modeling studies of iron recovery from red mud using thermal plasma. *Plasma Sci. Technol.* **2013**, *15*, 459–464, doi:10.1088/1009-0630/15/5/13.

115. Liu, Y.; Mei, Z. Study on coal-based direct reduction of high-iron-content red mud. *Sinter. Pelletizing* **1995**, *20*, 5–9.

116. Qiu, G.; Liu, Y.; Jiang, T.; Hu, Y.; Mei, X. Influence of additives on slag-iron separation during direct reduction of coal-base high-iron-content red mud. *Trans. Nonferrous Met. Soc. China* **1996**, *6*, 1–7.

117. Rao, M.; Zhuang, J.; Li, G.; Zeng, J.; Jiang, T. Iron Recovery from Red Mud by Reduction Roasting-Magnetic Separation. In *Minerals, Metals and Materials Series*; 2016; pp. 125–130.

118. Guo, Y.; Gao, J.; XU, H.; Zhao, K.; Shi, X. Nuggets Production by Direct Reduction of High Iron Red Mud,. *J. Iron Steel Res. Int.* **2013**, *20*, 24–27, doi:10.1016/S1006-706X(13)60092-8.

119. Debadatta, D.; Pramanik, K. A study on chemical leaching of iron from red mud using sulphuric acid. *Res. J. Chem. Environ.* **2013**, *17*, 50–56.

120. YU, Z.; SHI, Z.; CHEN, Y.; NIU, Y.; WANG, Y.; WAN, P. Red-mud treatment using oxalic acid by UV irradiation assistance. *Trans. Nonferrous Met. Soc. China* **2012**, *22*, 456–460, doi:10.1016/S1003-6326(11)61198-9.

121. Eisele, T. C.; Gabby, K. L. Review of Reductive Leaching of Iron by Anaerobic Bacteria. *Miner. Process. Extr. Metall. Rev.* **2014**, *35*, 75–105, doi:10.1080/08827508.2012.703627.

122. Aghaie, E.; Pazouki, M.; Hosseini, M. R.; Ranjbar, M. Kinetic modeling of the bioleaching

process of iron removal from kaolin. *Appl. Clay Sci.* **2012**, *65–66*, 43–47, doi:10.1016/j.clay.2012.04.011.

123. Štyriaková, I.; Mockovčiaková, A.; Štyriak, I.; Kraus, I.; Uhlík, P.; Madejová, J.; Orolínová, Z. Bioleaching of clays and iron oxide coatings from quartz sands. *Appl. Clay Sci.* **2012**, *61*, 1–7, doi:10.1016/j.clay.2012.02.020.

124. Anand, P.; Modak, J. M.; Natarajan, K. A. A. Biobeneficiation of bauxite using Bacillus polymyxa: calcium and iron removal. *Int. J. Miner. Process.* **1996**, *48*, 51–60, doi:10.1016/S0301-7516(96)00013-0.

125. Papassiopi, N.; Vaxevanidou, K.; Paspaliaris, I. Effectiveness of iron reducing bacteria for the removal of iron from bauxite ores. *Miner. Eng.* **2010**, *23*, 25–31, doi:10.1016/j.mineng.2009.09.005.

126. Vasan, S. S.; Modak, J. M.; Natarajan, K. A. Some recent advances in the bioprocessing of bauxite. *Int. J. Miner. Process.* **2001**, *62*, 173–186, doi:10.1016/S0301-7516(00)00051-X.

127. Laguna, C.; González, F.; García-Balboa, C.; Ballester, A.; Blázquez, M. L.; Muñoz, J. A. Bioreduction of iron compounds as a possible clean environmental alternative for metal recovery. *Miner. Eng.* **2011**, *24*, 10–18, doi:10.1016/j.mineng.2010.08.026.

128. Thostenson, E. T.; Chou, T.-W. Microwave processing: fundamentals and applications. *Compos. Part A Appl. Sci. Manuf.* **1999**, *30*, 1055–1071, doi:10.1016/S1359-835X(99)00020-2.

129. Méndez, U. O.; Kharissova, O. V.; Rodríguez, M. Synthesis and morphology of nanostructures via microwave heating. *Rev. Adv. Mater. Sci.* **2003**, *5*, 398–402.

130. Zlotorzynski, A. The Application of Microwave Radiation to Analytical and Environmental Chemistry. *Crit. Rev. Anal. Chem.* **1995**, *25*, 43–76, doi:10.1080/10408349508050557.

131. Hassani, F.; Nekoovaght, P. M.; Gharib, N. The influence of microwave irradiation on rocks for microwave-assisted underground excavation. *J. Rock Mech. Geotech. Eng.* **2016**, *8*, 1–15, doi:10.1016/j.jrmge.2015.10.004.

132. Pickles, C. A. Microwaves in extractive metallurgy: Part 1 - Review of fundamentals. *Miner. Eng.* **2009**, *22*, 1102–1111, doi:10.1016/j.mineng.2009.02.015.

133. Griffiths, D. *Introduction to electrodynamics*; 3rd ed.; Upper Saddle River, NJ: Prentice Hall, 1999;

134. Clark, D. E.; Folz, D. C.; West, J. K. Processing materials with microwave energy. *Mater. Sci. Eng. A* **2000**, *287*, 153–158, doi:10.1016/S0921-5093(00)00768-1.

135. Chantrey, P.; Metaxas, A. C.; Meredith, R. . *Industrial Microwave Heating*; Peter Pere.; London, 1983; Vol. 29; ISBN 9781849194242.

136. Tang, J. Unlocking Potentials of Microwaves for Food Safety and Quality. *J. Food Sci.* **2015**, *80*,

E1776–E1793, doi:10.1111/1750-3841.12959.

137. Standish, N.; Worner, H. K.; Obuchowski, D. Y. Particle size effect in microwave heating of granular materials. *Powder Technol.* **1991**, *66*, 225–230, doi:10.1016/0032-5910(91)80034-G.

138. Churyumov, G.; Qiu, J.; Wang, N. Vacuum Microwave Sources of Electromagnetic Radiation. In *Electromagnetic Fields and Waves*; IntechOpen, 2019.

139. Humphries, S. Principles of Charged Particle Acceleration. **1999**, 356–407, doi:10.1063/1.2811424.

140. Kitagawa, K.; Kanuma, Y. The reliability of magnetrons for microwave ovens. *J. Microw. Power* **1986**, *21*, 149–158.

141. Gerling, J. Microwave oven power: a technical review. *J. Microw. Power* **1987**, *22*, 149 – 158.

142. Ludwig, R. *RF Circuit Design - Theory and Applications*; 2000; ISBN 0-13-095323-7.

143. Sun, J.; Wang, W.; Yue, Q. Review on Microwave-Matter Interaction Fundamentals and Efficient Microwave-Associated Heating Strategies. *Materials (Basel).* **2016**, *9*, 231, doi:10.3390/ma9040231.

144. Javad Koleini, S. M.; Barani, K.; Javad, S. M.; Barani, K.; Javad Koleini, S. M.; Barani, K. Microwave Heating Applications in Mineral Processing. In *The Development and Application of Microwave Heating*; InTech, 2012; pp. 79–104.

145. Dorn, C.; Behrend, R.; Giannopoulos, D.; Napolano, L.; Baños, B. G.; James, V.; Uhlig, V.; Catalá, J. M.; Founti, M.; Trimis, D. KPI and LCA evaluation of integrated microwave technology for high temperature processes. *Procedia CIRP* **2015**, *29*, 492–497, doi:10.1016/j.procir.2015.02.033.

146. Hertel, T.; Cardenia, C.; Balomenos, E.; Panias, D.; Pontikes, Y. Microwave treatment of bauxite residue for the production of inorganic polymers. In *Proceedings of the 2nd International Bauxite Residue Valorisation and Best Practices Conference*; 2018.

147. Chen, T. T.; Dutrizac, J. E.; Haque, K. E.; Wyslouzil, W.; Kashyap, S. The Relative Transparency of Minerals to Microwave Radiation. *Can. Metall. Q.* **1984**, *23*, 349–351, doi:10.1179/cmq.1984.23.3.349.

148. Cook, N. P. Microwave Principles and System. In; 1986.

149. Schiffmann, R. F. Microwave and dielectric drying. In *Handbook of Industrial Drying.*; 1987; pp. 327–356.

150. Doelling, M. K.; Jones, D. M.; Smith, R. A.; Nash, R. A. The Development of a Microwave Fluid-Bed Processor. I. Construction and Qualification of a Prototype Laboratory Unit. *Pharm. Res.* **1992**, *9*, 1487–1492, doi:10.1023/A:1015875300053.

151. Walkiewicz, J. W.; Kazonich, G.; McGill, S. L. Microwave heating characteristics of selected minerals and compounds. *Miner. Metall. Process.* **1988**, *5*, 39–42, doi:10.1007/BF03449501.

152. Walkiewicz, J. W.; Clark, A. E.; McGill, S. L. Microwave-assisted grinding. *IEEE Trans. Ind. Appl.* **1991**, *27*, 239–243, doi:10.1109/28.73604.

153. Javad Koleini, S. M.; Barani, K.; Rezaei, B. The Effect of Microwave Treatment on Dry Grinding Kinetics of Iron Ore. *Miner. Process. Extr. Metall. Rev.* **2012**, *33*, 159–169, doi:10.1080/08827508.2011.562947.

154. Seflek, C.; Bayat, O. Microwave-Assisted Grinding of Bolkardag (Nigde, Turkey) Gold Ore and Enhanced Cyanide Leachability. *Metall. Res. Technol.* **2018**, *115*, 508, doi:10.1051/metal/2018039.

155. Vorster, W.; Rowson, N. . A.; Kingman, S. . W. The effect of microwave radiation upon the processing of Neves Corvo copper ore. *Int. J. Miner. Process.* **2001**, *63*, 29–44, doi:10.1016/S0301-7516(00)00069-7.

156. Panias, D.; Krestou, A.; Panias D., K. A. Use of Microwave energy in Metallurgy. In *1st International Conference in Advance in Mineral Resources Management and Environmental Geotechnology · AMIREG 2004*; 2004; pp. 215–220.

157. N. Standish, H. W. & G. G. Temperature Distribution in Microwave-Heated Iron Ore-Carbon Composites. *ournal Microw. Power Electromagn. Energy* **1990**, *25*, 78–80, doi:10.1080/08327823.1990.11688114.

158. Lu, T.; Pickles, C. A.; Kelebek, S. Carbothermal reductive upgrading of a bauxite ore using microwave radiation. *High Temp. Mater. Process.* **2012**, *31*, 139–148, doi:10.1515/htmp-2012-0002.

159. Kelly, R. M.; Rowson, N. A. Microwave reduction of oxidised ilmenite concentrates. *Miner. Eng.* **1995**, *8*, 1427–1438, doi:10.1016/0892-6875(95)00106-Z.

160. Samouhos, M.; Hutcheon, R.; Paspaliaris, I. Microwave reduction of copper(II) oxide and malachite concentrate. *Miner. Eng.* **2011**, *24*, 903–913, doi:10.1016/j.mineng.2011.03.026.

161. Nanthakumar, B.; Pickles, C. A.; Kelebek, S. Microwave pretreatment of a double refractory gold ore. *Miner. Eng.* **2007**, *20*, 1109–1119, doi:10.1016/j.mineng.2007.04.003.

162. Avraamides, J.; Miovski, P.; Van Hooft, P. Thermal reactivation of carbon used in the recovery of gold from cyanide pulps and solutions, Research and Development in Extractive Metallurgy. *Aus. I.M.M, Adelaide Branch.* **1987**.

163. Kingman, S. W. Recent developments in microwave processing of minerals. *Int. Mater. Rev.* **2006**, *51*, 1–12, doi:10.1179/174328006X79472.

164. Oder, R. R. High gradient magnetic separation theory and applications. *IEEE Trans. Magn.* **1976**, *12*, 428–435, doi:10.1109/TMAG.1976.1059076.

165. Svoboda, J.; Fujita, T. Recent developments in magnetic methods of material separation. *Miner. Eng.* **2003**, *16*, 785–792, doi:10.1016/S0892-6875(03)00212-7.

166. Ge, W.; Encinas, A.; Araujo, E.; Song, S. Magnetic matrices used in high gradient magnetic separation (HGMS): A review. *Results Phys.* **2017**, *7*, 4278–4286, doi:10.1016/j.rinp.2017.10.055.

167. Hällberg, L. P.; Stevens, T.; Almqvist, B.; Snowball, I.; Wiers, S.; Költringer, C.; Lu, H.; Zhang, H.; Lin, Z. Magnetic susceptibility parameters as proxies for desert sediment provenance. *Aeolian Res.* **2020**, *46*, 100615, doi:10.1016/j.aeolia.2020.100615.

168. Svoboda, J. *Magnetic techniques for the treatment of materials*; Kluwer Academic, 2004; Vol. 53; ISBN 1-4020-2038-4.

169. *Kirk-Othmer Encyclopedia of Chemical Technology*; John Wiley & Sons, I., Ed.; Wiley, 2000; ISBN 9780471484943.

170. Parodi, F. Physics and Chemistry of Microwave Processing. *Compr. Polym. Sci. Suppl.* **1989**, 669–728, doi:10.1016/b978-0-08-096701-1.00258-5.

171. Spain, E.; Venkatanarayanan, A. *Review of Physical Principles of Sensing and Types of Sensing Materials*; Elsevier, 2014; Vol. 13; ISBN 9780080965338.

172. Tripathy, S. K.; Singh, V.; Rama Murthy, Y.; Banerjee, P. K.; Suresh, N. Influence of process parameters of dry high intensity magnetic separators on separation of hematite. *Int. J. Miner. Process.* **2017**, *160*, 16–31, doi:10.1016/j.minpro.2017.01.007.

173. Anagnostou, C. Bauxite resource exploitation in Greece vs sustainability. *Bull. Geol. Soc. Greece* **2017**, *43*, 2426, doi:10.12681/bgsg.11644.

174. Aluminum of Greece Available online: https://www.alhellas.com/en-us/home/homepage.

175. Lavalou, E.; Bosca, B.; Keramidas, O. Alumina Production from Diasporic Bauxites. *Light Met. 1999* **1999**, 55–62.

176. Papanastassiou, D.; Contaroudas, D.; Solymàr, K. Processing and Marketing of Greek Diasporic Bauxite for Metallurgical and Non-Metallurgical Applications. In *17th International Symposium of ICSOBA*; Montrèal, QC, Canada, 2006.

177. Balomenos, E.; Gianopoulou, I.; Panias, D.; Paspaliaris, I. ENEXAL: Novel technologies for enhanced energy and exergy efficiencies in primary aluminium production industry. *Assoc. Metall. Eng. Serbia* **2009**, *15*, 203–217, doi:669.71.056.

178. Chin, L. A. D. The state-of-the-art in Bayer process technology. In *Light Metals 1988*; 1988; pp. 49–53.

179. Schumacher, B. A.; Shines, K. C.; Burton, J. V.; Papp, M. L. Comparison of three methods for soil homogenization. *Soil Sci. Soc. Am. J.* **1990**, *54*, 1187–1190,

doi:10.2136/sssaj1990.03615995005400040046x.

180. Sglavo, V. M.; Campostrini, R.; Maurina, S.; Carturan, G.; Monagheddu, M.; Budroni, G.; Cocco, G. Bauxite 'red mud' in the ceramic industry. Part 1: thermal behaviour. *J. Eur. Ceram. Soc.* **2000**, *20*, 235–244, doi:http://dx.doi.org/10.1016/S0955-2219(99)00088-6.

181. Atasoy, A. An investigation on characterization and thermal analysis of the Aughinish red mud. *J. Therm. Anal. Calorim.* **2005**, *81*, 357–361, doi:10.1007/s10973-005-0792-5.

182. Földavári, M.; Földvári, M.; Földavári, M. *Handbook of thermogravimetric system of minerals and its use in geological practice*; Geological Institute of Hungary: Budapest, Hungary, 2011; Vol. 213; ISBN 9789636712884.

183. Bale, C. W.; Chartrand, P.; Degterov, S. A.; Eriksson, G.; Hack, K.; Mahfoud, R. Ben; Melançon, J.; Pelton, A. D.; Petersen, S.; *CRCT FactSage Thermochemical Software and Databases. *Calphad* **2002**, *26*, 189–228.

184. Li, C.; Sun, H.; Bai, J.; Li, L. Innovative methodology for comprehensive utilization of iron ore tailings. Part 1. The recovery of iron from iron ore tailings using magnetic separation after magnetizing roasting. *J. Hazard. Mater.* **2010**, *174*, 71–77, doi:10.1016/j.jhazmat.2009.09.018.

185. Li, C.; Sun, H.; Yi, Z.; Li, L. Innovative methodology for comprehensive utilization of iron ore tailings. Part 2: The residues after iron recovery from iron ore tailings to prepare cementitious material. *J. Hazard. Mater.* **2010**, *174*, 78–83, doi:10.1016/j.jhazmat.2009.09.019.

186. Xu, Z.; Hwang, J.; Greenlund, R.; Huang, X.; Luo, J.; Anschuetz, S. Quantitative Determination of Metallic Iron Content in Steel-Making Slag. *J. Miner. Mater. Charact. Eng.* **2003**, *02*, 65–70, doi:10.4236/jmmce.2003.21006.

187. Buchmann, M.; Schach, E.; Tolosana-Delgado, R.; Leißner, T.; Astoveza, J.; Kern, M.; Möckel, R.; Ebert, D.; Rudolph, M.; van den Boogaart, K.; Peuker, U. Evaluation of Magnetic Separation Efficiency on a Cassiterite-Bearing Skarn Ore by Means of Integrative SEM-Based Image and XRF–XRD Data Analysis. *Minerals* **2018**, *8*, 390, doi:10.3390/min8090390.

188. Sanchez-Segado, S.; Monti, T.; Katrib, J.; Kingman, S.; Dodds, C.; Jha, A. Towards sustainable processing of columbite group minerals: Elucidating the relation between dielectric properties and physico-chemical transformations in the mineral phase. *Sci. Rep.* **2017**, *7*, 3–9, doi:10.1038/s41598-017-18272-3.

189. Chen, G. Particularities of heat conduction in nanostructures. *J. Nanoparticle Res.* **2000**, *2*, 199–204, doi:10.1023/A:1010003718481.

190. Kreith, F.; Black, W. Z. Basic heat transfer. 1980.

191. Fukushima, J.; Hayashi, Y.; Takizawa, H. Structure and magnetic properties of FeAl2O4synthesized by microwave magnetic field irradiation. *J. Asian Ceram. Soc.* **2013**, *1*, 41–45, doi:10.1016/j.jascer.2013.02.001.

192. LI, X. bin; XIAO, W.; LIU, W.; LIU, G. hua; PENG, Z. hong; ZHOU, Q. sheng; QI, T. gui Recovery of alumina and ferric oxide from Bayer red mud rich in iron by reduction sintering. *Trans. Nonferrous Met. Soc. China (English Ed.* **2009**, doi:10.1016/S1003-6326(08)60447-1.

193. Liu, W.; Sun, S.; Zhang, L.; Jahanshahi, S.; Yang, J. Experimental and simulative study on phase transformation in Bayer red mud soda-lime roasting system and recovery of Al, Na and Fe. *Miner. Eng.* **2012**, *39*, 213–218, doi:http://dx.doi.org/10.1016/j.mineng.2012.05.021.

194. Cardenia, C.; Balomenos, E.; Panias, D. Optimization of Microwave Reductive Roasting Process of Bauxite Residue. *Metals (Basel).* **2020**, *10*, 1083, doi:10.3390/met10081083.

195. Joyce, P. J.; Björklund, A. Using Life Cycle Thinking to Assess the Sustainability Benefits of Complex Valorization Pathways for Bauxite Residue. *J. Sustain. Metall.* **2019**, *5*, 69–84, doi:10.1007/s40831-019-00209-x.

196. Adrados, A.; De Marco, I.; López-Urionabarrenechea, A.; Solar, J.; Caballero, B.; Gastelu, N. Biomass Pyrolysis Solids as Reducing Agents: Comparison with Commercial Reducing Agents. *Materials (Basel).* **2015**, *9*, 3, doi:10.3390/ma9010003.

197. Javad Koleini, S. M.; Barani, K. Microwave Heating Applications in Mineral Processing. In *The Development and Application of Microwave Heating*; 2012; pp. 79–104.

198. Pickles, C. A.; Marzoughi, O. Towards a Microwave Metal Extraction Process. In; The Minerals, Metals & Materials Series; Springer International Publishing, 2018; pp. 1039–1060.

199. Peng, Z.; Hwang, J.-Y. Microwave-assisted metallurgy. *Int. Mater. Rev.* **2015**, *60*, 30–63, doi:10.1179/1743280414Y.0000000042.

200. V.V. A.A. RemovAL: Removing the waste streams from the primary Aluminium production in Europe Available online: https://www.removal-project.com.